

UNIVERSITY OF NAPLES FEDERICO II

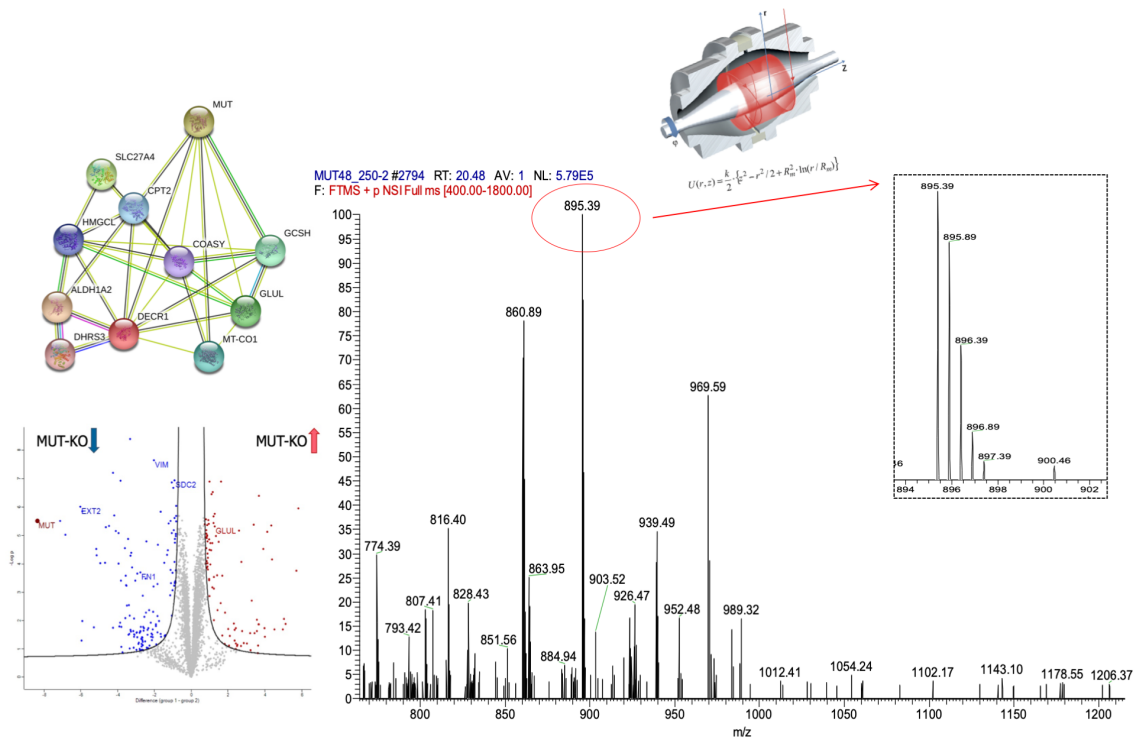
DOCTORATE IN
MOLECULAR MEDICINE AND MEDICAL BIOTECHNOLOGY

XXXII CYCLE



Michele Costanzo

THE PROTEOMIC LANDSCAPE OF CELLULAR MODELS
FOR METHYLMALONIC ACIDEMIA



Year 2020

UNIVERSITY OF NAPLES FEDERICO II

DOCTORATE IN
MOLECULAR MEDICINE AND MEDICAL BIOTECHNOLOGY

XXXII CYCLE



THE PROTEOMIC LANDSCAPE OF CELLULAR MODELS
FOR METHYLMALONIC ACIDEMIA

Tutor
Prof. Margherita Ruoppolo

Candidate
Dr. Michele Costanzo

Coordinator
Prof. Vittorio Enrico Avvedimento

Year 2020

Index

1. INTRODUCTION

1.1. Methylmalonic acidemias (MMA)

- 1.1.1. Background and molecular characterization of MMA*
- 1.1.2. Biochemical and pathophysiologic mechanisms in MMA*
- 1.1.3. MMA diagnosis and Expanded Newborn Screening*
- 1.1.4. Results of the research group on MMA*

2. AIM

3. MATERIALS AND METHODS

3.1. Cell cultures and treatments

3.2. Cell transfections

- 3.2.1. siRNA for MUT silencing in SH-SH5Y cell line*
- 3.2.2. CRISPR/Cas9-MUT KO HEK293 cell line generation*
- 3.2.3. MUT-FLAG expression for MUT rescuing in MUT-KO*
- 3.2.4. MMACHC-FLAG expression in HepG2 cell line*

3.3. Cell viability and apoptosis assays

- 3.3.1. Apoptosis by Flow Cytometry*
- 3.3.2. MTT and Neutral-Red assay*

3.4. ROS detection

3.5. WGA staining

3.6. Proteomics

- 3.6.1. Global proteomic analysis for SH-SY5Y siRNA_MUT cells*
 - 3.6.1.1. Sample preparation*
 - 3.6.1.2. LC-MS/MS analysis*
 - 3.6.1.3. Spectral counts-based proteomics*
- 3.6.2. Global proteomic analysis for HEK293 MUT-KO cells*
 - 3.6.2.1. Sample preparation*
 - 3.6.2.2. LC-MS/MS analysis*
 - 3.6.2.3. LFQ-based proteomics*
- 3.6.3. Global proteomic analysis for HEK293 MUT-KO and MUT-Rescue cells*
 - 3.6.3.1. Sample preparation*
 - 3.6.3.2. LC-MS/MS analysis*
 - 3.6.3.3. DIA-based proteomics*

3.7. Metabolomics

3.7.1. Sample preparation and targeted LC-MS/MS

3.8. Bioinformatics

3.9. Western blotting

3.10. Quantitative real-time PCR

3.11. Co-Immunoprecipitation of MMACHC protein and MS-based identification of putative interactors

4. RESULTS

4.1. MUT knockdown in SH-SY5Y cell line

4.1.1. MUT silencing does not induce apoptosis in SH-SY5Y cells

4.1.2. Spectral counts-based global proteomic analysis of MUT-silenced SH-SY5Y cells

4.1.3. Bioinformatic analysis and functional annotation

4.1.4. Mut silencing decreases cell viability and mitochondrial functionality in propionate-enriched culture medium

4.2. MUT knockout in SH-SY5Y cell line

4.3. MUT knockout in HEK293 cell line

4.3.1. CRISPR/Cas9-based cell model generation and biochemical characterization

4.3.2. LFQ-based global proteomic analysis of MUT-KO cells

4.3.3. Bioinformatic analysis

4.3.4. Rescuing MUT expression in MUT-KO cells

4.3.5. Validation of proteomic results and protein expression analysis

4.3.6. MUT knockout impairs cell viability and mitochondrial functionality in propionate-enriched culture medium

4.3.7. MUT knockout increases the intracellular levels of ROS

4.3.8. MUT knockout hampers proteoglycan levels

4.3.9. DIA-based global proteomic analysis of MUT-KO and MUT-Rescue cells

4.4. Mapping the interactome of MMACHC protein

4.4.1. Stable generation of MMACHC-FLAG and GFP-FLAG HepG2-expressing cell lines

4.4.2. Co-immunoprecipitation of MMACHC protein

4.4.3. MS-based identification of putative MMACHC interactors

5. DISCUSSION

- 5.1. MUT knockdown in SH-SY5Y cells induces alterations in proteins related to mitochondrial functionality*
- 5.2. MUT knockout in SH-SY5Y and HEK293 cells*
- 5.3. Proteomic analysis of HEK293 MUT-KO cells reveals impairment in metal homeostasis*
- 5.4. Proteomic analysis of HEK293 MUT-KO cells reveals impairment in mitochondrial metabolic pathways*
- 5.5. Effects of MUT-KO and MUT-rescuing on cell adhesion, cytoskeleton and structural organization*
- 5.6. Production of ROS and hyperammonemia in MUT-KO*
- 5.7. Impact of propionate-induced stress in MUT-KO and siRNA_MUT cells*
- 5.8. Exploring HEK293 MUT-KO and MUT-Rescue proteomes using Data-Independent Acquisition mass spectrometry*
- 5.9. Mapping the interactome of MMACHC protein*

6. ACKNOWLEDGEMENTS

7. REFERENCES

8. LIST OF PUBLICATIONS

9. ABBREVIATIONS

ABSTRACT

The present PhD thesis project concerned the development of novel cellular models to be used for the study and the advancing knowledge about methylmalonic acidemia (MMA), a rare inborn error of metabolism that occurs as consequence of specific defects in propionyl-CoA and cobalamin (vitamin B12) metabolism. Isolated MMA is caused by specific mutations in methylmalonyl-CoA mutase (MUT) gene, whose protein product converts methylmalonyl-CoA into succinyl-CoA, an intermediate of the Krebs cycle. Mutations in one of the genes involved in the intracellular metabolism of cobalamin, used for the synthesis of MUT cofactor, the adenosylcobalamin, are causative of secondary forms of MMA with or without homocystinuria. Methylmalonic acid is the metabolite that accumulates downstream MUT reaction impairment and, therefore, is used as diagnostic biomarker of MMA. Metabolic alterations of this disease include tissue (mostly brain, liver, kidney) damage and necessity of transplantation to ensure a long-term survival. The causes of metabolic instability are often addressed to the action of secondary metabolites of propionyl-CoA pathway, ammonium accumulation, reactive oxygen species production and mitochondrial impairment with global energy production imbalance and irreversible damages. For all these altered processes, the acting mechanisms are not known. Here, the generation of different cell models that may recapitulate MMA physiopathology was accompanied by the application of different mass spectrometry-based proteomic strategies, employing different instrumentations and techniques, with the aim to describe and elucidate perturbed pathways and unravel possible pathogenetic mechanisms that are still unknown.

The first cellular model for isolated MMA was created by silencing *MUT* gene in human neuroblastoma SH-SY5Y cell line via siRNA-mediated RNA interference. The proteome of these cells was resolved by monodimensional SDS-PAGE and analyzed by liquid chromatography-tandem mass spectrometry (LC-MS/MS) using a LTQ-Orbitrap XL mass spectrometer. Label-free proteomic analysis by means of the spectral counts approach highlighted common dysregulated signatures related to mitochondrial energy production and oxidation-reduction processes unbalances.

Subsequently, a second cell model for isolated MMA was generated knocking out (KO) *MUT* gene in human embryonic kidney (HEK) 293 cells using CRISPR/Cas9 genome editing technology. *MUT*-KO proteome was analyzed by shotgun LC-MS/MS using an Orbitrap-Q Exactive Plus mass spectrometer. Label-free quantitative proteomics based on LFQ method and biochemical assays suggested that *MUT*-KO cells are adapting to the changes triggered upon *MUT* knock out by altering their structure with modifications in extracellular matrix, cell adhesion and cytoskeletal components. *MUT* KO induced metabolic alterations related to toxic compounds accumulations, such as ammonia, and production of ROS that are known damaging cells by interfering in the oxidation-reduction homeostasis. The *MUT*-deficient cells

modify their proteome by a modulation of gene expression that still permits to survive, even in conditions of stress and mitochondrial impairment. On the other hand, an additional stress induced by propionate overload on a system already stressed became fatal. All the alterations found were monitored in an additional cell model of MUT rescuing that was generated from MUT-KO cells in order to control the specificity of the effects of MUT knockout.

In addition to the previous investigation, proteome alterations were deeper investigated in MUT-KO and MUT-Rescue through the employment of a sophisticated high resolution Data-Independent Acquisition-based proteomic analysis carried out with an Orbitrap-Q Exactive HF mass spectrometer.

Finally, to complete the picture of the proteomic landscape of MMA, the possible role of MMACHC protein in the cell was investigated. Interactomics experiments provided the identification of many putative interactors of MMACHC, which may take part in the formation of MUT cofactor. Alternatively, new roles for MMACHC protein in the cell may be discovered making a valuable contribution in the knowledge of vitamin B12 metabolism.

1. INTRODUCTION

1.1. Methylmalonic acidemias (MMA)

1.1.1. Background and molecular characterization of MMA

Methylmalonic acidemias (MMA) are rare inborn errors of metabolism included in the family of organic acidemias, a group of more than 65 metabolic disorders affecting amino acid metabolism, lipid metabolism, purine and pyrimidine metabolism, urea cycle, Krebs cycle and fatty acid oxidation. MMA together with other organic acidemias, such as propionic acidemia (PA), isovaleric acidemia and maple syrup urine disease, are sometimes referred to as classical organic acidemias (Villani et al., 2017).

MMA is a rare autosomal recessive disease, with an incidence around 1:100000 in Italy that occurs as consequence of specific defects in propionyl-CoA and cobalamin (cbl; vitamin B12) metabolism. The onset of the disease is commonly around the first months of life, even though it can be very variable and unpredictable, ranging from the newborn period to the adulthood. Infants and children can experience a broad range of clinical manifestation. At the beginning, signs can be absolutely non-specific, like gastrointestinal disturbances, vomiting, feeding rejection, and subsequent loss of weight. Then, clinical signs can, rapidly or in a progressive way, turn into more severe neurological manifestations, including hypotonia, lethargy, seizures and epilepsy, movement and neuromuscular abnormalities, and mental retardation. If not immediately treated, patients undergo coma, respiratory distress, hypothermia, and die within a few days or develop permanent brain damage. The neurological damage is the major complication for MMA patients (Dionisi-Vici et al., 2002).

The molecular defect related to MMA affects propionyl-Coenzyme A (CoA) catabolism into the mitochondrion. Propionyl-CoA is produced from branched-chain amino acids (valine, isoleucine, threonine, methionine) degradation, cholesterol side chains degradation and odd-chain fatty acids β -oxidation. In the mitochondrion, the propionyl-CoA is carboxylated to D-methylmalonyl-CoA in a reversible reaction catalyzed by the biotin-dependent propionyl-CoA carboxylase enzyme. The molecule D-methylmalonyl-CoA racemizes into its epimer, L-methylmalonyl-CoA, thanks to the activity of the methylmalonyl-CoA epimerase (also called methylmalonyl-CoA racemase). Finally, the vitamin B12-dependent methylmalonyl-CoA mutase (MUT) apoenzyme catalyzes the reversible isomerization of the L-methylmalonyl-CoA to succinyl-CoA, a key molecule involved in the last steps of metabolic energy production via tricarboxylic acid (Krebs) cycle. Methylmalonyl-CoA mutase is a key enzyme in the pathogenesis of MMA because mutations leading to inactivity or absence of the protein are responsible for the so-called isolated MMA (Figure 1).

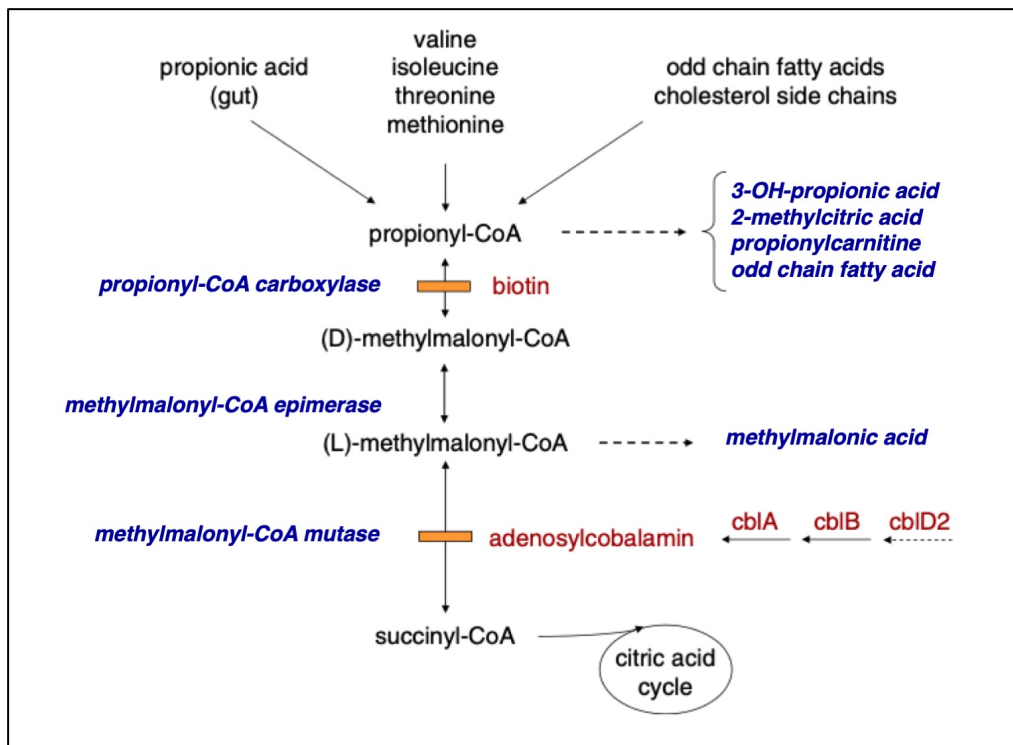


Figure 1. Schematic representation of the propionyl-CoA pathway involved in MMA.

Picture taken from Baumgartner et al., 2014.

MUT is a protein widely distributed in all living organisms, except plants (Takahashi-Iñiguez et al., 2012). In humans, MUT protein (UniProt ID P22033, Enzyme entry: EC 5.4.99.2) is encoded by the *MUT* gene that lies at the chromosome location 6p12.3 and consists of 13 exons, spanning over 35kb. Ledley et al. (1988) were the first to identify the human *MUT* gene by screening an expression library with MUT antibodies to isolate the first human *MUT* cDNA. MUT protein has been studied in several model organisms, such as *Saccharomyces cerevisiae*, *Caenorhabditis elegans*, in order to understand the nature of the molecular alterations due to mutation of the enzyme. In 1996, Mancía et al. obtained the crystal structure of MUT protein at 2Å of resolution by X-ray crystallography in *Propionibacterium shermanii*. The mature enzyme is a homodimer ($\alpha\beta$ dimer) that has several functional domains: a N-terminal domain linked to a CoA ester binding pocket domain, a C-terminal cobalamin binding motif, a mitochondrial importation signal, a dimerization domain, and a spacer or linker region. Figure 2 shows an adaptation of the 3D crystal structure of MUT by Mancía et al. (1996) elaborated using the RCSB Protein Data Bank (PDB, <https://www.rcsb.org>) (Berman et al., 2000); two colors distinguish the active α -chain, which contains the active domains of the protein, and the inactive β -chain. Several mutational mechanisms operating at *MUT* locus, such as mutations of premature stop codons, missense mutations, splice site mutations, mRNA stability mutations, deletions, and isodisomy, were identified over the years and listed and reviewed by Chandler et al. (2005). Such mutations are able

to impair MUT activity/expression causing a block at the reaction step catalyzed by MUT. In this context, there are two possible pathologic phenotypes related to MUT apoenzyme defect with which is possible to classify patients with isolated MMA: 1) *mut*⁰, in which patients are characterized by a totally absent enzymatic activity and 2) *mut*⁻, in which patients only have a low-to-moderate residual deficiency. *Mut*⁻ patients are more responsive to vitamin B12 (MUT cofactor) treatment because the reduced enzymatic activity is due to the decrement of the enzyme-cofactor affinity constant value; it is possible, therefore, to operate on the formation of the complex increasing the amount of cofactor. To date, for *mut*⁰ phenotype patients no specific pharmacological therapy exists but they can partially recover the metabolic instability through a liver or a combined liver/kidney transplantation (Manoli et al., 2005). For this reason, *mut*⁰ patients have an earlier onset, worse neurological outcome and higher mortality rate than *mut*⁻ ones, who became symptomatic later in infancy and have better survival and outcome (Deodato et al., 2006).

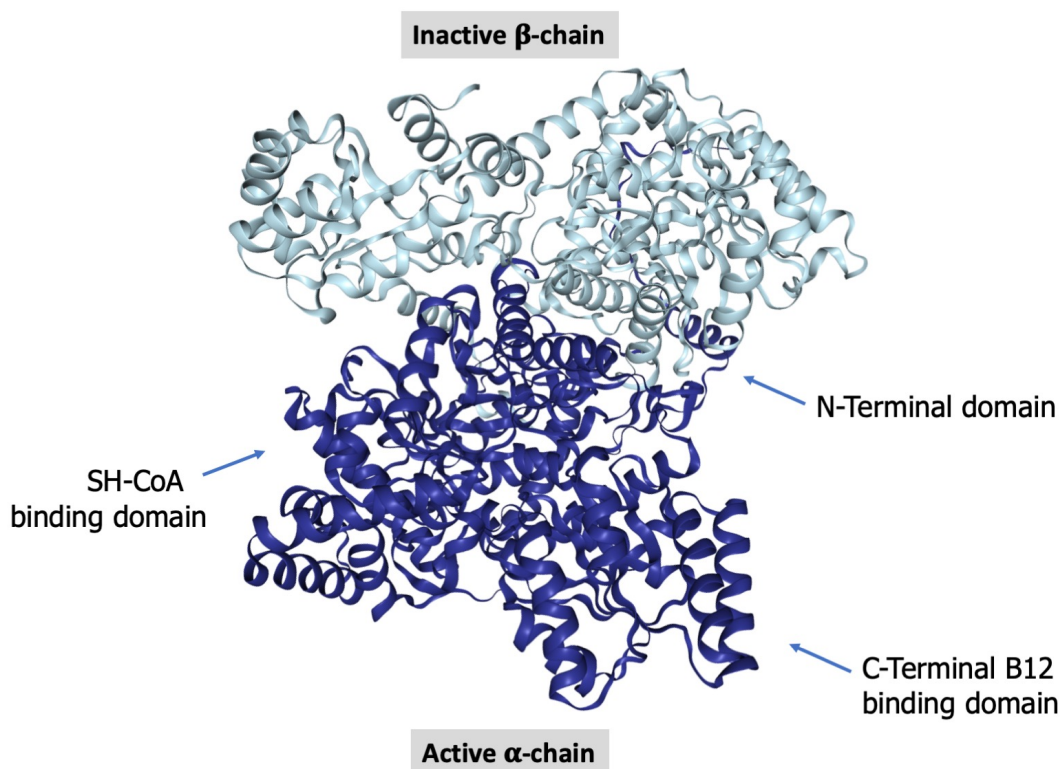


Figure 2. Crystal structure of methylmalonyl-CoA mutase enzyme. The $\alpha\beta$ -homodimer that forms the mature functioning enzyme is composed by an active α -chain (blue), which contains functional domains and binding sites, and an inactive β -chain (light blue), which contains no functional domains. The image was elaborated from the 3D structure of MUT within the Protein Data Bank database.

In order to undertake its task in the conversion of methylmalonyl-CoA to succinyl-CoA, MUT requires vitamin B12 in the form of adenosylcobalamin (AdoCbl) as cofactor. Dietary vitamin B12 enters the gastrointestinal tract via binding with a cobalamin transporter, the haptocorrin (HC), also called transcobalamin I (TCI), present in saliva. Its role is to protect cobalamin from acid degradation in the stomach. Once reached the duodenum, the complex cbl-TCI is released because of the action of pancreatic proteases that degrade the TCI. Then, free cbl makes a complex with the intrinsic factor (IF), a glycoprotein produced by the parietal cells of the stomach also known as gastric intrinsic factor, that is necessary for the absorption of vitamin B12 in the terminal ileum. The mechanisms of absorption and enterohepatic circulation of vitamin B12 are illustrated in Figure 3. In the terminal ileum, IF is degraded and free cbl uptake by ileal enterocytes is mediated by its binding with transcobalamin II (TCII) and further activation of the transcobalamin receptor (TCblR). Through a receptor-mediated endocytic event induced by activation of TCblR, the cbl-TCII complex is internalized and, thus, dissociates from TCblR itself in the endosomal compartment (Seetharam et al., 2000; Hannibal et al., 2013).

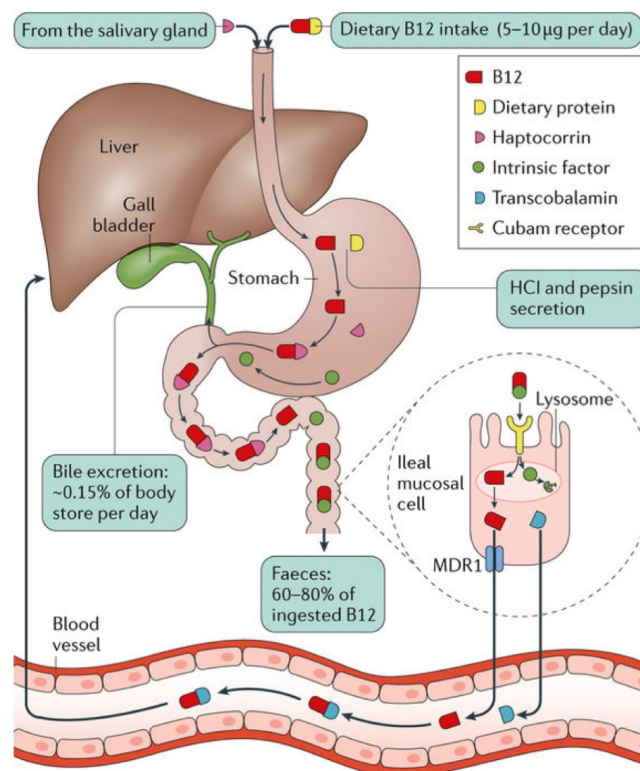


Figure 3. Mechanisms of absorption and enterohepatic circulation of vitamin B12. Vitamin B12 is derived from the diet and internalized in the organism. The transport of vitamin B12 is mediated by several proteins and carriers within an intricate mechanism that lead to the final processing for cofactors synthesis into the cells. Picture taken from Green et al., 2017.

When late endosomes get fused with lysosomes, TCII is degraded and free cobalamin is released into cytosol, where the cobalt of the molecule is reduced from the trivalent state (cob[III]alamin) to bivalent (cob[II]alamin) before entering the mitochondria, where a further reduction to cob[I]alamin takes place. Many proteins (such as ABCD4, LMBRD1, MMAA, MMAB, MMACHC, MMADHC, MTR, MTRR) are known to take part somehow to the final transformation of cbl to methylcobalamin (MeCbl) or AdoCbl, to serve as cofactors respectively for the cytosolic methionine synthase or the mitochondrial MUT, or both (Froese and Gravel, 2010). Probable lysosomal cobalamin transporter (LMBRD1) should carry cbl to the cytosol, in co-work with ATP-binding cassette sub-family D member 4 (ABCD4). Methylmalonic aciduria and homocystinuria type C protein (MMACHC) and methylmalonic aciduria and homocystinuria type D protein, mitochondrial (MMADHC) interact probably creating a complex that serves as chaperon for cbl trafficking and reduction of the cobalt atom. In the mitochondrion, the corrinoid adenosyltransferase (MMAB) generates AdoCbl and directly delivers the cofactor to MUT in a transfer that is stimulated by ATP-binding to MMAB and gated by methylmalonic aciduria type A protein, mitochondrial (MMAA), a G-protein chaperone that assists AdoCbl delivery. Methionine synthase (MTR) catalyzes the transfer of a methyl group from MeCbl to homocysteine, then reconstitutes the cofactor transferring the methyl from the methyltetrahydrofolate. When MeCbl is used it becomes oxidized from cob(I)alamin to cob(II)alamin and in this oxidation state MTR is not active; then, in order to keep MTR in a functional state, methionine synthase reductase (MTRR) catalyzes the reductive methylation of cob(II)alamin to cob(I)alamin using S-adenosylmethionine as a methyl donor (Sloan et al., 2008; Froese et al., 2015). However, the exact sequence of events that occur from the exit from lysosomes to the delivery to the two cbl-dependent enzymes is still unknown (Hannibal et al., 2013) (Figure 4).

Mutations in each gene encoding for the proteins involved in any steps of cofactors metabolism, impairing the synthesis or utilization of AdoCbl or MeCbl, are causative of a specific *cbl*-deficiency metabolic disorder, associated or not to MMA. In addition, other cbl-related defects are caused not only by alteration in the biosynthetic pathway of cofactors, but also by a lack of the vitamin in the diet or by malabsorption (Froese and Gravel, 2010). The nomenclature for inherited disorders of intracellular cobalamin metabolism is based on the biochemical phenotype, according to cellular complementation analysis, which was used for the first time to make diagnosis (Watkins and Rosenblatt, 1986) and that defines cobalamin complementation groups A-J (*cblA-cblJ*). AdoCbl deficiency caused by mutations in *MMAA*, *MMAB* and *MMADHC* genes (group *cblA*, *cblB*, *cblD*) is associated with MMA. Mutations in *MMADHC*, *MTRR* and *MTR* genes (group *cblD*, *cblE*, *cblG*) causing MeCbl deficiency are associated with homocystinuria. When both AdoCbl and MeCbl are deficient for mutations in genes involved in a common step of the biosynthetic pathway, *MMACHC*, *MMADHC*, *LMBRD1* and *ABCD4* (group *cblC*, *cblD*, *cblF*, *cblJ*), the pathologic disorder is referred to as combined

methylmalonic acidemia and homocystinuria. The name of each disorder is prefixed with "cbl" followed by a unique capital letter for its complementation group, e.g. cblC is for combined methylmalonic acidemia and homocystinuria cobalamin C type. CblC is the most frequent disorder of cbl metabolism among all (Sloan et al., 2008). Additionally, other unique cbl-associated disorders are recorded. A form biochemically related to cblC, called cblX, was discovered by Yu et al. (2013) as for mutations in *HCFC1*, a global transcriptional co-regulator. Only recently, Quintana et al. (2017) identified a cblX-like phenotype caused by mutations in *THAP11* gene. THAP11 is an interactor of the above-mentioned HCFC1, with which forms a complex that was discovered to regulate MMACHC expression. Another cblX-like patient was diagnosed to carry mutations in *ZNF143* gene (Pupavac et al., 2016), a transcriptional activator later proved also to interact with HCFC1 and, therefore, contribute to regulate MMACHC expression.

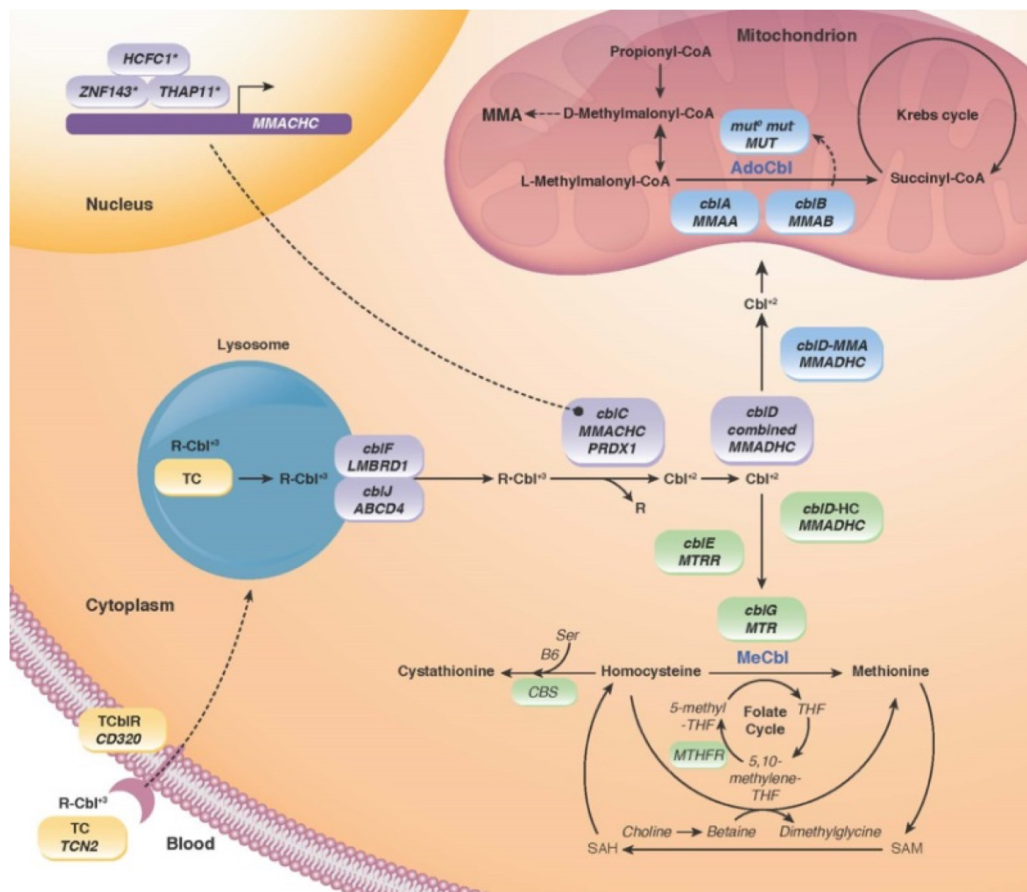


Figure 4. Picture representing the intracellular biosynthetic metabolism of cobalamin in the formation of cofactors for the completion of MUT reaction.

Picture taken from Sloan et al., 2008. MMA = methylmalonic acid; Cbl⁺³ = cobalamin at oxidation state +3; Cbl⁺² = cobalamin at oxidation state +2; CBS = cystathionine β-synthase; THF = tetrahydrofolate; MTHFR = methylenetetrahydrofolate reductase; SAM = S-adenosylmethionine; SAH = S-adenosylhomocysteine.

Therefore, mutations on the apoenzyme impairing MUT activity/expression lead to the most severe isolated MMA. Subsequently, the substrate L-methylmalonyl-CoA that cannot be converted in succinyl-CoA accumulates and is hydrolyzed to form methylmalonic acid and CoA. It is not sure whether the hydrolases enzymes catalyze this reaction acting on L-epimer of methylmalonyl-CoA; in fact, a highly specific hydrolase, called D-methylmalonyl-CoA hydrolase (Enzyme entry: EC 3.1.2.17), was identified and demonstrated to use D-methylmalonyl-CoA as substrate to remove CoA esters, but not to be active on L-methylmalonyl-CoA (Kovachy et al., 1983). Thus, a proposed mechanism for the accumulation of methylmalonic acid may be that, in case of block of MUT reaction, L-methylmalonyl-CoA is first racemized to D-methylmalonyl-CoA and then hydrolyzed, or probably L-methylmalonyl-CoA is hydrolyzed by unspecific hydrolases. Therefore, methylmalonic acid accumulates in tissues and organic fluids, representing the most important biomarker of isolated MMA disorders (Villani et al., 2017). Since MUT apoenzyme is AdoCbl-dependent, deficiencies in cbl metabolism impair MUT reaction. As consequence, methylmalonic acid can be accumulated in tissues and excreted in urines and blood. Rare secondary forms of MMA may be potentially caused by a block in the reaction catalyzed by methylmalonyl-CoA epimerase, codified by the *MCEE* gene. Then, D-methylmalonyl-CoA accumulates similarly to the L-methylmalonyl-CoA and methylmalonic acid is formed as well (Dobson et al., 2006). In addition, atypical mild forms of methylmalonic acidemias with increased urinary excretion of methylmalonic acid were reported by Villani et al. (2017) as due to succinate-CoA ligase (SUCL, EC 6.2.1.5) deficiency caused by mutations in *SUCLA2* and *SUCLG1* that impair the conversion of succinyl-CoA to succinate. Deficiency of methylmalonate semialdehyde dehydrogenase (MMSDH, EC 1.2.1.27), which converts (S)-methylmalonic semialdehyde to propionyl-CoA in the final enzymatic steps of valine degradation pathway, can also lead to transient MMA. Finally, moderate levels of methylmalonic acid and traces of 2-methylcitric acid without other propionate metabolites were observed in urine from patients affected by defect of the transcobalamin receptor (TCblR/CD320).

1.1.2. Biochemical and pathophysiologic mechanisms in MMA

The first case of MMA was reported for the first time in 1968 (Lindblad et al., 1968) when a 2 years old girl was diagnosed after showing apparently not well ascribed metabolic alterations. In fact, the patient was at first uncertainly diagnosed for hyperglycinemia with acidosis or infantile lactate acidosis. After the determination of ketone bodies, lactate, pyruvate, and plasma levels and urinary excretion of methylmalonic acid, it became possible to include all these apparently non-specific alterations under the name of methylmalonic acidemia. Acidosis, hyperglycinemia, and hyperlactatemia are only few of the metabolic and biochemical alterations commonly associated with MMA. In fact, other common MMA alterations include ketosis and ketonuria, hyperuricemia, hypoglycemia, hyperglycemia, anemia and other blood cells defects like leukopenia, neutropenia, and thrombocytopenia. In addition to all the metabolic unbalances indicated above, one the most severe life-threatening events that connect MMA patients is hyperammonemia (Baumgartner et al., 2014).

Hyperammonemia, which is developed in the newborn period and that frequently worsen during episodes of metabolic decompensation, is almost present in the majority of MMA patients and, in general, a common feature of all the organic acidemias (Häberle et al., 2018). In physiological conditions, urea cycle and Krebs cycle are fundamental for the control of ammonia levels. In fact, in the urea cycle (mostly active in liver), the incorporation of ammonia into urea is carried out to lower total ammonia levels in the form of amino groups of carbamyl phosphate and aspartate, passing out through the mitochondria for the urinary excretion. In periportal hepatocytes, N-acetylglutamate synthase (NAGS; EC 2.3.1.1) catalyzes the formation of N-acetylglutamate (NAG) from glutamate and acetyl-CoA; NAG is an essential activator for the first enzyme in the urea cycle, the carbamyl phosphate synthetase 1 (CPS-1), which synthesizes carbamyl phosphate to start the cycle. Ammonia that escapes the urea cycle in periportal hepatocytes produces glutamine in pericentral hepatocytes through conjugation with glutamate, explaining the increase in glutamine levels. In addition, in physiological conditions ammonia levels are lowered through conjugation with 2-oxoglutarate in favor of glutamate formation. Then, urea cycle is connected to Krebs cycle in relation to aspartate, which is converted from oxaloacetate via transamination (Kölker et al., 2013). The acetyl-CoA is one of the main substrates necessary for NAG synthesis and is normally produced during physiological catabolism by oxidation of fatty acids, carbohydrates and amino acids. On the other hand, the acyl-CoA esters produced as consequence of the impairment of methylmalonyl-CoA pathway, such as methylmalonyl-CoA, methylmalonic acid and 2-methylcitric acid (but also including those produced in the other organic acidemias), compete with acetyl-CoA, inhibiting the activity of NAGS and, subsequently, carbamyl phosphate synthesis (Häberle et al., 2018). In MMA and PA, succinyl-CoA synthesis is impaired, and acetyl-CoA is deficient, such as the molecules produced from propionyl-CoA catabolism that are important intermediates used to replenish

Krebs cycle. By the way, as for an inhibition mechanism or for a lack in intermediates, urea and Krebs cycle cannot absolve their complete function, leading to impairment of ammonia excretion and, thus, hyperammonemia (Filipowicz et al., 2006). The major effect of hyperammonemia toxicity is evident in the brain. Brain damaging is due to multiple mechanisms, including unbalances in amino acid metabolism and in the global energy metabolism, together with an increased oxidative stress (Braissant et al., 2013; Häberle et al., 2018).

So far, hyperammonemia contributes to severe organ injury in MMA but many mechanisms of damage have been proposed. The mentioned symptoms such as retardation, epilepsy, or motor dysfunction may be linked to known structural lesions in brain, especially in the basal ganglia and the globus pallidus (Larnaout et al., 1998). Others neuroradiological findings in MMA are brain atrophy, and abnormal myelination of various degree (Deodato et al., 2006). The exact mechanism by which methylmalonic acid exerts its damaging action is not known. Certainly, the principal cause of systemic and brain damage may be ascribed to its massive accumulation with consequent impairment of energy metabolism and redox unbalance. The major effects of the metabolite on brain mitochondrial function are primarily related to the inhibition of enzymatic activities and transport systems. In addition, mitochondria are prone for the uptake and storage of this metabolite, determining an increase in its concentrations of 3- to 9-fold within the mitochondrial matrix compared to the extramitochondrial environment, causing an irreversible bioenergetic stroke due to the inhibition of the mitochondrial respiratory chain and Krebs cycle (Melo et al., 2011). Methylmalonic acid is a dicarboxylic acid considered as metabotoxin because, due to the poor dicarboxylic acid transport system of the blood-brain barrier, it is effectively entrapped within the brain, leading to severe neurotoxic effects (Ballhausen et al., 2009). Neurotoxic effects may be due to the fact that the brain mitochondrial dicarboxylate carrier works to replenish Krebs cycle intermediates and methylmalonic acid may inhibit this transport, as well as the transport of glutathione into mitochondria, impairing cellular antioxidant defense. Furthermore, methylmalonic acid may be responsible for lipid peroxidation in cerebral tissues, increasing the evidence in support of the unbalance in redox homeostasis as major actor in MMA pathogenesis (Melo et al., 2011). In general, it is becoming convincing that neurological pathogenetic effects caused in MMA may be ascribed to many factors acting together on energy metabolism for inhibition of Krebs cycle and of mitochondrial respiratory chain, oxidative stress for impairment of the antioxidant defenses and disruption of redox homeostasis, neuronal apoptosis, impairment of intracellular trafficking, alteration of cell morphology and structure by cytoskeletal proteins modification (Villani et al., 2017).

Nonetheless, in addition to the toxic effect exerted by methylmalonic acid, MMA patients are characterized by the presence of other metabolites which can significantly contribute to the damage. Elevated levels of 2-methylcitric acid, propionic acid, 3-hydroxypropionic acid, malonic acid and other

metabolites linked to methylmalonyl-CoA and propionyl-CoA pathway are often detected. Malonic acid is a competitive inhibitor of mitochondrial complex II and could explain tissue lesions observed in the disease. 2-Methylcitric acid, propionic acid and propionyl-CoA also are connected to tissue degeneration (Melo et al., 2011; Jafari et al., 2013).

Mitochondrial methylmalonic acid- and MMA metabolites-induced impairment may also be configured as the cause of renal dysfunction and kidney failure which are well-known complications of MMA, in particular for isolated MMA subtype. The histological phenotype of kidney tissues from MMA patients is abnormal with extensive interstitial fibrosis, chronic inflammation and tubular atrophy (Haijes et al., 2019). Interestingly, especially in the proximal tubules of kidney, the functional alteration of mitochondria reflects a cytochrome c oxidase deficiency and increased markers of oxidative stress and, at the same time, structural alterations leading to the formation of large, circular, pale mitochondria with diminished cristae, called megamitochondria (Zsengellér et al., 2014). Patients may develop end-stage renal failure requiring dialysis and kidney transplantation (Manoli et al., 2005). Kidney transplantation is, often, accompanied by the necessity of liver transplantation. Hepatomegaly and fibrosis/cirrhosis states are common features of MMA patients that develop hepatic long-term complications. The presence of megamitochondria with dysmorphic and shortened, or absent, cristae and a less electron-dense mitochondrial matrix was also found in hepatocytes of MMA *Mut*^{-/-} mice. As guessed, similar morphological alterations were also found to characterize the hepatocytes of a patient with isolated MMA. Even in liver context, the damage and the structural modifications were ascribed to an alteration of mitochondrial function, with decreased activity of the respiratory chain complex and reduction of the oxidation rates of the substrate used for energy production within mitochondria (Chandler et al., 2009; Haijes et al., 2019).

1.1.3. MMA diagnosis and Expanded Newborn Screening

As described, a direct block of MUT activity for direct mutations in apoenzyme gene structure, or for alterations in the biosynthetic pathway of AdoCbl, leads to the accumulation of MUT substrate, L-methylmalonyl-CoA, which is not converted in succinyl-CoA anymore. The methylmalonyl-CoA epimerase converts the L-methylmalonyl-CoA into its D-epimer, which is then processed by the D-methylmalonyl-CoA hydrolase producing methylmalonic acid and releasing CoA. Therefore, methylmalonic acid is accumulated in elevated quantity in tissues and organic fluids, representing the most important biomarker of the disease. To this aim, the diagnosis of MMA (and other related organic acidemias) can be realized by measuring the concentrations of the metabolite in urine or blood by gas chromatography-mass spectrometry (GC-MS) or liquid chromatography-tandem mass spectrometry (LC-MS/MS) technologies (Costanzo et al., 2017; Villani et al., 2017).

Inborn errors of metabolism have very serious outcomes and for most of them no resolutive therapy exists; symptoms can express immediately after the birth and, unfortunately, most of the clinical damages, like brain malformations, are irreversible; in other cases, the disorder is asymptomatic at birth. For this reason, an early and precise diagnosis of the metabolic defect has a pivotal role on the management of therapy and future lifestyle of the baby. In this context, targeted LC-MS/MS has been totally employed in the diagnostic laboratories for the identification and quantification of biomarkers for the early diagnosis of metabolic disorders. Thus, MMA, together with more than other 70 metabolic disorders, has been included in the expanded newborn screening program in Italy. In particular, collecting on a paper a drop of blood from the heel of the baby within 48-72 hours from his birth, a dried blood spot (DBS) is obtained and sent to the laboratory. Targeted LC-MS/MS analysis is able to detect more than 100 metabolites in the DBS, including specific disease-biomarkers, amino acids, amino acid ratios, acylcarnitines, acylcarnitine ratios (Scolamiero et al., 2015). Acylcarnitines are the conjugation product of a L-carnitine molecule with an acyl-CoA, after removal of CoA group, coming from the degradation of fatty acids and branched-chain amino acids. The enzymes that catalyze this conjugation reaction are called carnitine acyl-transferases. Because in their form acyl-CoA intermediate are not able to exit mitochondria due to the lack of specific transporters, carnitines have the role to transport each specific acyl-CoA across mitochondrial membrane. Thus, acylcarnitine profiling is a reflection of the intramitochondrial acyl-CoA status at a particular time. In case of metabolic disorders, the block in a catabolic pathway with accumulation in particular acyl-CoA intermediates is reflected in an accumulation of the corresponding acylcarnitine (Millington et al., 2011).

A common profile for MMA may include elevation in the levels of methylmalonic acid, propionylcarnitine (C3), methylmalonylcarnitine (C4DC) with reduction of free carnitine (C0). Because abnormal levels of C3 may be detected in several disorders, like in PA, C3 taken alone is not considered a real

diagnostic marker (la Marca et al., 2007). Also acylcarnitine ratios may be altered, like increased C3/C0 or C3/acetylcarnitine (C2). Common alterations in amino acid profiles include increased glycine and alanine levels (Deodato et al., 2006; Sloan et al., 2008; Ombrone et al., 2016).

In addition to targeted LC-MS/MS, GC-MS analysis may be employed for metabolic profiling of organic acids in urine of patients in order to quantify MMA-related urinary biomarkers or detect a specific metabolic disorder. Methylmalonic acid can reach high concentrations of 10-30 mmol/mol creatinine in the urines of patients with isolated MMA (Deodato et al., 2006). A chromatogram representative of a urinary organic acid profile from a MMA patient reveals a very large peak relative to methylmalonic acid (Figure 5, Villani et al., 2017).

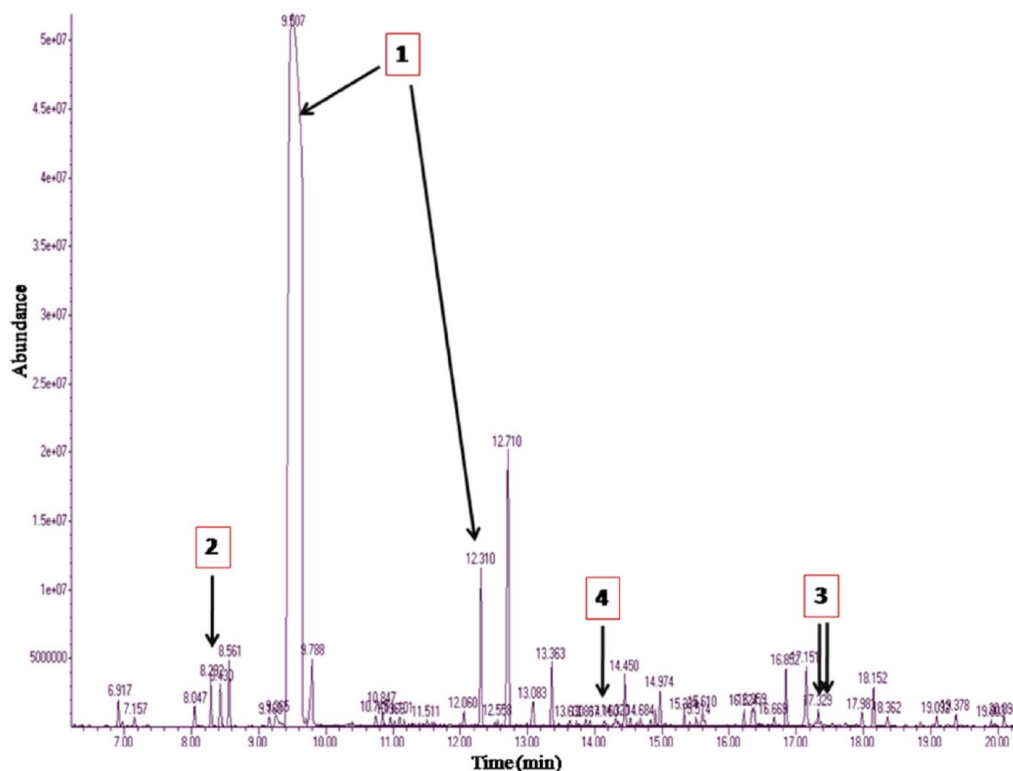


Figure 5. Chromatogram representative of an organic acids profile from the urine of a patient affected by MMA. A huge peak relative to the presence of methylmalonic acid (1) in the sample is easy detectable. Metabolite quantification is carried out by comparing the area under the curve with that of internal standards. 1 = Methylmalonic acid (RT 9.50 min: 2TMS; RT 12.31min: 3TMS), 2 = 3-hydroxypropionic acid (RT 8.29 min), 3 = 2-methylcitric acid (RT 17.32 min: 4TMS, isomer I; RT 17.38 min: 4TMS, isomer II) and 4 = tiglylglycine (RT 14.05 min: 2TMS). RT = retention time; TMS = (number of units of) trimethylsilyl derivative.

Despite methylmalonic acid represents the most important biomarker of the disease, other metabolites are detected and used for MMA diagnosis. Even in case of MMA with homocystinuria it is possible to detect increased levels of methylmalonic acid; however, for cobalamin deficiency defects the clinical picture is different and, thus, a combined set of biomarker metabolites, such as total vitamin B12, TC, MMA and homocysteine, should be considered (Green et al., 2017). The deficiency of the enzymes related to propionyl-CoA metabolism leads to a build-up of their precursors. In case of MMA, methylmalonyl-CoA and propionyl-CoA and their corresponding organic acids are accumulated and possibly detected (Villani et al., 2017; Häberle et al., 2018). In addition, secondary metabolites of the propionic acid, namely 3-hydroxypropionic acid, 2-methylcitric acid, and tiglylglycine are produced from secondary pathways and frequently detected at abnormal levels (Figure 5).

Generally, the interpretation of the metabolic profile obtained by MS analysis and its correlation with the disease-specific metabolic fingerprint allow the early diagnosis. Several different metabolic disorders can be detected on a single DBS collected in the first hours from birth or urine samples, without any painful or invasive procedure for the newborn. For these reasons, the employment of the expanded newborn screening is able to decrease early mortality by rapid intervention on patients carried out by pediatricians that are allowed to start appropriate therapeutic approaches before the irreversible and severe worsening of symptoms and complications for the patients.

1.1.4. Results of the research group on MMA

In the context of the rare metabolic diseases, the laboratory of expanded newborn screening, directed by Prof. Margherita Ruoppolo, has diagnosed from 2007 to 2018 around 50 newborns affected by a metabolic disorder in Campania region. Of these, twenty newborns were diagnosed of organic acidemias, of which 3 cases of isolated MMA and 6 cases of MMA with homocystinuria.

Additionally, two previous projects of the research group relative to the study of molecular alterations in MMA were published by Caterino et al. in 2015 and 2016. The first study (Caterino et al., 2015) was conducted to study proteome alteration in MMA with homocystinuria cblC type patients, the most common inborn error of cobalamin metabolism. The proteome of control and MMACHC lymphocytes obtained from patients was quantitatively analyzed by two dimensional-differential in-gel electrophoresis (2D-DIGE) technology. From this study, MS analysis detected 23 up-regulated and 38 down-regulated proteins in MMACHC lymphocytes. The altered pathways were ascribed to proteins involved in energy metabolism, oxidative stress and cellular detoxification, trafficking and protein folding, and cytoskeleton organization and assembly. The second study (Caterino et al., 2016) was a proteomic investigation performed on liver samples obtained from patients with isolated MMA undergone liver transplantation. Proteomic analysis was carried out by

2D-DIGE, in order to investigate the alterations in the liver proteome correlated to altered hepatic metabolism in patients. From proteomic results mitochondrial alterations were clearly evident. The alterations described in this study highlighted that MUT absence or diminished expression is able to induce differential regulation of proteins involved in energy metabolism, gluconeogenesis and Krebs cycle anaplerosis. Furthermore, the pattern of proteome changes is suggestive of an attempt from liver of MMA patients toward a process of metabolic adaptation, as a probable compensation rearrangement for mitochondrial dysfunction derived from MUT deficiency.

2. AIM

The present PhD research project was developed to study molecular alterations and impaired pathways in suitable cellular models for isolated MMA in order to elucidate the molecular basis that underlies the mechanism of damage induced by the metabolic disorder. The molecular mechanisms and protein actors involved in this context are not completely known and, in addition, several processes are supposed to contribute in the enhancement of the metabolic complications. Therefore, the main purpose of this PhD project aimed at developing cell systems that recapitulated the molecular alterations of MMA.

The first cell model generated reflected the alterations induced by a knockdown of *MUT* gene expression via siRNA-mediated RNA interference. Subsequently, in order to better characterize the effects coming from *MUT* deficiency, it became necessary to establish a stable cell line in which *MUT* gene was knocked out employing CRISPR/Cas9 genome editing technology.

In addition, a cell model of *MUT*-rescued expression was created to control that the specificity of the effects and alterations shown were effectively induced by and linked to *MUT* knockout.

Different proteomics experiments were conducted with different label-free quantitative proteomics methodologies in order to determine quantitative changes in protein expression profiles within cell models comparison. Complementation of bioinformatics analysis with functional assays will be helpful in determining the protein classes that deserve to be further investigated with a view of future application for targeted therapies to be translated in patients.

Finally, experiments of interactomics of the MMACHC protein were performed in order to elucidate the role of this protein in the formation of cobalamin cofactors, biologically relevant for many cellular processes.

3. MATERIALS AND METHODS

3.1. Cell cultures and treatments

SH-SH5Y cells (human bone marrow neuroblastoma; ATCC no. CRL-2266) were cultured in Dulbecco's Modified Eagle Medium (DMEM) (Sigma-Aldrich, St. Louis, MO, USA) supplemented with 15% fetal bovine serum (FBS) (Gibco/Life Technologies, Rockville, MA, USA) and 2 mM L-Glutamine (EuroClone, Paington, UK) at 37°C in 5% CO₂ atmosphere.

HEK293 cells (human embryonic kidney, ATCC no. CRL-1573) were cultured with High Glucose Dulbecco's Modified Eagle Medium (DMEM) (EuroClone, Paington, UK) supplemented with 15% FBS (EuroClone, Paington, UK), 4 mM L-Glutamine (Sigma-Aldrich, St. Louis, MO, USA), 1% penicillin-streptomycin solution (Sigma-Aldrich, St. Louis, MO, USA) at 37°C in 5% CO₂ atmosphere.

HepG2 cells (human hepatocellular carcinoma, ATCC no. HB-8065) were cultured with RPMI 1640 medium (EuroClone, Paington, UK) supplemented with 20% fetal bovine serum (FBS) (EuroClone, Paington, UK), 2 mM glutamine (Sigma-Aldrich, St. Louis, MO, USA), 1% penicillin-streptomycin solution (Sigma-Aldrich, St. Louis, MO, USA) at 37°C in 5% CO₂ atmosphere.

For treatments of cells with propionate-enriched culture medium, the normal medium used for each cell line was supplemented with sodium propionate (Sigma Aldrich, St. Louis, MO, USA) at the desired concentration.

3.2. Cell transfections

3.2.1. siRNA for MUT silencing in SH-SH5Y cell line

SH-SH5Y cells were kept in culture and 24 h before MUT siRNA transfection 4.2×10^2 cells/mm² were seeded into 60 mm-diameter plates. Transfections of small interfering RNA (siRNA) were carried out with 100 pmol/mL MUT siRNA (sc-95089, Santa Cruz Biotechnology, Dallas, TX, USA) added to 0.05 µL/pmol siRNA of Lipofectamine® 2000 Reagent (Thermo Fisher, Waltham, MA, USA). Lipofectamine-siRNA complexes were added to the medium and incubated for 5 h. After the incubation, fresh medium replaced culture medium with siRNAs. In parallel, the cells used as negative control were transfected with a scramble siRNA (sc-37007, Santa Cruz Biotechnology, Dallas, TX, USA) known to have no targets into the cells, following the same protocol used for MUT siRNA. Two time points (24 and 48 h) were chosen for the collection of the transfected cells. In addition, other cells were not transfected and used as an additional control (0 h time point). Each time point experiment was carried out in three independent plates replicates. Western blot (WB) was used to reveal the levels of MUT protein knockdown at tested time points. The

48 hours-time points were chosen for all the following experiments and samples were named as siRNA_MUT and scramble.

3.2.2. CRISPR/Cas9-MUT KO HEK293 cell line generation

Before the application of CRISPR/Cas9 technology for MUT knockout in HEK293 cell line, 1.5×10^3 cells/mm² of wild type (WT) HEK 293 cells were cultured in a 10 cm diameter plate in medium without antibiotics. After 24 hours, cells were transfected with 12 µg of “MUT CRISPR/Cas9 KO Plasmid (h2)” (Santa Cruz Biotechnology, Dallas, TX, US) and 12 µg of “MUT HDR Plasmid (h2)” (Santa Cruz Biotechnology, Dallas, TX, USA), using Lipofectamine® 2000 Reagent (Thermo Fisher Scientific, Waltham, MA, USA) following the supplier instructions. After 48 hours from the transfection, the culture medium was replaced with selective medium containing 1 µg/mL puromycin (Santa Cruz Biotechnology, Dallas, TX, USA). The pool of transfected cells (MUT-KO pool) was kept in culture in selective medium for 4 days, with proper phosphate buffered saline (PBS) washes and medium changes, in order to eliminate detached cells and select adherent puromycin-resistant cells. Then, the cells of MUT-KO pool were detached from the plate and properly diluted in a 10 cm diameter plate with selective medium, and seeded in order to have few isolated cells able to form distinct colonies each constituted by a single cell clone (MUT-KO clone). After that, the generated colonies were detached and kept in separate cultures. MUT-KO pool and clones (MUT-KO clone 1 and clone 2) protein lysates were then analyzed by Western blot (WB) to test the absence of MUT protein. MUT-KO clone 2 was then chosen and employed in all the following experiments and simply indicated as MUT-KO. In addition, qRT-PCR was performed to analyze the levels of MUT RNA in the tested cells.

3.2.3. MUT-FLAG expression for MUT rescuing in MUT-KO

HEK293 cells engineered with CRISPR/Cas9 system (MUT-KO) were transfected in order to rescue MUT protein and stably ensure its expression. In detail, 1.5×10^3 cells/mm² of MUT-KO clone 2 cells were cultured in a 10 cm diameter plate in medium without antibiotics. After 24 hours, cells were transfected with 24 µg of “pCMV3-FLAG-MUT” plasmid (Sino Biological, Beijing, China). 48 hours after the transfection, the culture medium was replaced with selective medium containing 1 µg/mL puromycin and 150 µg/mL hygromycin. The transfected cells for MUT rescuing were kept in culture in selective medium; a pool of stably transfected (hygromycin-resistant) cells (MUT-Rescue pool) and distinct single cell clones (MUT-Rescue clone 1, clone 2 and clone 3) were obtained as described for MUT-KO (*Materials and Methods*, 3.2.2). MUT-Rescue pool and MUT-Rescue clones protein lysates were then analyzed by WB to test the signals of recombinant MUT-FLAG protein. MUT-

Rescue clone 2 was then chosen and employed in all the following experiments and simply indicated as MUT-Rescue.

3.2.4. MMACHC-FLAG expression in HepG2 cell line

For the stable expression of recombinant MMACHC-FLAG and GFP-FLAG, the coding sequences of MMACHC and GFP were cloned into a pcDNA3-CT10HF-LIC plasmid (Heuberger et al., 2019). In detail, 1.5×10^3 cells/mm² of HepG2 cells were seeded in a 10 cm diameter plate and kept in culture in medium without antibiotics. After 24 hours, cells were transfected with 24 µg of the MMACHC-FLAG or GFP-FLAG constructs, respectively. After 48 hours from the transfection, the culture medium was replaced with selective medium containing 400 µg/mL hygromycin (Sigma-Aldrich, St. Louis, MO, USA). The transfected cell pools were kept in culture in selective medium for 7 days, with proper PBS washes and medium changes, in order to eliminate detached cells and select adherent hygromycin-resistant cells. Then, the cells were detached from the plate, properly diluted and seeded again in a 10 cm diameter plate with selective medium, in order to have few isolated cells able to form distinct colonies each constituted by a single cell clone. The colonies were detached and kept in culture separately and, then, tested by WB to verify the presence of recombinant MMACHC-FLAG and GFP-FLAG protein expression.

3.3. Cell viability and apoptosis assays

3.3.1. Apoptosis by Flow Cytometry

Apoptosis was tested in MUT-silenced and control SH-SY5Y cells by flow cytometry. MUT siRNA- and scramble-transfected cells were pelleted and resuspended in 100 µL 1X Binding Buffer solution (0.1 M HEPES pH = 7.4, 1.4 M NaCl, 25 mM CaCl₂) containing 5 µL fluorescein isothiocyanate (FITC)-conjugated Annexin V (BD Biosciences, San Jose, CA, USA) and 5 µL propidium iodide (PI) (Sigma Aldrich, St. Louis, MO, USA) for 15 min at room temperature in the dark. Then, 400 µL of 1X Binding Buffer was added to each sample and the cells were analyzed using a FACSCanto II flow cytometer (BD Biosciences, San Jose, CA, USA). The cells with high Annexin V and low PI signals were considered to be in the early stages of the apoptotic process. The cells with both high Annexin and PI signals were considered to be in late apoptosis or necrosis. Cell transfections and subsequent flow cytometric analyses were performed in three independent replicates.

3.3.2. MTT and Neutral-Red assay

Both MTT and Neutral-Red assays were employed to test cell viability of SH-SY5Y siRNA_MUT and HEK293 MUT-KO and MUT-Rescue cells and performed in all the experiments with same procedures. Before each experiment, cells were washed with phosphate buffered saline (PBS) (EuroClone, Paington, UK), and the culture medium replaced with a fresh medium containing 0.5 $\mu\text{g}/\mu\text{L}$ MTT or 0.33 $\mu\text{g}/\mu\text{L}$ Neutral-Red reagents (both Sigma-Aldrich, St. Louis, MO, USA). The incubation time was 2 h at 37°C and then PBS washing followed to completely remove the reagents. Subsequently, in the case of MTT assay, a solution of 1 N HCl-isopropanol (1:24, v:v) was added to dissolve the dark-blue formazan crystals formed. After a few minutes of gentle agitation on a rocking platform at room temperature, the assay was completed by reading the absorbance of the samples at 570 nm in a Perkin Elmer Enspire plate reader (Perkin Elmer, Waltham, MA, USA). For the Neutral-Red assay, a solution of acetic acid–water–ethanol (1:49:49, v:v:v) was added to solubilize the dye and, after a few minutes of gentle agitation on a rocking platform at room temperature, absorbances of the samples were read at 540 nm in the same plate reader.

3.4. ROS detection

Reactive Oxygen Species (ROS) levels were measured in HEK293 MUT-KO and MUT-Rescue cells; WT cells were used as control. In particular, 2×10^3 cells/ mm^2 were cultured in a 24-wells plate. After 24 hours, cells were washed two times with Hank's balanced saline solution (HBSS) (EuroClone, Paington, UK) and 10 μM 2',7'-dichlorofluorescein diacetate (H₂DCFDA) (Sigma-Aldrich, St. Louis, MO, USA) in HBSS was added to the cells for 1-hour incubation at 37°C in 5% CO₂ atmosphere. Subsequently, the H₂DCFDA solution was removed and cells washed twice with HBSS. Part of the samples were incubated for one additional hour in HBSS with 100 μM H₂O₂, in order to stress the cells by over-production of ROS, and then washed twice with HBSS. Native and H₂O₂-treated cells were collected and lysed with RIPA buffer (Sigma-Aldrich, St. Louis, MO, USA) supplemented with protease inhibitors (Thermo Fisher Scientific, Waltham, MA, USA). Cell extracts were centrifuged at 15000 g for 10 minutes at 4°C and supernatants collected in a 96-wells black plate. Fluorescence was read in a Perkin Elmer Enspire plate reader (Perkin Elmer, Waltham, MA, USA) using 485 nm and 527 nm as excitation and emission wavelengths, respectively. Protein concentration in the supernatants was measured by Bradford assay and used to normalize the fluorescence levels.

3.5. WGA staining

In order to carry out an analysis of plasmatic membrane proteoglycans, a staining of HEK293 MUT-KO and MUT-Rescue cells (WT used as control) was performed with wheat germ agglutinin (WGA) labelled with Oregon Green 488 (excitation maximum at 496 nm; emission maximum at 524 nm) (Thermo Fisher Scientific, Waltham, MA, USA). Before the staining, 1.5×10^3 cells/mm² were seeded in a 24-wells plate. After 24 hours and two washings with PBS, cells were fixed for 5 minutes in a solution with 4% (w/v) paraformaldehyde (Sigma-Aldrich, St. Louis, MO, USA) in PBS. The cells were then washed twice with PBS and incubated in PBS containing 5.0 µg/mL WGA for 10 minutes. Cells were again washed twice and incubated with a solution 300 nM DAPI (Thermo Fisher Scientific, Waltham, MA, USA) in PBS for 5 minutes. After two washings, cells were covered with a solution containing Prolong Gold antifade reagent 50% (v/v) in PBS and observed with a Leica DMI 4000 B inverted microscope, equipped with Leica GFP (bandpass: 470±40 nm excitation; 525±50 nm suppression) and DAPI (bandpass: 420±30 nm excitation; 465±20 nm suppression) filter cubes, using a 20X objective. Experiments were performed in three independent biological replicates and four microscope fields were acquired from each replicate using the Leica LAS AF software. The values of Oregon Green 488 were normalized with those of DAPI. ImageJ (Image J, NIH, USA) software was employed to perform quantitative analysis of fluorescent signals.

3.6. Proteomics

3.6.1. Global proteomic analysis for SH-SY5Y siRNA_MUT cells

3.6.1.1. Sample preparation

For the proteomic preparation of SH-SY5Y, siRNA_MUT and scramble cells were lysed in lysis buffer (40 mM Tris pH = 8.6, 7 M urea, 2 M thiourea, 4% CHAPS) supplemented with protease inhibitor cocktail (Roche, Indianapolis, IN, USA). Cellular lysates were sonicated and then centrifuged at 15000 g for 30 min at 4 °C. Supernatant (proteins) was collected and protein concentration determined by Bradford assay. Then, as described by Costanzo et al. (2018), 100 µg of each protein sample were fractionated on a preparative 16 x 20 cm gel by sodium dodecyl sulfate - polyacrylamide gel electrophoresis (SDS-PAGE). The resulting gel was stained using Gel Code Blue Stain Reagent (Thermo Fisher Scientific, Waltham, MA, USA) and each lane of the gel was cut into 40 slices. In order to obtain peptide mixtures, a *in situ* hydrolysis followed for each gel slice: each sample underwent reduction of disulfide bonds (10 mM DTT, 1 h, 37 °C), alkylation (20 mM IAA, 30 min, in the dark, RT) and in-gel digestion using Trypsin, Proteomics Grade (Sigma-Aldrich, St. Louis,

MO, USA) in the ratio enzyme:substrate 1:10 (O/N, 37 °C). Peptide mixtures were analyzed by liquid chromatography – tandem mass spectrometry (LC-MS/MS).

3.6.1.2. *LC-MS/MS analysis*

Digested peptides were resuspended in 0.2% formic acid (FA) and loaded on a EASY-nLC II chromatographic system coupled with a LTQ-Orbitrap XL (both Thermo Scientific, Bremen, Germany). Samples were concentrated and desalted onto a 2 cm trapping column (C18, ID 100 μ m, 5 μ m) and then fractionated onto 20 cm C18 reverse phase silica capillary column (ID 75 μ m, 5 μ m) (Nanoseparations). Peptides were eluted by a nonlinear gradient with buffer A (0.1% FA) and B (80% acetonitrile (ACN), 0.08% FA) at flow rate of 250 nL/min: 4% B for 5 min, from 4 to 40% B in 45 min, and from 40 to 90% B in 1 min. The LTQ-Orbitrap XL operated in data-dependent acquisition (DDA) mode, MS resolution was set to 30000 and mass range of scans from m/z 400 to 1800. Collision Induced Dissociation (CID) energy was used to fragment the three most intense doubly, triply, and fourthly charged ions.

3.6.1.3. *Spectral counts-based proteomics*

Proteomic identifications were obtained using Proteome Discoverer™ platform (version 1.3.0.339; Thermo Scientific, Bremen, Germany), interfaced with an in-house Mascot server (version 2.3, Matrix Science, London, UK), set as: min precursor mass 350 Da, max. precursor mass 5000 Da, minimum peak count 1; protein database SwissProt, enzyme trypsin, maximum missed cleavage sites 2, instrument ESI-FTICR, taxonomy Homo sapiens; precursor mass tolerance 5 ppm, fragment mass tolerance 0.8 Da. Methionine oxidation, N-terminal glutamine cyclization to pyroglutamic acid and N-terminal protein acetylation were set as dynamic modifications; cysteine carbamidomethylation was set as static modification. After quantitative analysis, only proteins identified with at least 3 peptides were included in the final list.

The spectral counts (SpC) approach (De Pasquale et al., 2020; Costanzo et al., 2018; Old et al., 2005) was used as label-free quantification strategy, employing two related quantitative indices, R_{SC} and $Fold_{NSAF}$.

Fold changes of protein abundances were expressed as R_{SC} (log ratio of abundance between scramble and siRNA_MUT) according to the formula:

$$R_{SC} = \log_2 [(n2 + f)/(n1 + f)] + \log_2 [(t1 - n1 + f)/(t2 - n2 + f)]$$

$n1$ and $n2$ are the SpCs (peptide-to-spectrum matches, PSMs) for the given protein in sample groups 1 and 2, respectively; $t1$ and $t2$ are the total numbers of

spectra in each group, respectively; f is a correction factor set to 0.5 and used to eliminate discontinuity due to $SpC = 0$.

In addition, the normalized spectral abundance factor (NSAF) was calculated for each protein as spectral abundance factor (SAF), namely the spectral counts (PSMs) divided by protein length (number of amino acids), normalized to the sum of all SAFs detected within the same gel lane. Then, fold changes of protein abundances were expressed in the \log_2 form as $Fold_{NSAF}$ that is the ratio of NSAFs of siRNA MUT and scramble.

Protein regulation was reported if proteins showed at the same time $R_{SC} > +3.5$ and $Fold_{NSAF} > +3.5$ (up-regulation) or $R_{SC} < -3.5$ and $Fold_{NSAF} < -3.5$ (down-regulation).

3.6.2. Global proteomic analysis for HEK293 MUT-KO cells

3.6.2.1. Sample preparation

The sample preparation adopted for the proteomic experiment of MUT-KO vs HEK293 WT cells started with lysis of samples in RIPA buffer (Sigma-Aldrich, St. Louis, MO, USA) supplemented with protease inhibitor cocktail (Roche, Indianapolis, IN, USA). Lysates were centrifuged at 15000 g for 30 min at 4°C. Supernatants were collected and protein concentrations determined using Bio-Rad Protein Assay Dye Reagent Concentrate (Hercules, CA, USA). For each sample, the volume corresponding to 50 μ g of protein was reduced with TCEP (Sigma-Aldrich, St. Louis, MO, USA) for 10 min and subsequently carbamidomethylated with iodoacetamide (Sigma-Aldrich, St. Louis, MO, USA) for 30 min in the dark. Protein digestion was then performed using Sequencing Grade Modified Trypsin (Promega, Madison, WI, USA), in the ratio enzyme:substrate 1:20, on S-Trap (ProtiFi, Huntington, USA) micro spin columns, following manufacturer's instruction. Digested peptides were eluted from the S-Trap columns, vacuum dried and kept at -80 °C until analysis.

3.6.2.2. LC-MS/MS analysis

Samples were resuspended in 100 μ L of 10% ACN, 0.1% trifluoroacetic acid (TFA) in HPLC-grade water. For each run, 1 μ L was injected in a nanoRSLC-Q Exactive PLUS (RSLC Ultimate 3000) (Thermo Scientific, Waltham, MA, USA). Peptides were loaded onto a μ -precolumn (Acclaim PepMap 100 C18, cartridge, 300 μ m i.d. \times 5 mm, 5 μ m) (Thermo Scientific), and were separated on a 50 cm reversed-phase liquid chromatographic column (0.075 mm ID, Acclaim PepMap 100, C18, 2 μ m) (Thermo Scientific). Chromatography solvents were: A) 0.1% FA in water; B) 80% ACN, 0.08% FA. Peptides were eluted from the column with the following gradient 5% to 40% B (180 minutes), 40% to 80% (1 minutes). At 181 minutes, the gradient stayed at

80% for 5 minutes and, at 187 minutes, it returned to 5% to re-equilibrate the column for 20 minutes before the next injection. One blank was run between each series to prevent sample carryover. Peptides eluting from the column were analyzed by DDA MS/MS, using top 10 acquisition method. Peptides were fragmented using higher-energy collisional dissociation (HCD). Briefly, the instrument settings were as follows: resolution was set to 70,000 for MS scans and 17,500 for the MS/MS scans in order to increase speed. The MS automatic gain control (AGC) target was set to 3×10^6 counts with maximum injection time set to 60 ms, while MS/MS AGC target was set to 1×10^5 with maximum injection time set to 60 ms. The MS scan range was from 400 to 2000 m/z. Dynamic exclusion was set to 30 seconds duration. The analysis included 4 independent biological replicates per condition, each run in technical triplicates.

3.6.2.3. *LFQ-based proteomics*

Raw MS data were processed using MaxQuant software version 1.5.8.3 for the identification and label-free quantification (LFQ) of the proteins. Andromeda was used as engine for the search against the human SwissProt Database (UniProt Release 07/2017). The specific parameters for the group were set as follows: carbamidomethylation of the cysteines as “fixed modifications”; oxidation of the methionine and N-terminal protein acetylation as “variable modifications”. Parameters for the *in silico* digestion of protein sequences were set selecting minimum peptide length as 7 amino acids, Trypsin as specific proteolytic enzyme and allowing up to two missed cleavages. In the global parameters, the false discovery rate (FDR) for the identification both at the peptide spectrum match level and at the protein level (both determined by the target-decoy approach) was set at 1%. Unique and razor peptides were used for the quantification of proteins. The “match between runs” option has been checked besides the advanced identification tools. All the other parameters were used as in the default settings of MaxQuant. The table (.txt) for “proteinGroups” exported from MaxQuant was loaded in the starting matrix in the Perseus software (version 1.6.0.7). Protein groups were filtered out for reverse hits, contaminants and hits that are only identified by site. Experimental conditions were created comparing MUT-KO vs WT samples. The obtained matrix was further reduced by excluding proteins with any missing value (100% of valid values). The \log_2 function was used to transform all the intensities. Finally, two sample t-test was used to point out the significative differences between intensities referring to the expression level of the same protein in the two different experimental conditions; values setting: FDR = 0.01; $s_0 = 0.9$. Alterations of the MUT-deficient proteome were clustered and visualized as a volcano plot that shows in detail the distribution of some proteins whose regulation was validated. The mass spectrometry proteomics data have been deposited to the ProteomeXchange Consortium via the PRIDE Partner repository with the dataset identifier PXD017977.

3.6.3. Global proteomic analysis for HEK293 MUT-KO and MUT-Rescue cells

3.6.3.1. Sample preparation

HEK293 cells (WT, MUT-KO, MUT-Rescue) for data-independent acquisition (DIA) proteomics analysis were lysed with 1% SDS buffer containing 50 mM Tris-Cl pH = 7.8, 150 mM NaCl, with complete mini protease inhibitors (Roche, Indianapolis, IN, USA). To degrade all nucleic acids (DNA and RNA), lysates were incubated at 37°C for 30 min with benzonase enzyme (Sigma-Aldrich, St. Louis, MO, USA) plus 2 mM MgCl₂. Next, cell lysates were centrifuged at 18000 g at room temperature (RT) for 30 min. The clear supernatant was collected and used for determining protein concentration with BCA assay as per manufacturer's instructions. Aliquots corresponding to 50 µg of protein of each sample were subjected to reduction of disulfide bonds with 10 mM DTT (30 min, 56 °C) followed by alkylation (carbamidomethylation) of free thiol groups with 30 mM IAA (30 min, in the dark, RT). Sample cleaning and proteolysis were performed using the filter aided sample preparation (FASP) protocol (Manza et al., 2005; Wisniewski et al., 2009) with minor changes. 100 µL of digestion buffer comprising Sequencing Grade Modified Trypsin (Promega, Madison, WI, USA) in the ratio enzyme:substrate 1:20, 0.2 M GuHCl, 2 mM CaCl₂ in 50 mM NH₄HCO₃ buffer, pH = 7.8 were added to the devices and incubated at 37°C for 14 h. Finally, peptides were acidified to pH < 3 with 10% TFA and digests were desalted with C18 solid phase extraction cartridges (SPEC; 4 mg, Varian) according to the manufacturer's instructions. After desalting, dried peptides were resolubilized in 0.1% TFA and quality controlled on a Monolithic-HPLC as described (Burkhart et al., 2012).

Peptide quantification was performed by amino acid analysis (AAA), as previously described by Cohen et al. (1993) and Shindo et al. (1997). A "master mix" was generated by combining 1 µg of peptides (based on AAA) from each HEK293 cell line and their corresponding replicates (N = 15) resulting in 15 µg of pooled sample. The peptide "master mix" was dried in a SpeedVac, resolubilized in 10 mM ammonium formate, pH 8.0 and fractionated by high-pH reversed-phase chromatography at pH 8.0 on a Biobasic (C18, 0.5 x 150 mm, 5 µm particle size) column using an UltiMate 3000 LC system (both Thermo Scientific, Bremen, Germany) with buffer A: 10 mM ammonium formate, pH 8.0, and B: 84% ACN in 10 mM ammonium formate, pH 8.0. Peptides were loaded onto the column with buffer A at a flowrate of 12.5 µL/min and separation was carried out using the following gradient: 3% B for 10 min, 3-38% B in 55 min, 38-95% B in 5 min, 95% B hold for 5 min, 95%-3% B in 5 min and finally re-equilibrate the column with 3% B for 20 min. In total 16 fractions were collected at 1 min intervals from min 5 to 70 in a concatenation mode. Finally, all the fractions were completely dried in a SpeedVac and stored at -40°C until further use.

3.6.3.2. *LC-MS/MS analysis*

Each fraction, resolubilized in 15 μL of 0.1% TFA containing 1.5 μL of diluted iRT standard, was analyzed by nano-LC-MS/MS using an Ultimate 3000 nano RSLC system coupled to a Q Exactive HF mass spectrometer (both Thermo Scientific, Bremen, Germany). Peptides were preconcentrated on a 100 μm x 2 cm C18 trapping column for 5 min using 0.1% TFA with a flow rate of 20 $\mu\text{L}/\text{min}$ followed by separation on a 75 μm x 50 cm C18 main column (both Acclaim Pepmap nanoviper, Thermo Scientific, Bremen, Germany) with a 120 min LC gradient ranging from 3-35% of B (84% ACN in 0.1% FA) at a flow rate of 250 nL/min. The Q Exactive HF was operated in data-dependent acquisition mode and MS survey scans were acquired from m/z 300 to 1500 at a resolution of 60000 using the polysiloxane ion at m/z 371.1012 as lock mass (Olsen et al., 2005). The fifteen most intense ions were isolated with a 1.2 m/z window and fragmented by HCD with a normalized collision energy (NCE) of 27%, taking into account a dynamic exclusion of 20 s. MS/MS were acquired at a resolution of 15000. AGC target values and maximum fill times were set to 3×10^6 and 120 ms for MS and 5×10^4 and 200 ms for MS/MS, respectively.

3.6.3.3. *DIA-based proteomics*

Peptides corresponding to 0.5 μg (based on AAA) of each sample containing 1.5 μL of diluted iRT standard were analyzed using DIA method. These measurements were performed directly after the DDA runs on the same set of LC-MS instruments as above and using an identical HPLC separation time as well as the gradient. All 15 samples were analyzed in a randomized order in order to minimize systematic errors and, additionally, to check for any carryover; dedicated blank measurements were performed in between samples. Furthermore, prior starting DIA runs of real samples, a quick DIA run was performed (called "scouting method") in order to (i) determine m/z scan range, (ii) assess the number of data points per peak, and (iii) calculate number of DIA segments (Bruderer et al., 2017). Based on the information from the scouting measurement, the Q Exactive HF was operated in DIA mode and MS survey scans were acquired from m/z 300 to 1201 at a resolution of 60000. The AGC target and maximum fill time values were set to 3×10^6 and 20 ms, respectively. For DIA, the settings were: resolution 30000; AGC target value 3×10^6 ; isolation window 43.9 m/z; DIA segments 21, with each isolation width overlapping 1.0 m/z; HCD NCE: 27% and the maximum fill time was set to auto. Both full MS and DIA data were acquired in profile mode.

The acquired DDA MS data of all 16 fractions were processed together with PD version 1.4 (Thermo Scientific, Bremen, Germany) software. Database searches were performed against the human UniProt database, downloaded on 23rd of July 2018, containing 20734 target sequences including iRT sequence (Escher et al., 2012), using Mascot (Perkins et al., 1999) and Sequest (Eng et al.,

1994) algorithms. The search parameters were identical for both algorithms i.e. precursor and fragment ion tolerances of 10 ppm and 0.02 Da for MS and MS/MS, respectively; trypsin as enzyme with a maximum of 2 missed cleavages; carbamidomethylation of cysteine as fixed modification and oxidation of methionine as variable modification. The data analysis of all DIA runs including the “scouting method” measurement was performed with Spectronaut Pulsar software (version 12.0.20491.8.23937). To generate the spectral library, the same human UniProt database and the .msf PD 1.4 output file (as mentioned above) were uploaded in the Spectronaut software as per the recommended settings including 1% false discovery rate and search engine rank 1 on the peptide to spectrum match level (from PD). Next, all DIA raw files were processed using the Spectronaut default settings i.e. MS and MS/MS filtering, extracted ion chromatogram (XIC) extraction, calibration and identification. The settings under quantification were also set to default except with minor changes. The Min and Max values of Major Group Top N values were set to 2 and 4, respectively; Proteotypicity Filter was set to Only Proteotypic; Data Filtering was set to Qvalue (type Qvalue sparse), Cross Run Normalization set as True, Normalization Strategy was set as Global Normalization and Normalize on set to Median. Lastly, the protein group (PG) identifications with their respective abundance (PG.Quantity) values, PG.Qvalue, PG. Nr Of Modified Sequences Identified, PG. Nr Of Modified Sequences Used For Quantification were exported from Spectronaut for further data analysis. The \log_2 ratio of protein abundances was calculated for the compared conditions. Protein regulation was considered true if \log_2 value for a given protein was higher than 2-fold total standard deviation (calculated on the total list of \log_2 values of the considered ratio) and t-test ≤ 0.05 between replicates.

3.7. Metabolomics

3.7.1. Sample preparation and targeted LC-MS/MS

Metabolites from HEK293 cells, in particular methylmalonic acid and propionylcarnitine, were measured by targeted LC-MS/MS by multiple reaction monitoring (Ruoppolo et al., 2018; Scolamiero et al., 2015; la Marca et al., 2007). Briefly, the cells were lysed in 500 μ L of cold methanol. A centrifugation was performed at 14000 g for 20 minutes at 4°C to separate and collect the supernatant from proteins and cell debris. The supernatant was used for the detection of methylmalonic acid and propionylcarnitine. Protein pellet was resuspended in RIPA buffer (Sigma-Aldrich, St. Louis, MO, USA) and protein concentration determined using Bio-Rad Protein Assay Dye Reagent Concentrate (Hercules, CA, USA). The instrumentation employed to analyze metabolites was a API 4000 triple quadrupole mass spectrometer (Applied Biosystems-Sciex, Toronto, CA) coupled to a 1100 series Agilent high-performance liquid chromatograph (Agilent Technologies, Waldbronn,

Germany). Metabolites concentrations for each sample were normalized to the respective protein concentration and, finally, expressed as $\mu\text{M}/\mu\text{g}$ protein. Data were analyzed using GraphPad Prism version 7.0a. Statistical analysis was performed by paired t-test using a total of 9 replicates per condition.

3.8. Bioinformatics

For the bioinformatic analysis of proteomics datasets, different bioinformatic tools and databases were employed.

The PANTHER (Protein Analysis Through Evolutionary Relationship) database (<http://www.pantherdb.org>) (Mi et al., 2013) was used to cluster the regulated proteome of siRNA_MUT cells according to Molecular Function and Biological Process Gene Ontology (GO) terms. For both terms, a double-level analysis was performed investigating the “catalytic activity” and “metabolic process” subcategories, respectively.

MUT-KO proteome was analyzed using Cytoscape software (version 3.6.1) (Shannon et al., 2003) with employment of the STRING app and the ClueGO plugin. The STRING app allowed the construction of a graph in which the connected nodes represent interaction partners; the design of the nodes and edges was custom, with respect of the quantitative values of proteins provided from the proteomic analysis. The statistical test used for enrichment/depletion of GO categories provided within the ClueGO plugin was a two-sided hypergeometric test with Bonferroni step down as correction method. A single cluster analysis was performed setting a Kappa Score Threshold = 0.4, including in the resulting cluster terms with minimum number of genes = 3 and percentage of associated genes = 4.0. A final group size of 12 ‘true’ terms, according Over View Term column, was created.

The STRING (Search Tool for the Retrieval of Interacting genes) version 11 (Caterino et al., 2017; Szklarczyk et al., 2019) was used for the generation of the interacting network of mitochondrial proteins. A minimum of required interaction score of 0.150 (low confidence) was set.

3.9. Western blotting

All Western Blot (WB) analysis performed for this thesis underwent the same procedure. Protein lysates from cells were obtained from lysis in RIPA buffer (Sigma-Aldrich, St. Louis, MO, USA) and centrifugation at 14000 g for 30 minutes at 4°C to collect the protein supernatant. For urine proteins, urine samples were centrifuged in centrifugal filters Amicon Ultra-15 3k (Millipore, Burlington, Massachusetts, USA). Concentrated samples were further concentrated using centrifugal filters Amicon Ultra-0.5 3k (Millipore, Burlington, Massachusetts, USA) and stored at – 20 °C. Protein extracts were fractionated by 10% SDS-PAGE, and transferred onto nitrocellulose membranes

using Trans-Blot Turbo Transfer System (Bio-Rad, Hercules, CA, USA). Membranes were blocked for 3 h at room temperature with 5% milk in PBS with 0.05% Tween-20. Each primary antibody used for WB against MUT (sc-136541, Santa Cruz Biotechnology, Dallas, TX, USA), FLAG (F1804, Sigma-Aldrich, St. Louis, MO, USA), vimentin (sc-373717, Santa Cruz Biotechnology), exostosin-2 (sc-514092, Santa Cruz Biotechnology), syndecan-2 (sc-365624, Santa Cruz Biotechnology), glutamine synthetase (sc-74430, Santa Cruz Biotechnology), fibronectin (sc-271098, Santa Cruz Biotechnology), MMACHC (66609-1-Ig, Proteintech), and MMADHC (23191-1-AP, Proteintech) was incubated O/N at 4°C. Primary antibodies used for detection of GAPDH (sc-32233, Santa Cruz Biotechnology), β -actin (ab8226, Abcam, Cambridge, UK) and α -tubulin (T6074, Sigma-Aldrich, St. Louis, MO, USA) normalizing proteins were incubated for 2 h at RT. Immunoblot detections were carried out using horseradish peroxidase-conjugated antibodies (GE Healthcare, Piscataway, NJ, USA) and enhanced chemiluminescence (GE Healthcare, Piscataway, NJ, USA). Signals were visualized on X-ray films. Images were acquired using the GS-800 calibrated densitometer scan (Bio-Rad, Hercules, CA, USA) and elaborated using the Fiji (Image J, NIH, USA) image processing program. Urine protein signals were normalized to the intensity of the respective gel lane detected over the nitrocellulose membranes by Ponceau S staining.

3.10. Quantitative real-time PCR

1.5×10^3 cells/mm² of HEK 293 cells were seeded in a 6 cm diameter plate and kept in culture in standard conditions (see above). After 24 hours, cells were washed twice with PBS, detached from the plate by trypsinization, resuspended in PBS containing 5% FBS and centrifuged at 250 g for 10 minutes. Supernatant was discarded and total RNA was extracted from cell pellets by using a RNeasy Mini Kit (Qiagen, Hilden, Germany), after which 500 ng RNA were reverse transcribed using SuperScript™ VILO™ MasterMix (Thermo Fisher Scientific, Bremen, Germany). Quantitative real-time polymerase chain reaction (qRT-PCR) was carried out in a 7500 Real-Time PCR System PCR Thermal Cycler with appropriate primers using a SYBR® Select Master Mix (Applied Biosystems, Monza, Italy). Relative gene expression levels of vimentin (VIM) and exostosin-2 (EXT2) were normalized to RNA polymerase II (POLR2A), α -tubulin (TUBA1A) and β -actin (ACTB) and calculated using the $2^{-\Delta\Delta C_t}$ method. Average values from at least three independent experiments were graphically reported as relative units. Statistical significance was calculated by two-tail unpaired t-test. Table 1 reports the sequences of the primers used for the qRT-PCR experiments.

Table 1. Primers sequences for qRT-PCR.

PRIMERS		
Gene name	Orientation	Sequence
POLR2A	Forward	CAACGCACACATCCAGAACG
	Reverse	TCCTTGACTCCCTCCACCAC
TUBA1A	Forward	TCGCCTTCGCCTCCTAATCC
	Reverse	CAAGTCTACAAACACAGCCCG
ACTB	Forward	CGACAGGATGCAGAAGGAGA
	Reverse	CTGCATACTCCTGCTTGCTG
VIM	Forward	CCGGGAGAAATTGCAGGAGG
	Reverse	CCTGGATTTCTCTTCGTGG
EXT2	Forward	AACCAGCCAGGAGAGAGAAC
	Reverse	CACTTCACAGCAGGAGGGTC

3.11. Co-Immunoprecipitation of MMACHC protein and MS-based identification of putative interactors

HepG2 cells expressing recombinant FLAG-MMACHC and FLAG-GFP were lysed in lysis buffer containing 150 mM NaCl, 50 mM Tris-HCl, pH 7.4, 1 mM PMSF, 1% NP-40, and protease inhibitor cocktail (Roche, Indianapolis, IN, USA). Total protein extracts were incubated overnight at 4 °C with M2 anti-FLAG magnetic beads-conjugated antibody (Sigma-Aldrich, St. Louis, MO, USA) to immunoprecipitate (IP) FLAG-tagged proteins and their respective interactors. Beads were washed with lysis buffer containing 300 mM NaCl. The IP protein complexes were then specifically eluted from the beads by competition with FLAG peptide (Sigma-Aldrich, St. Louis, MO, USA) for 5 hours at 4 °C (1st elution). Later, a non-specific elution of IP complexes was performed incubating beads with 2X Laemmli buffer at 99 °C for 5 min (2nd elution). WB was performed on FLAG-MMACHC and FLAG-GFP IPs (1st and 2nd elution) to reveal an enrichment of the respective proteins with respect to whole cell extracts. An anti-FLAG antibody was used for FLAG-MMACHC and FLAG-GFP proteins detection.

One part of the specific eluted protein complexes (1st elution) was resolved by 10% SDS-PAGE on a 16 x 20 cm gel and stained with Gel Code Blue Stain Reagent (Thermo Fisher Scientific, Waltham, MA, USA). Protein bands were excised from the gel and subjected to the same procedure of proteolytic digestion reported in *Materials and Methods*, 3.6.1. A second part of the 1st elution was digested using S-Trap columns, as reported in *Materials and Methods*, 3.6.2. LC-MS/MS analysis and subsequent protein identification processing of FLAG-MMACHC and FLAG-GFP samples, for both gel-based and S-Trap-based sample preparations, were carried out using the same LC-MS/MS setup reported

in *Materials and Methods*, 3.6.1., with only one exception related to liquid chromatographic separation gradient for S-Trap samples (3 h gradient with buffer B).

The two generated lists of putative interactors were filtered removing the proteins common to both GFP-FLAG and MMACHC-FLAG IPs, or those proteins only found in GFP-FLAG samples, and removing affinity MS-related contaminants according to CRAPome Contaminant Repository (Mellacheruvu et al., 2013). Proteins identified with 1 or 0 peptides in GFP-FLAG were included in the final lists as absent in GFP-FLAG condition and only present in MMACHC-FLAG condition. Proteins for MMACHC-FLAG were kept, for gel-based and shotgun identification strategies, only if identified with at least 2 peptides in both replicates or two out of three replicates, respectively.

4. RESULTS

4.1. MUT knockdown in SH-SY5Y cell line

One of the aims of this PhD thesis was the creation of a suitable cell model to study MMA and focus on altered pathways responsible for the damage induced in patients. To this purpose, the first attempt toward this direction was made by silencing MUT gene via siRNA in SH-SY5Y neuroblastoma cell line. Specific siRNAs against MUT and scrambled siRNAs unable to target any cell transcripts were used for samples and negative controls, respectively.

The reduction of protein expression was evaluated 24 and 48 hours after siRNA transfection. Figure 6 shows a reduction of MUT expression by about 50% after 24 h and 70% ($p < 0.001$) after 48 h (Costanzo et al., 2018). The 48 hours-time points (siRNA_MUT and scramble) were chosen for the following experiments.

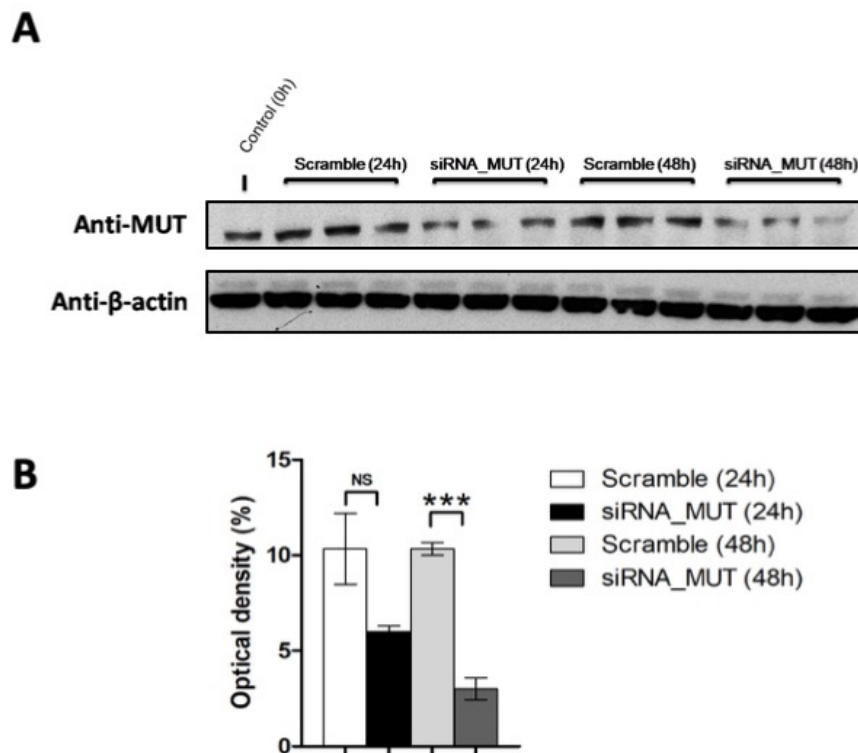


Figure 6. Reduction of MUT protein expression in SH-SY5Y cells after siRNA silencing. MUT silencing was performed in three independent experiments and tested 24 and 48 h after siRNA transfection by Western blot (A). MUT optical density was normalized to β-actin protein and compared to that of scramble samples (B). Results are reported as mean ± standard deviation (SD). Control (0 h) is untransfected cells. Statistical significance was calculated by one-way two tail paired t-test. p-values are indicated as: NS = not significant = $p > 0.05$; *** = $p < 0.005$

4.1.1. MUT silencing does not induce apoptosis in SH-SY5Y cells

In order to understand whether MUT silencing could affect cell viability, the apoptosis rate was measured by flow cytometry in siRNA_MUT cells. Scramble and untransfected cells were used as controls. The results revealed a very low percentage of cells with a high Annexin V signal and low PI signal (cells in early apoptosis), with no significant difference between the siRNA_MUT and control cells. No significant differences were reported for healthy cells (both low Annexin V and PI) or cells in necrotic or late apoptotic state (both high Annexin V and PI) as well (Figure 7). Since that the number of cells in the samples in which apoptosis was tested was comparable (by Neutral-Red assay, data not shown), it was possible to conclude that MUT knockdown is not able to induce apoptosis in SH-SY5Y cells (Costanzo et al., 2018).

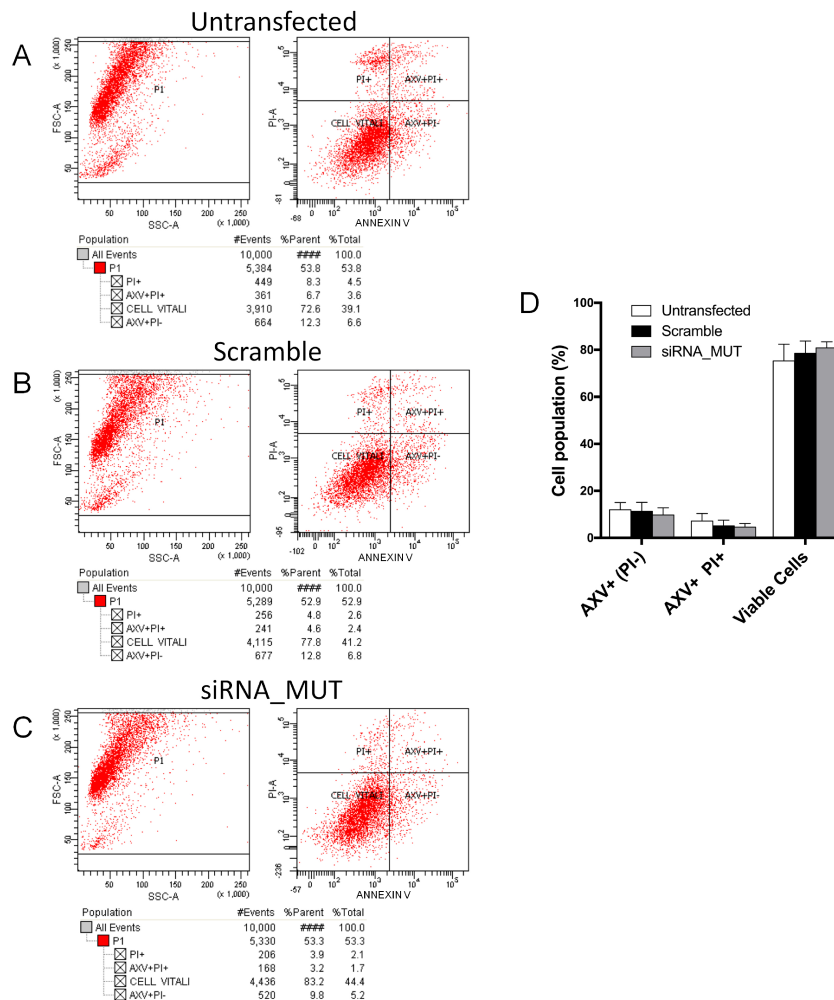


Figure 7. Analysis of apoptosis rate in siRNA_MUT SH-SY5Y cells. Apoptosis was tested by flow cytometry after Annexin V-FITC and PI staining in untransfected (A), scramble (B) and siRNA_MUT (C) cells. Cell populations % are all reported in (D) with no significant differences between the conditions. Each result is the mean of three independent experiments \pm SD. AXV+ (PI-) = Annexin V positive (and PI negative) cells; AXV+ PI+ = Annexin V and PI positive cells.

4.1.2. Spectral counts-based global proteomic analysis of MUT-silenced SH-SY5Y cells

A global proteomic analysis was performed in siRNA_MUT and scramble SH-SY5Y cells. Cell proteomes were separated by SDS-PAGE and proteins digested with trypsin by *in situ* hydrolysis. LC-MS/MS analysis resulted in two datasets consisting in about 1000 proteins identified at least with two peptides. Spectral counts parameters, R_{SC} and $Fold_{NSAF}$, were used to determine the relative abundance of each protein. Protein regulation was tracked for values higher than +3.5 or lower than -3.5 for both the indices. In total, 57 and 56 proteins were found to be up- and down-regulated in siRNA_MUT condition. Differentially regulated proteins were reported in Table 2, ordered from the most down- to the most up-regulated by R_{SC} values, including for each protein the UniProt accession number, gene name, protein name, and R_{SC} and $Fold_{NSAF}$ values (Costanzo et al., 2018).

Table 2. Differentially regulated proteins in siRNA_MUT cells.

UniProt Accession	Gene Name	Protein Name	R_{SC}	$Fold_{NSAF}$
Q9Y678	<i>COPG1</i>	Coatomer subunit gamma-1	-4.62	-6.22
O14776	<i>TCRG1</i>	Transcription elongation regulator 1	-4.62	-5.89
Q02952	<i>TCRG1</i>	A-kinase anchor protein 12	-4.50	-5.07
P08865	<i>RSSA</i>	40S ribosomal protein SA	-4.37	-7.53
Q15365	<i>PCBP1</i>	Poly(rC)-binding protein 1	-4.37	-7.25
Q02978	<i>M2OM</i>	Mitochondrial 2-oxoglutarate/malate carrier protein	-4.37	-7.44
P11717	<i>MPRI</i>	Cation-independent mannose-6-phosphate receptor	-4.37	-6.89
P62913	<i>RL11</i>	60S ribosomal protein L11	-4.23	-4.45
P48643	<i>TCPE</i>	T-complex protein 1 subunit epsilon	-4.23	-8.10
O43242	<i>PSMD3</i>	26S proteasome non-ATPase regulatory subunit 3	-4.23	-6.50
Q15477	<i>SKIV2</i>	Helicase SKI2W	-4.23	-6.52
P50395	<i>GDIB</i>	Rab guanosine diphosphate dissociation inhibitor beta	-4.06	-5.30
Q14240	<i>IF4A2</i>	Eukaryotic initiation factor 4A-II	-4.06	-6.61
Q01433	<i>AMPD2</i>	AMP deaminase 2	-4.06	-6.74
P35222	<i>CTNB1</i>	Catenin beta-1	-4.06	-5.63
P04792	<i>HSPB1</i>	Heat shock protein beta-1	-3.88	-5.80
P00568	<i>KAD1</i>	Adenylate kinase isoenzyme 1	-3.88	-7.54
Q14232	<i>EDBA</i>	Translation initiation factor eIF-2B subunit alpha	-3.88	-7.62
P09960	<i>LKHA4</i>	Leukotriene A-4 hydrolase	-3.88	-6.96
P43686	<i>PRS6B</i>	26S protease regulatory subunit 6B	-3.88	-5.96
Q14155	<i>ARHG7</i>	Rho guanine nucleotide exchange factor 7	-3.88	-6.51
Q13045	<i>FLII</i>	Protein flightless-1 homolog	-3.88	-5.57
Q14444	<i>CAPR1</i>	Caprin-1	-3.88	-6.29
P15924	<i>DESP</i>	Desmoplakin	-3.88	-6.56
Q96JQ0	<i>PCD16</i>	Protocadherin-16	-3.88	-5.92
Q9NR31	<i>SAR1A</i>	guanosine triphosphate (GTP)-binding protein SAR1a	-3.68	-4.91
Q9Y3B7	<i>RM11</i>	39S ribosomal protein L11, mitochondrial	-3.68	-5.75
P30041	<i>PRDX6</i>	Peroxiredoxin-6	-3.68	-3.73
P84103	<i>SRSF3</i>	Serine/arginine-rich splicing factor 3	-3.68	-3.53
P61020	<i>RAB5B</i>	Ras-related protein Rab-5B	-3.68	-7.36
Q13126	<i>MTAP</i>	S-methyl-5'-thioadenosine phosphorylase	-3.68	-7.41
P81605	<i>DCD</i>	Dermcidin	-3.68	-7.19
O00232	<i>PSD12</i>	26S proteasome non-ATPase regulatory subunit 12	-3.68	-7.64
Q9UFN0	<i>NPS3A</i>	Protein NipSnap homolog 3A	-3.68	-7.25
P09972	<i>ALDOC</i>	Fructose-bisphosphate aldolase C	-3.68	-6.85
Q8NBJ7	<i>SUMF2</i>	Sulfatase-modifying factor 2	-3.68	-8.21
P09104	<i>ENOG</i>	Gamma-enolase	-3.68	-6.16
P13804	<i>ETFA</i>	Electron transfer flavoprotein subunit alpha, mitochondrial	-3.68	-7.05
O15173	<i>PGR2</i>	Membrane-associated progesterone receptor component 2	-3.68	-6.49
Q8NC51	<i>PAIRB</i>	Plasminogen activator inhibitor 1 RNA-binding protein	-3.68	-6.76

Q96HS1	<i>PGAM5</i>	Serine/threonine-protein phosphatase PGAM5, mitochondrial	-3.68	-6.23
Q9UJU6	<i>DBNL</i>	Drebrin-like protein	-3.68	-6.61
Q14194	<i>DPYL1</i>	Dihydropyrimidinase-related protein 1	-3.68	-7.19
Q96PZ0	<i>PUS7</i>	Pseudouridylylase 7 homolog	-3.68	-6.32
P62195	<i>PRSS8</i>	26S protease regulatory subunit 8	-3.68	-6.82
Q14247	<i>SRC8</i>	Src substrate cortactin	-3.68	-6.25
Q9P289	<i>STK26</i>	Serine/threonine-protein kinase 26	-3.68	-5.83
Q9Y6E0	<i>STK24</i>	Serine/threonine-protein kinase 24	-3.68	-5.62
O14579	<i>COPE</i>	Coatamer subunit epsilon	-3.68	-6.33
Q13330	<i>MTA1</i>	Metastasis-associated protein MTA1	-3.68	-5.89
Q16401	<i>PSMD5</i>	26S proteasome non-ATPase regulatory subunit 5	-3.68	-6.29
Q15075	<i>EEA1</i>	Early endosome antigen 1	-3.68	-6.20
Q92626	<i>PXDN</i>	Peroxidasin homolog	-3.68	-6.73
O60841	<i>IF2P</i>	Eukaryotic translation initiation factor 5B	-3.68	-6.02
Q13576	<i>IQGA2</i>	Ras GTPase-activating-like protein IQGAP2	-3.68	-4.53
Q5VYK3	<i>ECM29</i>	Proteasome-associated protein ECM29 homolog	-3.68	-4.46
Q96GQ7	<i>DDX27</i>	Probable ATP-dependent RNA helicase DEAD box (DDX) 27	3.73	6.71
Q86VM9	<i>ZCH18</i>	Zinc finger (ZNF) CCCH domain-containing protein 18 O	3.73	6.46
Q9Y2A7	<i>NCKP1</i>	Nck-associated protein 1	3.73	5.89
Q9BUJ2	<i>HNRL1</i>	Heterogeneous nuclear ribonucleoprotein U-like protein 1	3.73	5.36
Q9Y6K1	<i>DNM3A</i>	DNA (cytosine-5)-methyltransferase 3A	3.73	5.39
Q9NXE4	<i>SMPD4</i>	Sphingomyelin phosphodiesterase 4	3.73	5.13
Q9BZJ0	<i>CRNL1</i>	Crooked neck-like protein 1	3.73	4.88
Q13523	<i>PRP4B</i>	Serine/threonine-protein kinase pre-mRNA-processing factor 4 homolog	3.73	5.28
Q8IXT5	<i>RB12B</i>	RNA-binding protein 12B	3.73	5.19
Q7KZ85	<i>SPT6H</i>	Transcription elongation factor suppressor of Ty6	3.73	5.33
O75691	<i>UTP20</i>	Small subunit processome component 20 homolog	3.73	5.29
P20340	<i>RAB6A</i>	Ras-related protein Rab-6A	3.93	5.05
Q13185	<i>CBX3</i>	Chromobox protein homolog 3	3.93	5.05
O14979	<i>HNRLD</i>	Heterogeneous nuclear ribonucleoprotein D-like	3.93	4.27
Q5BKZ1	<i>ZN326</i>	DBIRD complex subunit ZNF326	3.93	3.58
Q9Y310	<i>RTCB</i>	tRNA-splicing ligase RtcB homolog	3.93	7.54
Q96A65	<i>EXOC4</i>	Exocyst complex component 4	3.93	7.73
Q00325	<i>MPCP</i>	Phosphate carrier protein, mitochondrial	3.93	6.53
O60282	<i>KIF5C</i>	Kinesin heavy chain isoform 5C	3.93	6.06
Q68E01	<i>INT3</i>	Integrator complex subunit 3	3.93	6.26
Q13620	<i>CUL4B</i>	Cullin-4B	3.93	5.32
P51531	<i>SMCA2</i>	Probable global transcription activator SNF2L2	3.93	6.74
O00299	<i>CLIC1</i>	Chloride intracellular channel protein 1	4.11	5.34
P83916	<i>CBX1</i>	Chromobox protein homolog 1	4.11	5.22
Q96E39	<i>RMXL1</i>	RNA binding motif protein, X-linked-like-1	4.11	5.41
Q14978	<i>NOLC1</i>	Nucleolar and coiled-body phosphoprotein 1	4.11	4.61
Q15061	<i>WDR43</i>	WD repeat-containing protein 43	4.11	7.52
Q8WTT2	<i>NOC3L</i>	Nucleolar complex protein 3 homolog	4.11	7.91
P23921	<i>RIR1</i>	Ribonucleoside-diphosphate reductase large subunit	4.11	6.83
O75400	<i>PR40A</i>	Pre-mRNA-processing factor 40 homolog A	4.11	5.99
P52948	<i>NUP98</i>	Nuclear pore complex protein Nup98-Nup96	4.11	6.03
O75367	<i>H2AFY</i>	Core histone macro-H2A.1	4.27	5.79
O43290	<i>SNUT1</i>	U4/U6.U5 tri-snRNP-associated protein 1	4.27	5.81
O00571	<i>DDX3X</i>	ATP-dependent RNA helicase DDX3X	4.27	5.53
P39023	<i>RL3</i>	60S ribosomal protein L3	4.27	4.61
Q14690	<i>RRP5</i>	Protein RRP5 homolog	4.27	7.07
Q13151	<i>ROA0</i>	Heterogeneous nuclear ribonucleoprotein A0	4.42	5.96
P38919	<i>IF4A3</i>	Eukaryotic initiation factor 4A-III	4.42	6.24
Q9UMS6	<i>SYNP2</i>	Synaptopodin-2	4.42	6.95
Q9NYF8	<i>BCLF1</i>	Bcl-2-associated transcription factor 1	4.42	4.74
Q9H0A0	<i>NAT10</i>	N-acetyltransferase 10	4.42	7.51
Q9UKV3	<i>ACINU</i>	Apoptotic chromatin condensation inducer in the nucleus	4.42	7.08
P68431	<i>H31</i>	Histone H3.1	4.55	5.66
Q8IY81	<i>SPB1</i>	pre-rRNA processing protein FTSJ3	4.55	5.91
Q9H6R4	<i>NOL6</i>	Nucleolar protein 6	4.55	5.76
Q9NVP1	<i>DDX18</i>	ATP-dependent RNA helicase DDX18	4.55	5.37
Q8WUM0	<i>NU133</i>	Nuclear pore complex protein Nup133	4.67	8.81
Q8NI27	<i>THOC2</i>	THO complex subunit 2	4.67	6.17
P28331	<i>NDUS1</i>	Nicotinamide adenine dinucleotide	4.78	5.73
P07197	<i>NFM</i>	-ubiquinone oxidoreductase 75 kDa subunit, mitochondrial Neurofilament medium polypeptide	4.78	6.51

Q9UIG0	<i>BAZ1B</i>	Tyrosine-protein kinase bromodomain adjacent to ZNF 1B	4.78	5.85
P62805	<i>H4</i>	Histone H4	4.88	5.38
O00159	<i>MYO1C</i>	Unconventional myosin-Ic	4.98	6.63
Q9H583	<i>HEAT1</i>	HEAT repeat-containing protein 1	4.98	6.30
P28370	<i>SMCA1</i>	Probable global transcription activator SNF2L1	5.24	5.60
P49792	<i>RBP2</i>	E3 small ubiquitin-like modifier-protein ligase RanBP2	5.31	9.56
POC055	<i>H2AZ</i>	Histone H2A.Z	5.38	6.29

4.1.3. Bioinformatic analysis and functional annotation

The differentially regulated proteome dataset was then analyzed using bioinformatic tools and protein annotation databases in order to characterize the altered cellular pathways subsequent MUT knockdown.

PANTHER analysis allowed to cluster 92/113 regulated proteins with the enrichment of three main categories, the most represented amongst the all, related to molecular function GO category term: binding, catalytic activity, and structural molecule activity (Figure 8A). “Catalytic activity” was the most represented class and it was further subdivided into eight enzymatic categories (Figure 8B). Of particular interest are the proteins related to oxidoreductase activity category, like the electron transfer flavoprotein subunit alpha, mitochondrial (ETFA) and Peroxiredoxin-6 (PRDX6), both down-regulated in the dataset and involved in fatty acid β -oxidation, electrons transport and cell redox homeostasis.

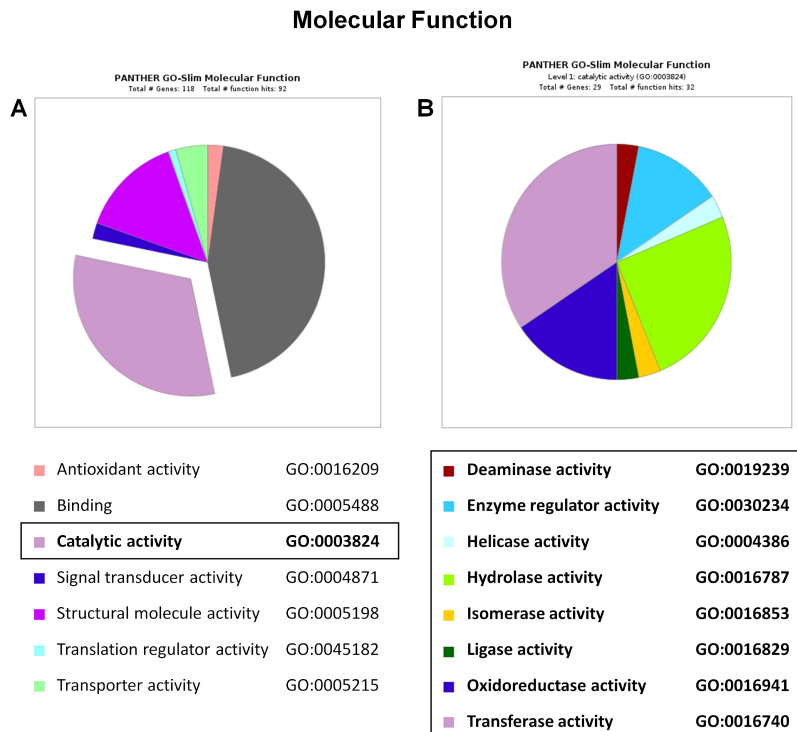


Figure 8. PANTHER analysis of Molecular Function categories within the differential siRNA_MUT proteome. Enrichment of the most represented categories with focus on “catalytic activity” (A) and detail of its subcategories (B).

PANTHER was also used to retrieve information about the biological processes perturbed after MUT silencing. Next to the more general “cellular process”, “metabolic process” was the most represented and interestingly investigated category because of the link of the cell system employed with the metabolic disease in study. Indeed, other seven subcategories were represented (Figure 9). Amongst these, Mitochondrial 2-oxoglutarate/malate carrier protein (M2OM), gamma-enolase (ENOG), and fructose bisphosphate aldolase C (ALDOC), involved in energy production and metabolism, were found down-regulated (Costanzo et al., 2018).

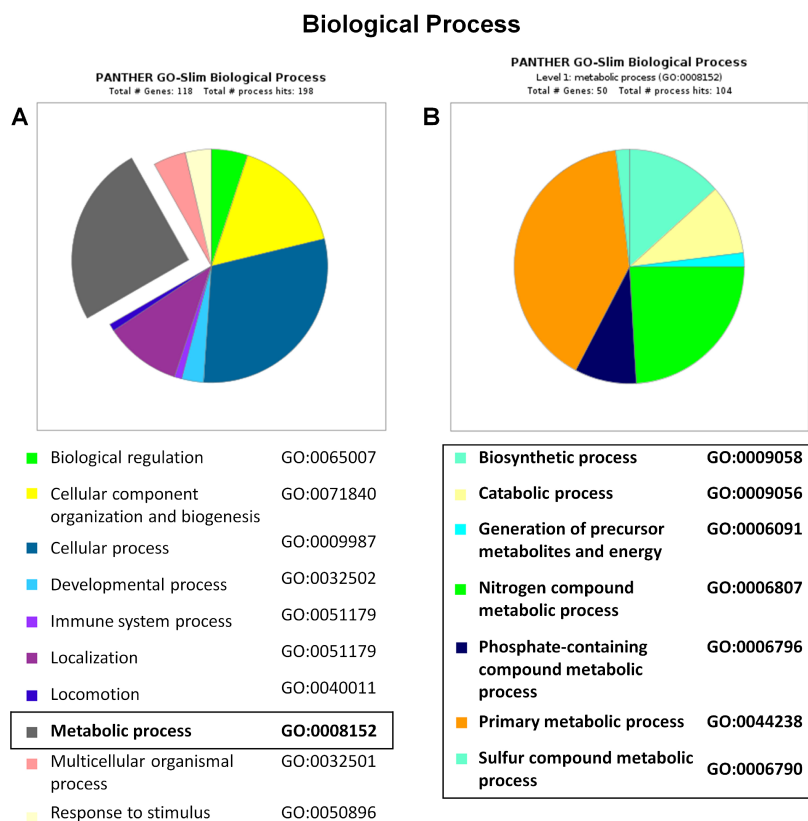


Figure 9. PANTHER analysis of Biological Process categories within the differential siRNA_MUT proteome. Enrichment of the most represented categories with focus on “metabolic process” (A) and detail of its subcategories (B).

4.1.4. Mut silencing decreases cell viability and mitochondrial functionality in propionate-enriched culture medium

In order to induce a stress similar to that of MMA patients, siRNA_MUT cells were treated for 48 h with propionate, a metabolic precursor of methylmalonyl-CoA. In a propionate-enriched culture medium, siRNA_MUT cells showed a slight but not significant reduction of the cell viability by Neutral-

Red assay. On the other hand, MTT assay showed a significant decreased mitochondrial functionality. The variation between the fold changes of Neutral-Red and MTT assays was calculated as $\Delta = 0.26$ (Figure 10). The reduction of mitochondrial functionality supports the proteomic results that showed the differential regulation of a group of mitochondrial proteins (Costanzo et al., 2018).

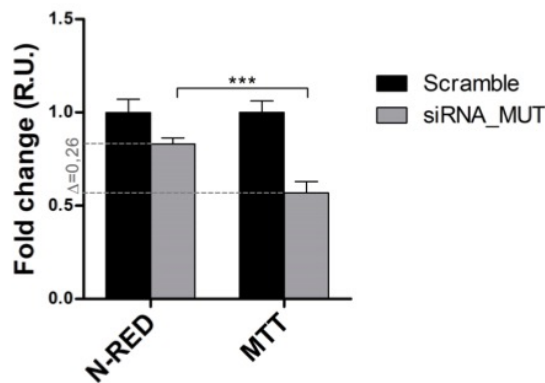


Figure 10. Viability and mitochondrial functionality of siRNA_MUT cells in propionate-enriched culture medium by Neutral-Red and MTT assay. Scramble and siRNA_MUT cells were compared. The fold changes were expressed as relative units (R.U.). The variation between the MTT and Neutral-Red fold-changes was calculated ($\Delta = 0.26$). Results are reported as mean of three independent replicates \pm SD. p-value for the statistical significance was calculated by one-way two-tail paired t-test; *** = $p < 0.005$.

4.2. MUT knockout in SH-SY5Y cell line

Despite the previous results were promising because well connected to the disease in study, a critical issue related to this kind of experiment is that the transient reduction of MUT protein induced by siRNA may prevent to go into the deep of the molecular alterations of MMA, for a fast recovery of protein expression levels. To this aim, total knockout cell models will be generated.

A first attempt (experimentally replicated three times) to produce a stable knock out cell model was made in human neuroblastoma SH-SY5Y cell line, unsuccessfully. Transfected cells were not able to replicate and survive, probably according to the notion that methylmalonic acid, 2-methylcitric acid and other metabolites that accumulate as consequence of MUT absence/inactivity are toxic for neuronal cells (Jafari P et al., 2013). A second attempt was, then, made on the human embryonic kidney (HEK) 293 cell line, successfully. Cells well survived after the transfection and started to replicate.

4.3. MUT knockout in HEK293 cell line

4.3.1. CRISPR/Cas9-based cell model generation and biochemical characterization

Two MUT CRISPR/Cas9 plasmids, a knockout (KO) and a homology-directed repair (HDR) plasmid, were used to generate a MUT KO in HEK293 cells. The vectors mediated the insertion of a red fluorescent protein (RFP) and a puromycin resistance gene. After 96 hours from the transfection, the cells that survived at antibiotic treatment showing red fluorescence (MUT-KO pool, Figure 11A) were kept in culture. Western blot (WB) analysis showed that this pool of cells still retained MUT protein expression, even if at very low level (Figure 11B). MUT-KO pool was further cultured in order to select single clones to be tested for the absence of MUT expression, monitoring RFP signals. The first two clones (namely, MUT-KO clone 1 and clone 2) analyzed by WB (Figure 11C) showed the complete absence of MUT expression and they still retained red fluorescence. Thus, clone 2 was selected to be used for the following experiments and, hereinafter, referred as MUT-KO.

Then, in order to test the validity of this cell model, the levels of some diagnostic biomarkers of MMA were measured. In particular, methylmalonic acid and propionylcarnitine were measured in the cells by targeted LC-MS/MS-MRM. As shown in Figure 12, an expected increase in the levels of methylmalonic acid and propionylcarnitine occurred in MUT-KO samples compared to WT ones. Thus, these results are convincing that this cell model is able to recapitulate in vitro the molecular alteration of MMA and, even more so, it may be employed in many further experiments for the study of the disease.

Similarly to the previous siRNA_MUT cell line, viability assays were performed for MUT-KO cell model as well. In particular, Neutral-Red and MTT assays showed no significant difference in viability comparing MUT-KO to WT cells (Figure 13). Neutral-Red assay showed no significant difference in proliferation rate between MUT-KO and WT cells. MTT showed a slight decrease ($p = 0.040$) in the absorbance of MUT-KO samples only at 72 hours. This is most likely accountable for a decreased mitochondrial succinate dehydrogenase activity rather than for a reduced proliferation rate, since Neutral-Red does not show a similar difference at the same time point. As conclusion, it is possible to assess that MUT knockout does not affect cell viability and proliferation.

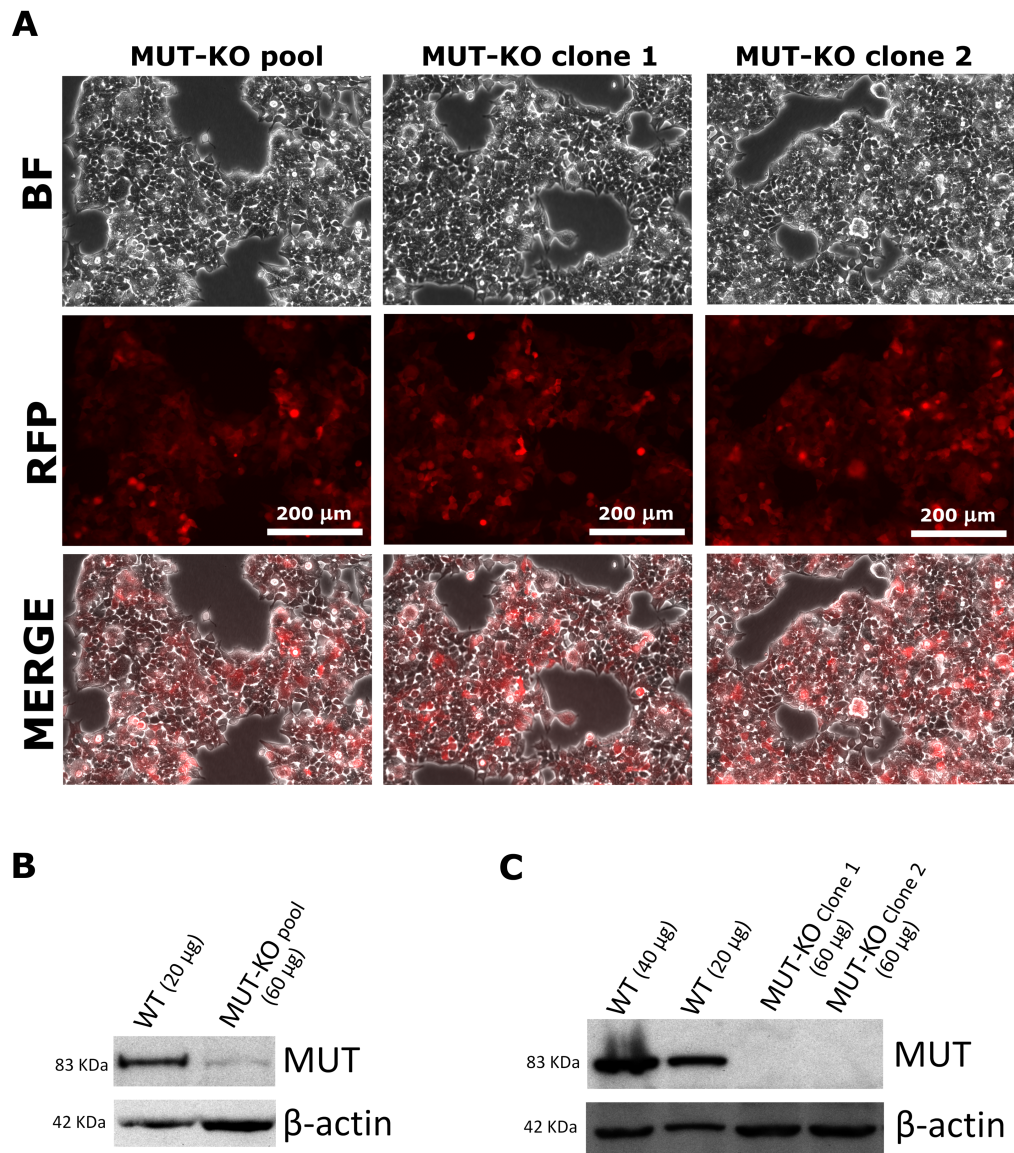


Figure 11. Microscopy and Western blot analysis of CRISPR/Cas9-treated HEK293 cells for MUT knockout. A) Microscopy images of CRISPR/Cas9-modified cells from Leica LAS AF software. After transfection, cells were observed with a 20X objective. MUT-KO pool = whole transfected cell population after selection with puromycin. MUT-KO clones = cell populations isolated from single progenitor cells within MUT-KO pool. BF = phase-contrast bright field. RFP = red fluorescent protein. B) WB analysis of MUT levels in the MUT-KO pool. C) WB analysis of the cell MUT-KO clones 1 and 2. In both WBs, WT cells were used as a control of MUT expression; β -actin was the loading control.

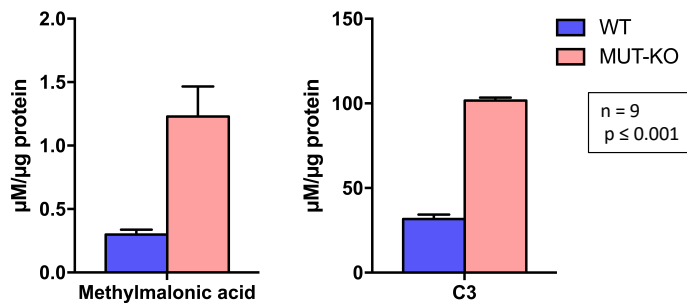


Figure 12. LC-MS/MS measurement of methylmalonic acid and propionylcarnitine in WT and MUT-KO cells. Both metabolites were significantly higher in MUT-KO, compared to WT cells. Metabolites concentrations, were normalized to the total µg protein content of each sample. For this measurement, 9 biological replicates were employed for each condition. Data are reported as mean ± Standard Error of the Mean (SEM). One-way two-tail t-test p value for both comparisons was < 0.001. C3 = propionylcarnitine.

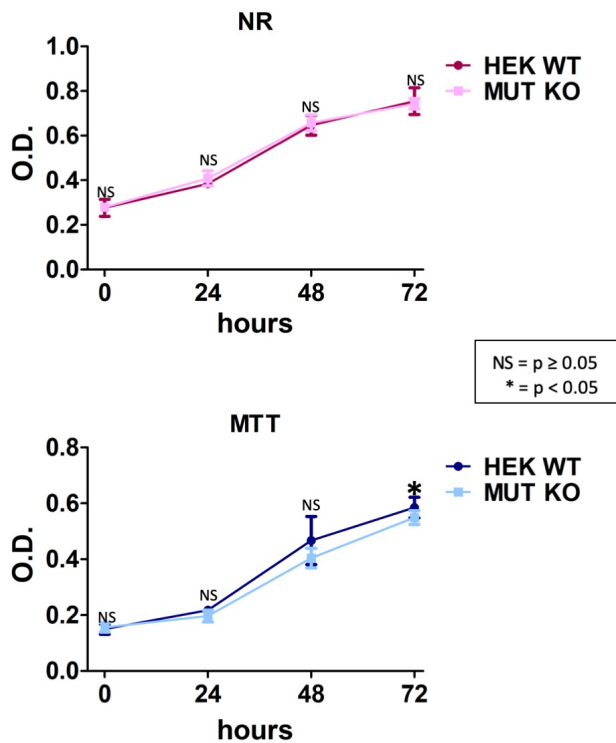


Figure 13. Growth curves of HEK293 cells are not affected by genome modification. WT and MUT-KO cells were analyzed by Neutral-Red (NR) and MTT assays. Data are the mean values of three experimental replicates and error bars represent SD. One-way two-tail paired t-test was used to calculate the statistical significance of differences between the tested cell types. O.D. = optical density; * = $p < 0.05$; NS = not significant = $p > 0.05$.

4.3.2. LFQ-based global proteomic analysis of MUT-KO cells

Using the new MUT-KO cell model and WT cells as control, a comparative global proteomics experiment was performed with four biological replicates per condition. Prior protein digestion, the same samples intended for the proteomic analysis were tested again by WB and MUT-KO samples showed no signals for MUT protein (data not shown). Each biological sample was analyzed in triplicates by shotgun LC-MS/MS. The label-free proteomic analysis was based on LFQ intensity values obtained from elaborating the MS raw files within the MaxQuant software. Each MS run could identify about 4500 proteins for each cell lysate. A combined bioinformatic and statistical analysis of the proteomic comparison with Perseus software (version 1.6.5.0) highlighted 178 differentially regulated proteins, of which 112 down- and 66 up-regulated in the MUT-KO condition. Proteome distribution is graphically reported in the volcano plot in Figure 14. MUT protein was uniquely identified in WT but not in MUT-KO samples, confirming once again WB data (Figure 11C). The list of the differentially regulated proteins in the MUT-KO cell model is reported in Table 3, including for each protein the UniProt ID, gene name, protein name and \log_2 difference, sorted in a crescent order for the \log_2 difference value.

In comparison with the previous proteomic experiment (*Results 4.1.2, Table 2*) no common protein was detected to have the same regulation. This was expected because of the different cell line and genome modification employed, and the different proteomic setup (LC and MS instruments, number of replicates, sample preparation, quantitative strategy). In addition, not surprisingly, this may also explain the different impact that MMA can have on different cell types.

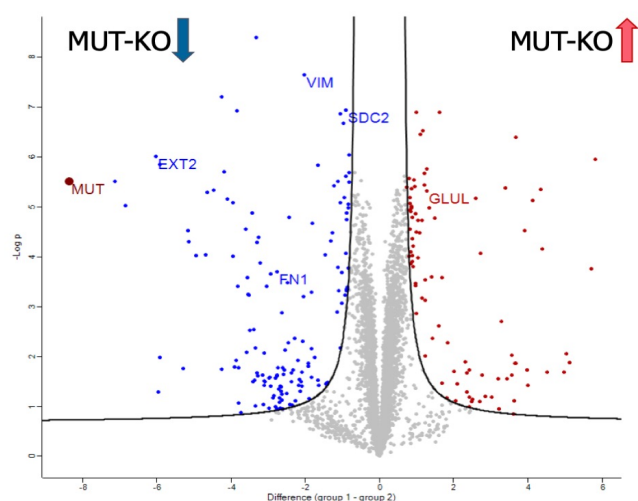


Figure 14. Representation of the label-free proteomic experiment in MUT-KO cell model. Volcano plot was used to visualize the global proteome distribution in MUT-KO according to the quantitative difference between KO and WT (group 1 and 2) and the statistical significance ($-\log p$) of the proteins. Blue and red dots represent the significant down- and up-regulated proteins, with detail of some proteins whose regulation has been validated (*Results 4.3.5*). MUT is indicated in the left part of the graph (brown dot) as the most strongly down-regulated protein.

Table 3. List of the differentially regulated proteins identified by LC-MS/MS analysis in MUT-KO cell line.

UniProt ID	Gene name	Protein name	Log ₂ Difference
P22033	MUT	Methylmalonyl-CoA mutase, mitochondrial	-8,5
Q13642	FHL1	Four and a half LIM domains protein 1	-7,1
Q16563	SYPL1	Synaptophysin-like protein 1	-7,1
O94763	URI1	Unconventional prefoldin RPB5 interactor 1	-6,1
Q93063	EXT2	Exostosin-2	-6,1
P31947	SFN	14-3-3 protein sigma	-6,0
O00622	CYR61	Protein CYR61	-5,8
P35625	TIMP3	Metalloproteinase inhibitor 3	-5,3
Q6PIJ6	FBXO38	F-box only protein 38	-5,1
Q96GS6	ABHD17A	Alpha/beta hydrolase domain-containing protein 17A	-5,1
A2RUR9	CCDC144A	Coiled-coil domain-containing protein 144A	-5,1
Q9BVC4	MLST8	Target of rapamycin complex subunit LST8	-4,7
Q9NPD8	UBE2T	Ubiquitin-conjugating enzyme E2 T	-4,6
Q9UBN6	TNFRSF10D	Tumor necrosis factor receptor superfamily member 10D	-4,3
O75096	LRP4	Low-density lipoprotein receptor-related protein 4	-4,2
Q9ULF5	SLC39A10	Zinc transporter ZIP10	-4,1
P78536	ADAM17	Disintegrin and metalloproteinase domain-containing protein 17	-4,1
Q9NPI1	BRD7	Bromodomain-containing protein 7	-4,0
Q00013	MPP1	55 kDa erythrocyte membrane protein	-4,0
Q9UI14	RABAC1	Prenylated Rab acceptor protein 1	-4,0
Q8IWB7	WDFY1	WD repeat and FYVE domain-containing protein 1	-4,0
O95639	CPSF4	Cleavage and polyadenylation specificity factor subunit 4	-3,9
Q8IUH5	ZDHHC17	Palmitoyltransferase ZDHHC17	-3,9
Q5T9L3	WLS	Protein wntless homolog	-3,8
Q9P2M7	CGN	Cingulin	-3,7
Q8TF71	SLC16A10	Monocarboxylate transporter 10	-3,7
Q9NVN8	GNL3L	Guanine nucleotide-binding protein-like 3-like protein	-3,6
Q07864	POLE	DNA polymerase epsilon catalytic subunit A	-3,6
Q9UL63	MKLN1	Muskelin	-3,6
Q2PZI1	DPY19L1	Probable C-mannosyltransferase DPY19L1	-3,6
Q96E15	TCEAL4	Transcription elongation factor A protein-like 4	-3,6
Q9UK99	FBXO3	F-box only protein 3	-3,6
P13747	HLA-E	HLA class I histocompatibility antigen, alpha chain E	-3,5
Q6P3X3	TTC27	Tetratricopeptide repeat protein 27	-3,5
P23434	GCSH	Glycine cleavage system H protein, mitochondrial	-3,5
Q8WW22	DNAJA4	DnaJ homolog subfamily A member 4	-3,5
Q99595	TIMM17A	Mitochondrial import inner membrane translocase subunit Tim17-A	-3,5
Q9Y388	RBMX2	RNA-binding motif protein, X-linked 2	-3,5
Q96IU4	ABHD14B	Alpha/beta hydrolase domain-containing protein 14B	-3,5
Q8N954	GPATCH11	G patch domain-containing protein 11	-3,4
Q9Y232	CDYL	Chromodomain Y-like protein	-3,4
Q8TEY7	USP33	Ubiquitin carboxyl-terminal hydrolase 33	-3,4
Q07617	SPAG1	Sperm-associated antigen 1	-3,4
Q6P1K8	GTF2H2C	General transcription factor IIH subunit 2-like protein	-3,2
Q9Y294	ASF1A	Histone chaperone ASF1A	-3,1
Q03519	TAP2	Antigen peptide transporter 2	-3,1
Q13370	PDE3B	cGMP-inhibited 3,5-cyclic phosphodiesterase B	-3,0
Q9UIC8	LCMT1	Leucine carboxyl methyltransferase 1	-3,0
Q13356	PPIL2	Peptidyl-prolyl cis-trans isomerase-like 2	-3,0
Q13530	SERINC3	Serine incorporator 3	-3,0
Q15139	PRKD1	Serine/threonine-protein kinase D1	-3,0
Q8N4T8	CBR4	Carbonyl reductase family member 4	-2,9
Q9Y2X9	ZNF281	Zinc finger protein 281	-2,9
Q7Z4S6	KIF21A	Kinesin-like protein KIF21A	-2,9

Q96AQ6	PBXIP1	Pre-B-cell leukemia transcription factor-interacting protein 1	-2,9
Q96ES7	CCDC101	SAGA-associated factor 29 homolog	-2,9
Q12841	FSTL1	Follistatin-related protein 1	-2,9
Q9H832	UBE2Z	Ubiquitin-conjugating enzyme E2 Z	-2,9
Q8IVL5	LEPREL1	Prolyl 3-hydroxylase 2	-2,9
Q14181	POLA2	DNA polymerase alpha subunit B	-2,9
Q8N138	ORMDL3	ORM1-like protein 3	-2,8
O75581	LRP6	Low-density lipoprotein receptor-related protein 6	-2,8
P22413	ENPP1	Ectonucleotide pyrophosphatase/phosphodiesterase family member 1	-2,7
Q9H0H0	INTS2	Integrator complex subunit 2	-2,7
Q8IZJ1	UNC5B	Netrin receptor UNC5B	-2,7
Q5TA45	CPSF3L	Integrator complex subunit 11	-2,7
P49848	TAF6	Transcription initiation factor TFIID subunit 6	-2,7
Q8N5L8	RPP25L	Ribonuclease P protein subunit p25-like protein	-2,7
Q9Y385	UBE2J1	Ubiquitin-conjugating enzyme E2 J1	-2,7
Q9H6U8	ALG9	Alpha-1,2-mannosyltransferase ALG9	-2,6
P13498	CYBA	Cytochrome b-245 light chain	-2,6
P98196	ATP11A	Probable phospholipid-transporting ATPase 1H	-2,5
O95825	CRYZL1	Quinone oxidoreductase-like protein 1	-2,5
O60779	SLC19A2	Thiamine transporter 1	-2,5
Q9NUQ2	AGPAT5	1-acyl-sn-glycerol-3-phosphate acyltransferase epsilon	-2,4
Q9H0U9	TSPYL1	Testis-specific Y-encoded-like protein 1	-2,4
O95716	RAB3D	Ras-related protein Rab-3D	-2,4
O00762	UBE2C	Ubiquitin-conjugating enzyme E2 C	-2,3
Q9UKB3	DNAJC12	DnaJ homolog subfamily C member 12	-2,3
P78368	CSNK1G2	Casein kinase I isoform gamma-2	-2,2
Q69YH5	CDCA2	Cell division cycle-associated protein 2	-2,2
Q12834	CDC20	Cell division cycle protein 20 homolog	-2,2
O75509	TNFRSF21	Tumor necrosis factor receptor superfamily member 21	-2,1
P02751	FN1	Fibronectin	-2,1
Q12929	EPS8	Epidermal growth factor receptor kinase substrate 8	-2,1
P12429	ANXA3	Annexin A3	-2,1
P19438	TNFRSF1A	Tumor necrosis factor receptor superfamily member 1A	-2,1
Q9BQE5	APOL2	Apolipoprotein L2	-2,0
P08670	VIM	Vimentin	-2,0
Q9BQT9	CLSTN3	Calsyntenin-3	-1,9
Q9NZN5	ARHGEF12	Rho guanine nucleotide exchange factor 12	-1,9
P80723	BASP1	Brain acid soluble protein 1	-1,8
O14686	KMT2D	Histone-lysine N-methyltransferase 2D	-1,7
P13591	NCAM1	Neural cell adhesion molecule 1	-1,7
Q9H9F9	ACTR5	Actin-related protein 5	-1,5
Q16890	TPD52L1	Tumor protein D53	-1,5
Q14699	RFTN1	Raftlin	-1,3
O43854	EDIL3	EGF-like repeat and discoidin I-like domain-containing protein 3	-1,3
Q16527	CSRP2	Cysteine and glycine-rich protein 2	-1,2
Q9NY26	SLC39A1	Zinc transporter ZIP1	-1,1
Q08345	DDR1	Epithelial discoidin domain-containing receptor 1	-1,1
Q6ZN17	LIN28B	Protein lin-28 homolog B	-1,1
Q13772	NCOA4	Nuclear receptor coactivator 4	-1,1
Q15004	KIAA0101	PCNA-associated factor	-1,1
O95235	KIF20A	Kinesin-like protein KIF20A	-1,1
P04818	TYMS	Thymidylate synthase	-1,0
Q5VV42	CDKAL1	Threonylcarbamoyladenine tRNA methylthiotransferase	-1,0
P02794	FTH1	Ferritin heavy chain	-1,0
P34741	SDC2	Syndecan-2	-0,9
Q8NEF9	SRFBP1	Serum response factor-binding protein 1	-0,9
Q99808	SLC29A1	Equilibrative nucleoside transporter 1	-0,9
O00461	GOLIM4	Golgi integral membrane protein 4	-0,9

P00568	AK1	Adenylate kinase isoenzyme 1	0,9
Q53T59	HS1BP3	HCLS1-binding protein 3	0,9
P48200	IREB2	Iron-responsive element-binding protein 2	0,9
Q13057	COASY	Bifunctional coenzyme A synthase	0,9
P35914	HMGCL	Hydroxymethylglutaryl-CoA lyase, mitochondrial	1,0
Q8WVC6	DCAKD	Dephospho-CoA kinase domain-containing protein	1,0
Q01628	IFITM3	Interferon-induced transmembrane protein 3	1,0
P23786	CPT2	Carnitine O-palmitoyltransferase 2, mitochondrial	1,0
P35270	SPR	Sepiapterin reductase	1,0
Q16698	DECR1	2,4-dienoyl-CoA reductase, mitochondrial	1,0
Q6YN16	HSDL2	Hydroxysteroid dehydrogenase-like protein 2	1,0
Q6P1M0	SLC27A4	Long-chain fatty acid transport protein 4	1,1
O94788	ALDH1A2	Retinal dehydrogenase 2	1,1
P16422	EPCAM	Epithelial cell adhesion molecule	1,1
Q05639	EEF1A2	Elongation factor 1-alpha 2	1,1
P12532	CKMT1A	Creatine kinase U-type, mitochondrial	1,2
Q8WWI5	SLC44A1	Choline transporter-like protein 1	1,2
Q3YEC7	RABL6	Rab-like protein 6	1,2
Q9BRX8	FAM213A	Redox-regulatory protein FAM213A	1,2
Q9Y657	SPIN1	Spindlin-1	1,2
P07196	NEFL	Neurofilament light polypeptide	1,3
P15104	GLUL	Glutamine synthetase	1,3
Q3LXA3	DAK	Bifunctional ATP-dependent dihydroxyacetone kinase/FAD-AMP lyase (cyclizing)	1,3
Q9NRG7	SDR39U1	Epimerase family protein SDR39U1	1,4
Q9NP58	ABCB6	ATP-binding cassette sub-family B member 6, mitochondrial	1,4
P50225	SULT1A1	Sulfotransferase 1A1	1,5
Q9BVL4	SELO	Selenoprotein O	1,6
P31321	PRKAR1B	cAMP-dependent protein kinase type I-beta regulatory subunit	1,6
Q9Y2Z9	COQ6	Ubiquinone biosynthesis monooxygenase COQ6, mitochondrial	1,7
Q16566	CAMK4	Calcium/calmodulin-dependent protein kinase type IV	1,9
Q3KQV9	UAP1L1	UDP-N-acetylhexosamine pyrophosphorylase-like protein 1	1,9
Q6VMQ6	ATF7IP	Activating transcription factor 7-interacting protein 1	2,0
Q86UT6	NLRX1	NLR family member X1	2,2
A0JLT2	MED19	Mediator of RNA polymerase II transcription subunit 19	2,2
Q9NZC9	SMARCAL1	SWI/SNF-related matrix-associated actin-dependent regulator of chromatin subfamily A-like protein 1	2,2
Q06330	RBPJ	Recombining binding protein suppressor of hairless	2,3
Q6PML9	SLC30A9	Zinc transporter 9	2,4
O00625	PIR	Pirin	2,4
Q13268	DHRS2	Dehydrogenase/reductase SDR family member 2, mitochondrial	2,6
Q15011	HERPUD1	Homocysteine-responsive endoplasmic reticulum-resident ubiquitin-like domain member 1 protein	2,6
Q8WVM7	STAG1	Cohesin subunit SA-1	2,6
Q70IA6	MOB2	MOB kinase activator 2	2,8
O95479	H6PD	GDH/6PGL endoplasmic bifunctional protein	2,9
Q14691	GINS1	DNA replication complex GINS protein PSF1	3,0
O75911	DHRS3	Short-chain dehydrogenase/reductase 3	3,3
Q9BUH6	C9orf142	Protein PAXX	3,4
A8MXV4	NUDT19	Nucleoside diphosphate-linked moiety X motif 19, mitochondrial	3,4
Q99758	ABCA3	ATP-binding cassette sub-family A member 3	3,5
Q9HBM0	VEZT	Vezatin	3,6
P08134	RHOC	Rho-related GTP-binding protein RhoC	3,6
Q9BQ75	CMSS1	Protein CMSS1	3,8
Q06136	KDSR	3-ketodihydrospingosine reductase	3,8
Q6ZRV2	FAM83H	Protein FAM83H	3,9

Q8IYQ7	THNSL1	Threonine synthase-like 1	3,9
P29323	EPHB2	Ephrin type-B receptor 2	3,9
Q05193	DNM1	Dynamin-1	4,0
Q2KHT3	CLEC16A	Protein CLEC16A	4,1
Q7LBR1	CHMP1B	Charged multivesicular body protein 1b	4,3
Q9P0M9	MRPL27	39S ribosomal protein L27, mitochondrial	4,4
Q0VGL1	LAMTOR4	Ragulator complex protein LAMTOR4	4,5
P12830	CDH1	Cadherin-1	4,6
Q9BSF4	C19orf52	Uncharacterized protein C19orf52	4,7
Q9Y6W3	CAPN7	Calpain-7	4,8
O43292	GPAA1	Glycosylphosphatidylinositol anchor attachment 1 protein	4,9
Q6Y288	B3GALTL	Beta-1,3-glucosyltransferase	5,3
P00395	MT-CO1	Cytochrome c oxidase subunit 1	5,9

4.3.3. Bioinformatic analysis

The list of differentially regulated proteins was analyzed with Cytoscape software (version 3.6.1) using the STRING app and the ClueGO plugin. A global interaction network was built with the STRING app (Figure 15A). STRING enrichment produced a network constituted by 133 nodes and 208 edges with a PPI Enrichment value of 3.31×10^{-7} . Nodes in figure were labelled according to the values of the LFQ intensities, ranging from intense blue to violet for the lowest and the highest LFQ values, respectively. Next, ClueGO application was used for a single cluster analysis in order to obtain a significant GO terms enrichment. Applying a Kappa Score Threshold = 0.4 and checking in the resulting list for the OverViewTerm equal to "TRUE", ClueGO provided a number of 12 significant enriched GO terms (Figure 15B). Amongst these, "Membrane lipid biosynthetic process", "Cellular transition metal ion homeostasis", and "Tetrapyrrole metabolic process" result strictly related to metabolic pathways of propionate metabolism.

Further, a number of proteins apparently belonging to mitochondrial compartment was recognized in the differential proteome. Thus, the protein list was intersected with the human MitoCarta2.0 dataset. This has highlighted 26 out of 178 proteins (the 14.6% of the differential proteome) that were analyzed using String software version 11.0. The resulted interaction network was shown in Figure 16. Of note, the GO sub-analysis (threshold of false discovery rate ≤ 0.015) enriched for these proteins some interesting biological process and molecular function categories related to "oxidation-reduction process" (Table 4). String enriched interesting KEGG and Reactome pathways as well (Table 4). This mitochondrial protein sub-analysis highlights possible mitochondrial dysfunctions related to energy deficiency, redox unbalance and alterations in fatty acid metabolism in our MUT-KO cell model, in part already known for MMA patients. By the way, since this analysis came out from a global dataset, a dedicated mitochondrial proteome analysis will be performed.

Table 4. Details of GO sub-analysis enrichment of regulated mitochondrial proteins in MUT-KO using STRING.

Biological Process (GO)			
<i>GO-term</i>	<i>description</i>	<i>count in gene set</i>	<i>false discovery rate</i>
GO:0051186	cofactor metabolic process	8 of 467	5.50e-05
GO:0044281	small molecule metabolic process	13 of 1779	5.50e-05
GO:0055114	oxidation-reduction process	9 of 923	0.00033
GO:0051188	cofactor biosynthetic process	5 of 218	0.0014
GO:0046916	cellular transition metal ion homeostasis	4 of 99	0.0014

Molecular Function (GO)			
<i>GO-term</i>	<i>description</i>	<i>count in gene set</i>	<i>false discovery rate</i>
GO:0048037	cofactor binding	7 of 481	0.00035
GO:0004140	dephospho-CoA kinase activity	2 of 2	0.00072
GO:0050662	coenzyme binding	5 of 274	0.0014
GO:0050661	NADP binding	3 of 46	0.0014
GO:0016491	oxidoreductase activity	7 of 716	0.0014

KEGG Pathways			
<i>pathway</i>	<i>description</i>	<i>count in gene set</i>	<i>false discovery rate</i>
hsa01100	Metabolic pathways	8 of 1250	0.0047
hsa00630	Glyoxylate and dicarboxylate metabolism	2 of 28	0.0108
hsa04216	Ferroptosis	2 of 40	0.0141
hsa00280	Valine, leucine and isoleucine degradation	2 of 48	0.0150

Reactome Pathways			
<i>pathway</i>	<i>description</i>	<i>count in gene set</i>	<i>false discovery rate</i>
HSA-8978868	Fatty acid metabolism	5 of 171	0.00020
HSA-1430728	Metabolism	12 of 2032	0.00020
HSA-556833	Metabolism of lipids	7 of 721	0.00073
HSA-196854	Metabolism of vitamins and cofactors	4 of 185	0.0017
HSA-8978934	Metabolism of cofactors	2 of 19	0.0046
HSA-9609507	Protein localization	3 of 122	0.0064
HSA-77289	Mitochondrial Fatty Acid Beta-Oxidation	2 of 37	0.0113

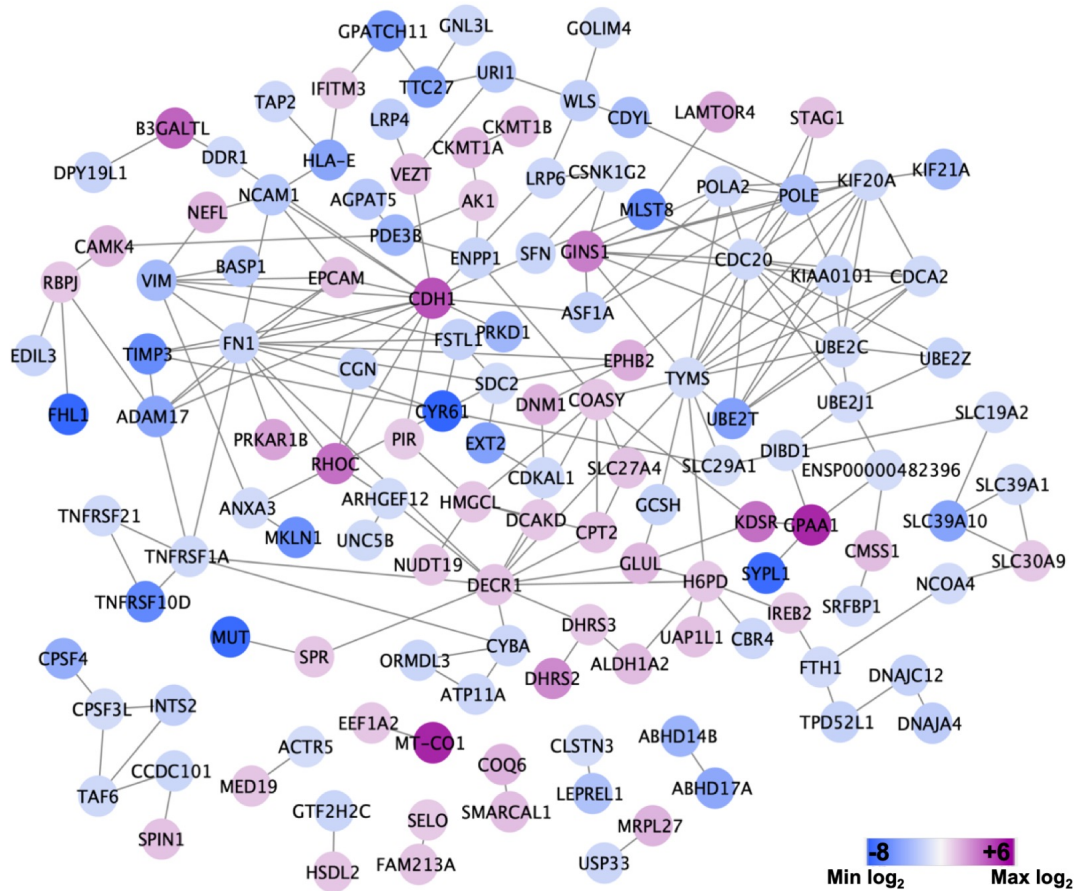
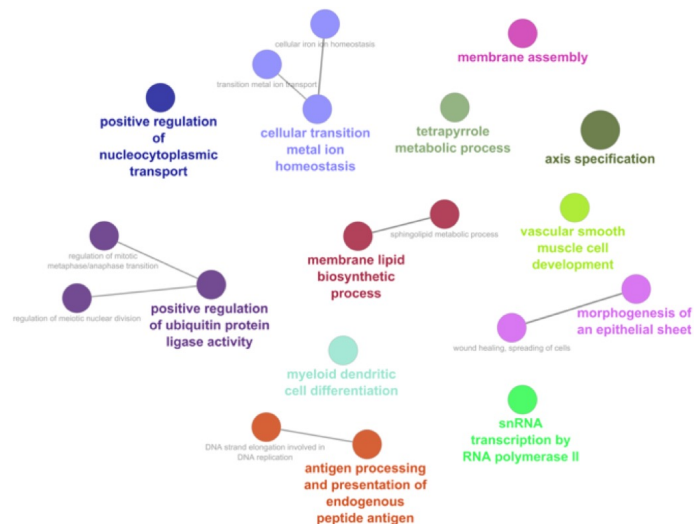
A**B**

Figure 15. Bioinformatic analysis of regulated proteome with Cytoscape. (A) Global interaction network of the differentially regulated proteins built with the STRING app within Cytoscape software. The nodes are differently coloured according to their LFQ values (from intense blue to purple for the lowest and the highest LFQ values, respectively). (B) ClueGO plugin provided a GO terms enrichment with a single cluster analysis. From the differential proteome dataset, 12 significant enriched GO terms were obtained.

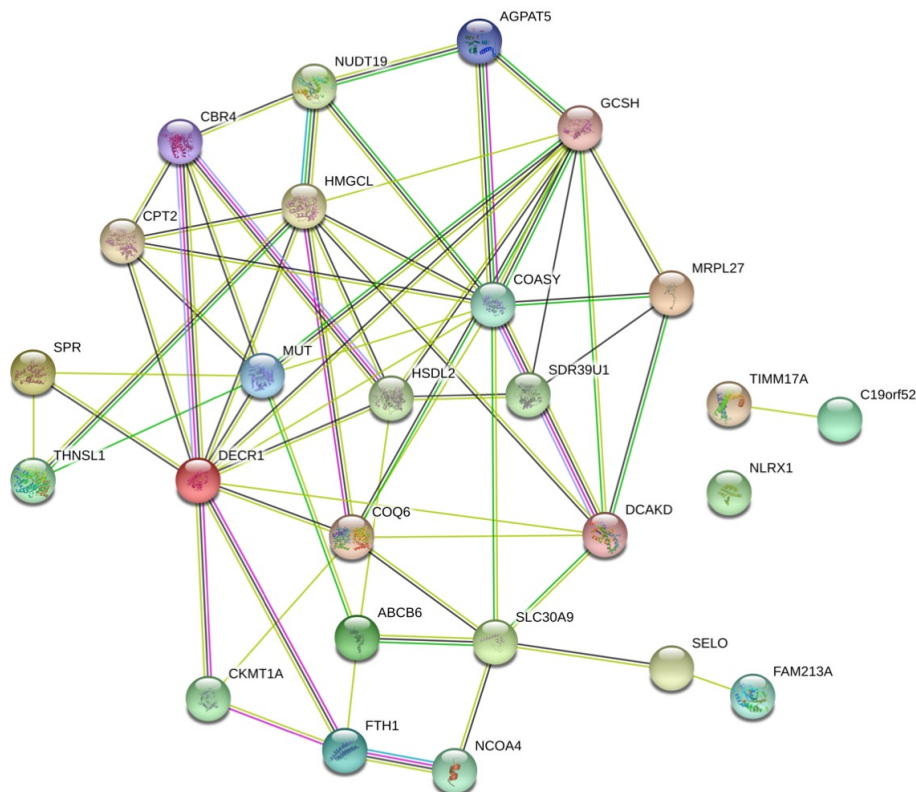


Figure 16. Protein-protein interaction network of differentially regulated mitochondrial proteins. From the list of differentially regulated proteins, 26 mitochondrial proteins were analyzed by String, in order to visualize their connections. For this network, a minimum of required interaction score of 0.150 was set.

4.3.4. Rescuing *MUT* expression in *MUT-KO* cells

In order to generate an additional cell model to control the specificity of KO effects, *MUT-KO* cells were transfected with a plasmid that ensured the stable expression of *MUT* protein. *MUT* expression was successfully rescued in the form of a *MUT-FLAG* (at N-terminus) protein. From a pool of transfected cells (*MUT-Rescue* pool), two single clones were cultured independently. The pool and the single clones showed by WB strong expression of *MUT* when compared with WT HEK293 cells (Figure 17A). Clones 1 and 2 were also tested for the presence of FLAG epitope fused to *MUT* recombinant protein and showed the expected FLAG signal (Figure 17B). Since clone 2 showed the best expression signals, it was selected to be used for the following experiments and, hereinafter, referred as *MUT-Rescue*. In addition, in order to test the influence of *MUT* rescuing on cell viability, Neutral-Red and MTT assays were performed on WT, *MUT-KO* and *MUT-Rescue* cells. Cell viability of *MUT-Rescue* samples showed no difference with the other two cell types (Figure 17C,D). From this point, all the experiments were conducted in parallel also using *MUT-Rescue* as additional control for the rescue of *MUT-KO*-induced effects.

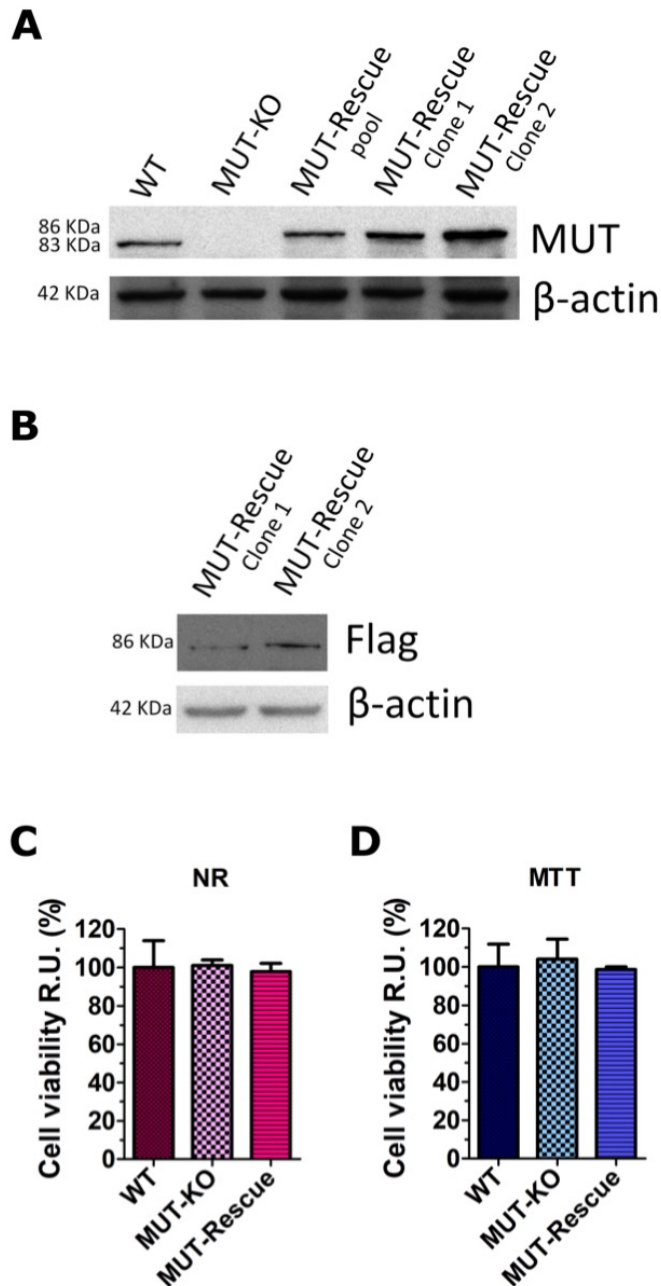


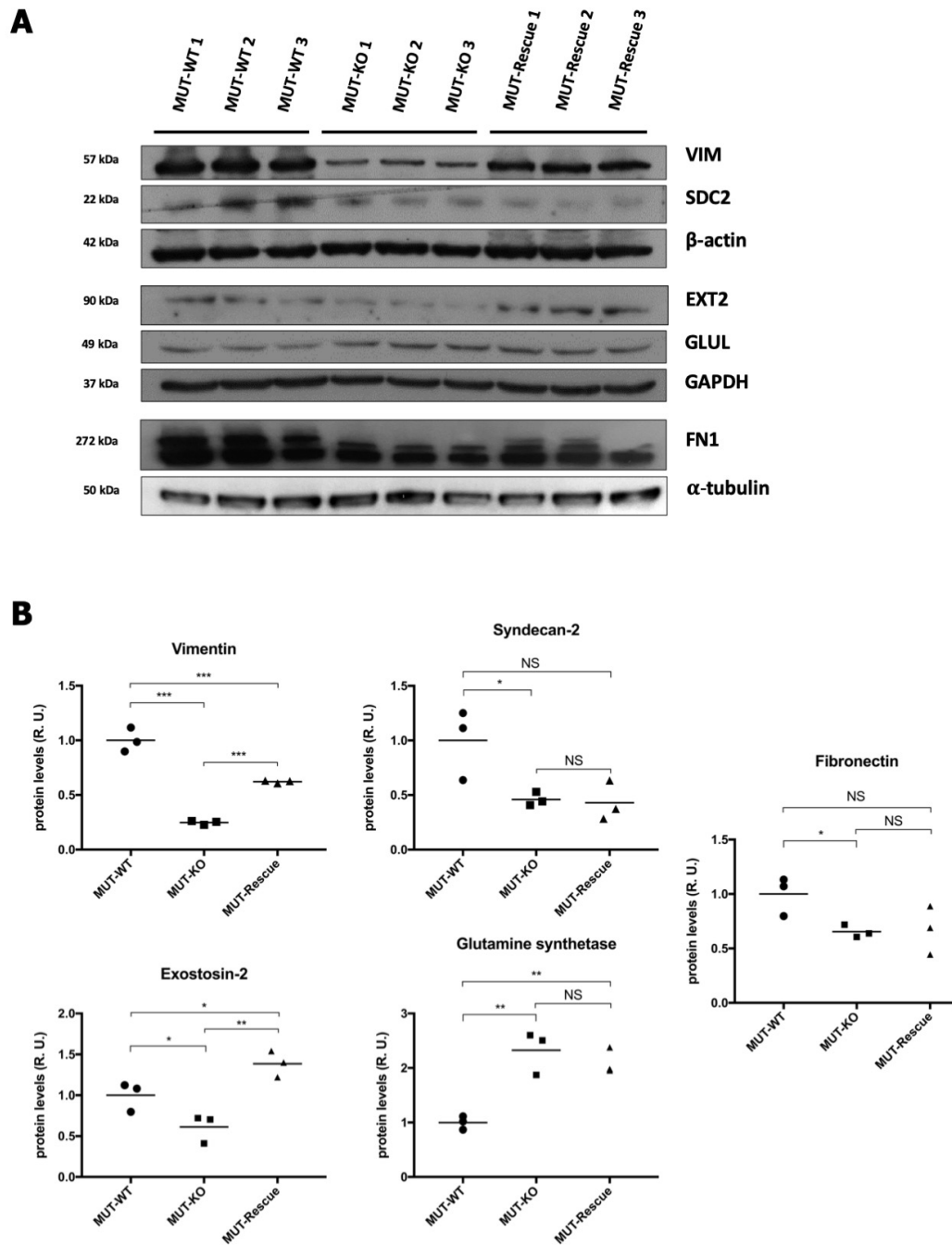
Figure 17. Western blot analysis and cell viability assays of MUT-KO cells after stable transfection for MUT rescuing. (A) WB analysis of the whole FLAG-MUT cell population (MUT-Rescue pool) and two single cell clones (MUT-Rescue clone 1 and 2) isolated from MUT-Rescue clone 1 and 2. WT and MUT-KO were used as control; β -actin was used as loading control. (B) Anti-FLAG detection of MUT-Rescue clones 1 and 2. WT and MUT-KO were used as control; β -actin was used as loading control. (C) Neutral-Red (NR) and (D) MTT assays for the comparison of cell viability of WT, MUT-KO and MUT-Rescue cells. Absorbance values were normalized to those of WT cells and expressed as cell viability percentage relative units (R.U.). Data are the mean of four biological replicates \pm SD. One-way two-tail paired t-test was used to calculate the statistical differences between the three groups. No statistically relevant difference was observed.

4.3.5. Validation of proteomic results and protein expression analysis

In order to confirm proteomic results, mass spectrometry-based protein identification was validated by WB in WT and MUT-KO cells. In addition, quantitative WB analysis was also performed on MUT-Rescue samples to track protein expression profiles changes in all the cell conditions. It can be supposed that specific MUT-KO effects should not be visible in the MUT-Rescue, if strictly dependent upon MUT absence, after its reintroduction into the cell. To carry on validation experiments, 5 proteins were chosen from the dataset: densitometry analysis confirmed the down-regulation of vimentin (VIM), syndecan-2 (SDC2), exostosin-2 (EXT2) and fibronectin (FN1), and the up-regulation of glutamine synthetase (GLUL) in MUT-KO (Figure 18A,B). For the MUT-Rescue condition, only EXT2 and VIM, but not SDC2, GLUL and FN1, seemed to show a trend of expression similar to WT (Figure 18A,B), suggesting that quantitative changes of these two proteins may be strictly related to MUT deficiency in the MUT-KO model.

In addition to WB experiments, qRT-PCR analysis revealed a diminished expression of VIM and EXT2 in MUT-KO cells also at the gene level (Figure 19). This could imply that the observed differences in VIM and EXT2 protein expression actually depend on a transcriptional regulation. Similarly to WB detection, the trend of expression of VIM is then reverted in MUT-Rescue resembling the WT condition. On the other hand, qRT-PCR analysis revealed that EXT2 gene expression is not reverted after rescuing MUT suggesting that in MUT-Rescue cells the regulation of EXT2 may be controlled at protein level.

Moreover, VIM expression was tested in the urine of MUT patients. Two MUT patients (MUT 1, MUT 2) and three healthy controls (control 1, control 2, control 3) were employed in WB experiments; two MMA with homocystinuria cblC type patients (CblC 1, CblC 2) were used as additional controls (Figure 20). Assuming an expected trend similar to proteomic results of MUT-KO, a diminished expression of VIM was validated only in one out of two MUT patients (namely MUT 2) while, surprisingly, both CblC 1 and 2 patients showed very low expression levels of the protein. This may indicate the involvement of VIM also in the Cbl-related MMA forms and not only in isolated MMA representing the result of a common alteration for both disorders.



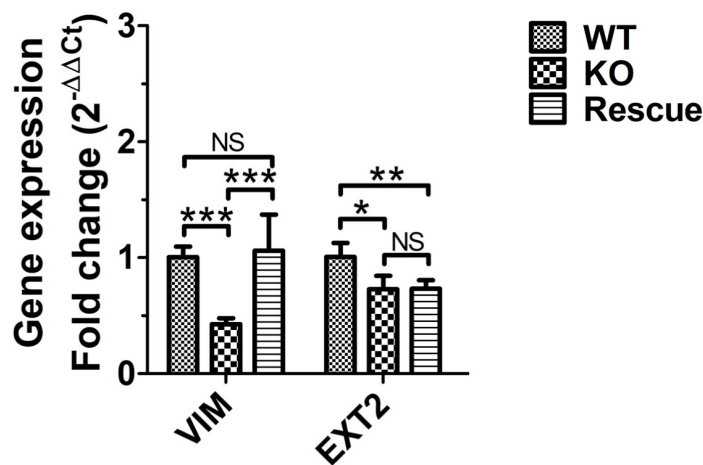


Figure 19. Analysis of gene expression levels in MUT-KO and MUT-Rescue by qRT-PCR. Vimentin and exostosin-2 transcript levels were measured by qRT-PCR in the analyzed cell lines. VIM expression resulted diminished in MUT-KO cells while its levels return similar to those of WT in MUT-Rescue. A significant reduction of EXT2 is detected in MUT-KO compared to WT, while gene expression is not reverted in MUT-Rescue. Relative gene expression levels were normalized to those of RNA polymerase II, α -tubulin and β -actin genes and calculated using the $2^{-\Delta\Delta C_t}$ method and reported as fold-change. Bars are the mean of four biological replicates while bar errors indicate SD. Statistical significance was calculated by one-way two-tail unpaired t-test; *** = $p < 0.005$.

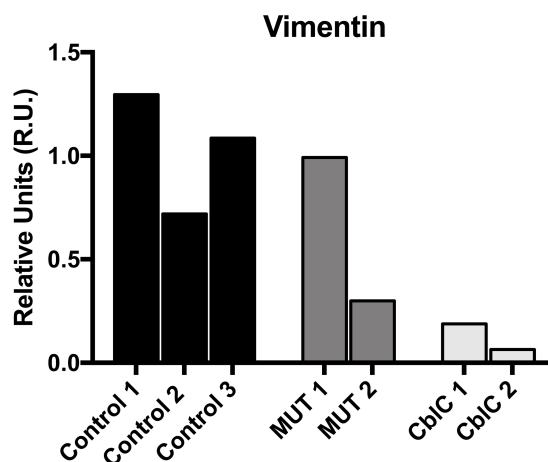


Figure 20. Western blot analysis of vimentin expression in urine from patients. Vimentin expression was tested in the urines of two MMA patients (MUT1, MUT 2). Three healthy donors (control 1, 2, 3) were used as controls; two MMA with homocystinuria cblC type patients (CblC 1, CblC 2) were used as additional control. One out of two MUT urines showed diminished VIM expression if compared to controls 1, 2 and 3, according to LFQ proteomics. Both CblC 1 and 2 patients also showed very low levels of the protein. VIM signals for each sample were normalized to the intensity of the respective lane detected by Ponceau S staining.

4.3.6. *MUT* knockout impairs cell viability and mitochondrial functionality in propionate-enriched culture medium

Since previous results on siRNA *MUT* cells showed impairment of mitochondrial functionality (*Results, 4.1.4*), Neutral-Red and MTT assays were repeated for *MUT*-KO cells in propionate-enriched culture medium. Both the assays were performed at three time points (24, 48 and 72 h) at 10 and 25 mM propionate concentration (Figure 21). Neutral-Red assay showed no significant difference between the three cell types (WT, *MUT*-KO and *MUT*-Rescue) at tested propionate concentrations at different time points. Even in MTT assay, 10 mM showed no significant effect, while treatment with 25 mM propionate caused significant reduction in MTT absorbance of *MUT*-KO cells at 48 and 72 hours. These results imply that 25 mM propionate is able to induce reduction of mitochondrial functionality (succinate dehydrogenase activity) in *MUT*-KO cells while this effect is not detectable in *MUT*-expressing cells.

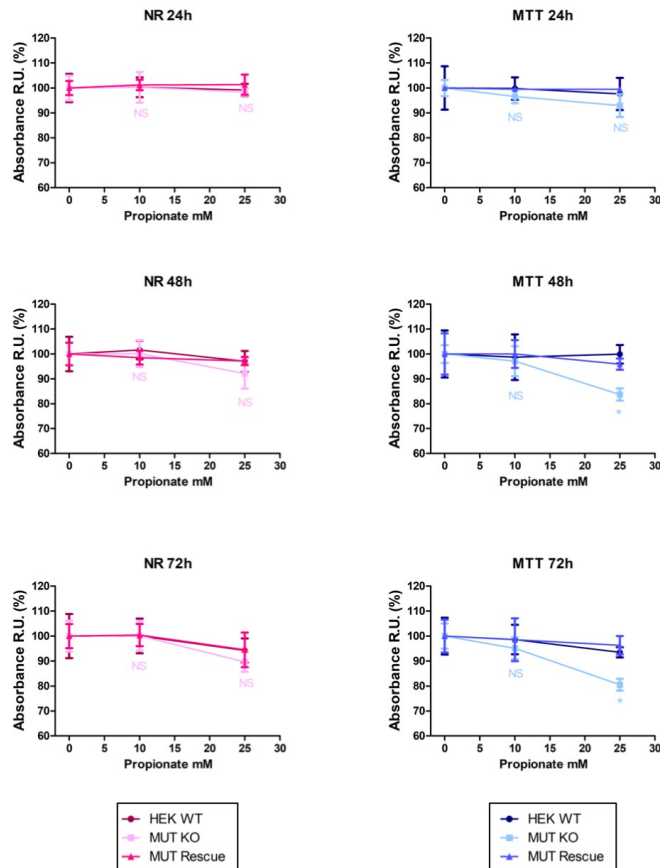


Figure 21. Viability and mitochondrial functionality of WT, *MUT*-KO and *MUT*-Rescue cells in propionate-enriched culture medium by Neutral-Red and MTT assay. Absorbance values were acquired at 10 and 25 mM propionate concentration at three time points (24, 48 and 72 h) for each cell type and expressed as fold change (relative units, R.U.) to the respective non-treated (0 h) time point. Data were reported as mean values of three independent experimental replicates \pm SD. One-way two-tail paired t-test was used to calculate the statistical significance of differences between the three tested cell types. * = $p < 0.05$; NS = not significant ($p > 0.05$).

4.3.7. *MUT* knockout increases the intracellular levels of ROS

As can be inferred from proteomics, bioinformatics and viability assays results, the alteration of mitochondrial functionality in *MUT*-KO is clearly evident. At this point, an unbalance in the redox state may be detected in *MUT*-KO cell model and, eventually, addressed to *MUT* absence. To this aim, the cellular oxidative stress was investigated by H₂DCFDA fluorescence assay measuring the intracellular levels of Reactive Oxygen Species (ROS) generated by WT, *MUT*-KO and *MUT*-Rescue cells. The assay was conducted in native conditions and after treatment with 100 μ M H₂O₂. Figure 22 shows that ROS detection was significantly higher in *MUT*-KO cells in native conditions if compared to WT and *MUT*-Rescue ones. An increase in ROS levels was relevant also after incubation with H₂O₂, thus suggesting that, in absence of *MUT* protein, the cells accumulate more ROS, even when oxidative stress is induced.

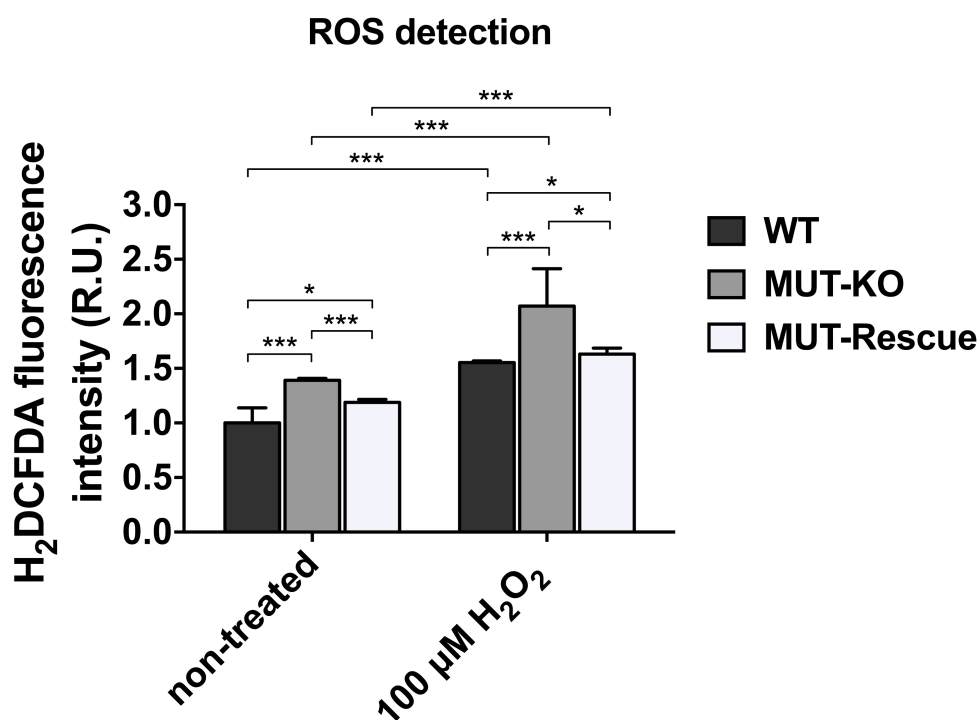


Figure 22. Determination of intracellular ROS levels in WT, *MUT*-KO and *MUT*-Rescue. H₂DCFDA fluorescence assay was employed to determine intracellular ROS levels in non-treated and 100 μ M H₂O₂-treated WT, *MUT*-KO and *MUT*-Rescue cells. Three technical measures of three independent biological replicates were averaged and normalized to the total protein amount of each sample. Normalized values were expressed as fold change (relative units, R.U.) with respect to WT control cells. Bars are mean values of the three replicate experiments \pm SD. The statistical significance of differences between the three cell types and in both treatment conditions was calculated by one-way two-tail paired t-test. * = $p < 0.05$; *** = $p < 0.005$. CTRL = control (non-treated) cells.

4.3.8. *MUT* knockout hampers proteoglycan levels

Through the analysis of proteomic results, it was possible to notice that the glycosyltransferase exostosin-2 and the glycoproteins syndecan-2 and fibronectin were down-regulated in *MUT*-KO cells (EXT2 was around 6-fold reduced). EXT2, SDC2 and FN1 down-regulation was confirmed in *MUT*-KO by WB (Figure 18A,B). Interestingly, EXT2 levels showed a trend of expression similar to WT after *MUT* rescuing (Figure 18A,B). Thus, in order to investigate the possible effects of *MUT* knockout on glycoproteins, a microscopy analysis was performed in WT, *MUT*-KO and *MUT*-Rescue cells after wheat germ agglutinin (WGA) staining. WGA is a lectin that, binding to glycoconjugates (N-acetyl-D-glucosamine and sialic acid residues), label cell membranes for imaging analyses (Monsigny et al., 1980). *MUT*-KO showed a significant lower fluorescent-WGA signal compared to WT and *MUT*-Rescue cells, while the rescue of *MUT* seems to partially revert this effect (Figure 23B). Moreover, the staining pattern is different in the three cell types. In WT cells, the appearance of WGA staining is very definite and delimits sharply the cell borders. On the contrary, the staining of *MUT*-KO seems much more diffuse, while in *MUT*-Rescue it seems halfway between the other two cell types (Figure 23A). These phenomena suggest that *MUT* knockout could impair either the distribution and organization of glycoproteins or the synthesis of their glycosidic chains, or both.

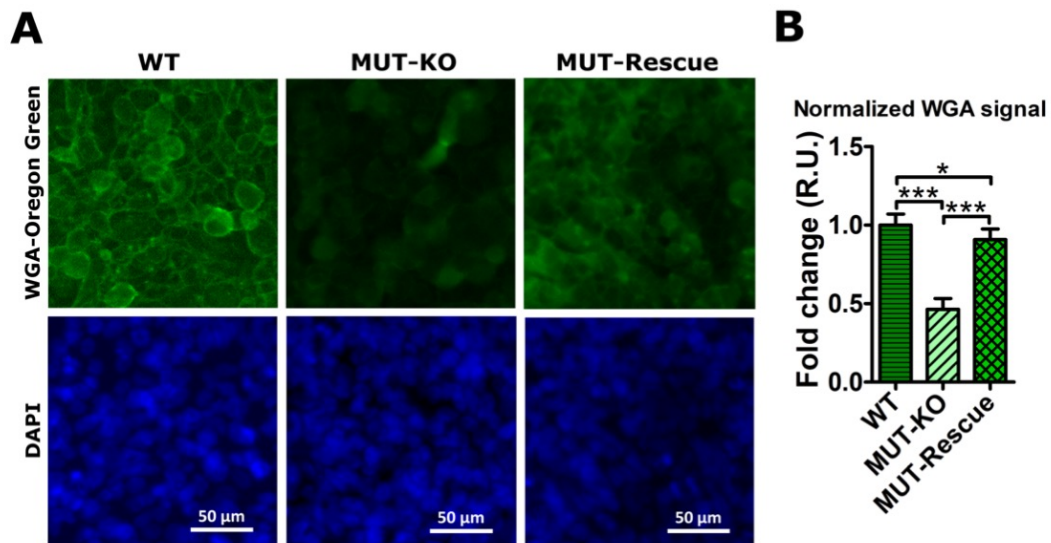


Figure 23. Microscopy analysis of fluorescent WGA staining. A) Microscopy images of WT, *MUT*-KO and *MUT*-Rescue cells after staining with Oregon Green-labeled wheat germ agglutinin (WGA) and DAPI. A Leica DMI 4000 B inverted microscope (40X objective) was used; images were acquired with Leica LAS AF software. B) Quantitative analysis of fluorescent signals was performed in three independent biological replicates and three microscope fields were acquired for each biological replicate. Signal intensity of acquired micrographs was measured by ImageJ software. WGA signals were normalized to DAPI signals and expressed as fold change (relative units, R.U.) with respect to WT. Data were reported as mean of the three biological replicates \pm SD. One-way two-tail paired t-test was used to calculate the statistical significance of differences between the three tested cell types. * = $p < 0.05$; *** = $p < 0.005$.

4.3.9. DIA-based global proteomic analysis of MUT-KO and MUT-Rescue cells

In order to have a comprehensive overview related to the omics investigation for MMA cell models, a new Data-Independent Acquisition (DIA) proteomic experiment was performed on MUT-KO including also MUT-Rescue as control for the recovery of MUT-KO effects. DIA experiment was designed in order to have a better identification coverage of proteomes and check rescue effect on protein expression levels by a proteomic point of view. In particular, five biological sample replicates per condition (WT, MUT-KO, MUT-Rescue) were analyzed by LC-MS/MS using a Q Exactive HF mass spectrometer. DIA runs, elaborated with Spectronaut Pulsar software, provided abundances, called Protein Group (PG).Quantity, for all the proteins of the dataset. A very stringent data analysis was carried out considering the comparisons KO/WT and KO/RES, in order to retrieve the relative abundance of protein in KO samples with respect to WT and MUT-Rescue. KO/WT comparison resulted in 90 regulated proteins, while KO/RES comparison in 70 regulated proteins, out of the around 6000 proteins identified in total. Amongst these, MUT protein was highly down-regulated in both comparisons, confirming once again positive results of CRISPR/Cas9 genome editing on MUT-KO cell line. Tables 5 and 6 report the lists of differentially regulated proteins for KO/WT and KO/RES ratios, respectively. Tables, including the UniProt ID, protein name and \log_2 of PG.Quantity, were sorted in a crescent order for the PG.Quantity values.

In addition, all the proteins common to both lists (regulated in both KO/WT and KO/RES) were found to have the same trend of regulation (Table 7). Interestingly, these proteins should be the ones whose dysregulated levels of expression in MUT-KO return similar to WT after MUT rescuing, thus suggesting that they may be strictly related to MUT absence. Of note, exostosin-1 (EXT1) was found up-regulated in MUT-KO and its levels are reverted in MUT-Rescue. EXT1 is a glycosyltransferase that forms a complex with EXT2 (which was validated to be down-regulated in MUT-KO, *Results*, 4.3.5) committed in the biosynthesis of heparan sulfates, thus reinforcing the hypothesis of proteoglycan alterations or involvement in the molecular mechanisms of MMA pathophysiology.

Table 5. List of the differentially regulated proteins identified by DIA-LC-MS/MS analysis in MUT-KO versus WT cell line.

UniProt ID	Protein name	PG.Quantity
Q9NRS6	Sorting nexin-15	-9,00
P09493	Tropomyosin alpha-1 chain	-8,89
P22033	Methylmalonyl-CoA mutase, mitochondrial	-8,01
Q13191	E3 ubiquitin-protein ligase CBL-B	-7,28
Q9H0R1	AP-5 complex subunit mu-1	-6,87
O95989	Diphosphoinositol polyphosphate phosphohydrolase 1	-6,21
Q92558	Wiskott-Aldrich syndrome protein family member 1	-6,06
Q96MW1	Coiled-coil domain-containing protein 43	-5,99
Q9H5N1	Rab GTPase-binding effector protein 2	-5,82
Q16890	Tumor protein D53	-5,79
Q9H008	Phospholysine phosphohistidine inorganic pyrophosphate phosphatase	-5,75
Q9UHK0	Nuclear fragile X mental retardation-interacting protein 1	-5,68
Q15283	Ras GTPase-activating protein 2	-5,61
Q96EM0	Trans-3-hydroxy-L-proline dehydratase	-5,57
Q6ZT21	Transmembrane protein with metallophosphoesterase domain	-5,32
Q6QNY1	Biogenesis of lysosome-related organelles complex 1 subunit 2	-5,09
P13591	Neural cell adhesion molecule 1	-4,70
P14649	Myosin light chain 6B	-4,59
O00221	NF-kappa-B inhibitor epsilon	-4,52
P16870	Carboxypeptidase E	-4,40
P03897	NADH-ubiquinone oxidoreductase chain 3	-4,32
Q96B97	SH3 domain-containing kinase-binding protein 1	-4,18
Q9H999	Pantothenate kinase 3	-3,91
P55854	Small ubiquitin-related modifier 3	-3,88
Q6ZN55	Zinc finger protein 574	-3,82
Q8NI22	Multiple coagulation factor deficiency protein 2	-3,74
Q96EQ0	Small glutamine-rich tetratricopeptide repeat-containing protein beta	-3,53
O75157	TSC22 domain family protein 2	-3,52
Q9U1L1	Short coiled-coil protein	-3,38
Q961Z7	Serine/Arginine-related protein 53	-3,17
P35226	Polycomb complex protein BMI-1	-3,15
Q96EA4	Protein Spindly	-2,75
Q5VXT5	Synaptophysin-like protein 2	-2,73
Q9H098	Protein FAM107B	-2,71
Q8N7R7	Cyclin-Y-like protein 1	-2,69
O14618	Copper chaperone for superoxide dismutase	-2,57
Q13614	Myotubularin-related protein 2	-2,49
O75496	Geminin	-2,31
Q14728	Major facilitator superfamily domain-containing protein 10	-2,29
Q9HD15	Steroid receptor RNA activator 1	-2,28
P23610	Factor VIII intron 22 protein	-2,23
Q96A54	Adiponectin receptor protein 1	-2,22
P08651	Nuclear factor 1 C-type	2,22
P00519	Tyrosine-protein kinase ABL1	2,23
Q7L3S4	Zinc finger protein 771	2,25
Q15361	Transcription termination factor 1	2,28
Q9Y4K1	Beta/gamma crystallin domain-containing protein 1	2,32
Q9BQE5	Apolipoprotein L2	2,45
Q9NTG7	NAD-dependent protein deacetylase sirtuin-3, mitochondrial	2,48
P51688	N-sulphoglucosamine sulphohydrolase	2,61
Q15642	Cdc42-interacting protein 4	2,71
P78549	Endonuclease III-like protein 1	2,72
Q8NDF8	Non-canonical poly(A) RNA polymerase PAPD5	2,72
Q96CS4	Zinc finger protein 689	2,79

Q12860	Contactin-1	2,80
Q9GZT4	Serine racemase	2,89
P40426	Pre-B-cell leukemia transcription factor 3	3,01
Q9H7Z3	Protein NRDE2 homolog	3,01
Q13509	Tubulin beta-3 chain	3,07
O14656	Torsin-1A	3,08
Q96LD4	Tripartite motif-containing protein 47	3,12
Q9UPW5	Cytosolic carboxypeptidase 1	3,26
Q8N4J0	Carnosine N-methyltransferase	3,37
Q16394	Exostosin-1	3,59
Q7Z392	Trafficking protein particle complex subunit 11	3,67
Q08AE8	Protein spire homolog 1	3,82
Q8N9N5	Protein BANP	3,87
Q6DT37	Serine/threonine-protein kinase MRCK gamma	3,92
Q96S19	Methyltransferase-like 26	4,02
Q14938	Nuclear factor 1 X-type	4,09
O43278	Kunitz-type protease inhibitor 1	4,30
Q05481	Zinc finger protein 91	4,35
O75582	Ribosomal protein S6 kinase alpha-5	4,39
Q9NWR8	Calcium uniporter regulatory subunit MCUb, mitochondrial	4,56
Q63HN8	E3 ubiquitin-protein ligase RNF213	4,59
Q6P5Z2	Serine/threonine-protein kinase N3	4,61
P42575	Caspase-2	4,92
Q14145	Kelch-like ECH-associated protein 1	5,02
Q8TEB9	Rhomboid-related protein 4	5,05
O14657	Torsin-1B	5,17
O95210	Starch-binding domain-containing protein 1	5,19
Q9UGJ1	Gamma-tubulin complex component 4	5,29
Q9NYM9	BET1-like protein	5,34
Q9UI14	Prenylated Rab acceptor protein 1	5,51
Q86WA6	Valacyclovir hydrolase	5,61
Q9H6S3	Epidermal growth factor receptor kinase substrate 8-like protein 2	5,65
Q9UDX5	Mitochondrial fission process protein 1	6,00
Q6UW68	Transmembrane protein 205	6,44
O00115	Deoxyribonuclease-2-alpha	6,57
Q8NFV4	Protein ABHD11	7,21

Table 6. List of the differentially regulated proteins identified by DIA-LC-MS/MS analysis in MUT-KO versus MUT-Rescue cell line.

UniProt ID	Protein name	PG.Quantity
P22033	Methylmalonyl-CoA mutase, mitochondrial	-10,69
Q7Z2E3	Aprataxin	-6,68
Q96MW1	Coiled-coil domain-containing protein 43	-5,87
Q92558	Wiskott-Aldrich syndrome protein family member 1	-5,73
Q6ZT21	Transmembrane protein with metallophosphoesterase domain	-5,72
P49459	Ubiquitin-conjugating enzyme E2 A	-5,58
P03886	NADH-ubiquinone oxidoreductase chain 1	-5,29
Q9H008	Phospholysine phosphohistidine inorganic pyrophosphate phosphatase	-5,15
O95989	Diphosphoinositol polyphosphate phosphohydrolase 1	-5,11
Q7Z6K5	Arpin	-4,80
Q9H6K5	Proline-rich protein 36	-4,67
Q9NX18	Succinate dehydrogenase assembly factor 2, mitochondrial	-4,65
Q96B97	SH3 domain-containing kinase-binding protein 1	-4,61
P14649	Myosin light chain 6B	-4,36

Q9NQS1	Cell death regulator Aven	-4,32
Q9UIL1	Short coiled-coil protein	-4,27
P13591	Neural cell adhesion molecule 1	-4,03
P55854	Small ubiquitin-related modifier 3	-3,91
Q9H999	Pantothenate kinase 3	-3,85
Q9Y625	Glypican-6	-3,70
O14763	Tumor necrosis factor receptor superfamily member 10B	-3,65
P16870	Carboxypeptidase E	-3,57
P19419	ETS domain-containing protein Elk-1	-3,46
Q6NZ67	Mitotic-spindle organizing protein 2B	-3,28
Q96EQ0	Small glutamine-rich tetratricopeptide repeat-containing protein beta	-3,06
Q92994	Transcription factor IIIB 90 kDa subunit	-3,05
P17900	Ganglioside GM2 activator	-2,99
Q8N7R7	Cyclin-Y-like protein 1	-2,93
O14618	Copper chaperone for superoxide dismutase	-2,84
Q8TAP8	Protein phosphatase 1 regulatory subunit 35	-2,57
Q96B23	Uncharacterized protein C18orf25	-2,52
Q8WWB7	Glycosylated lysosomal membrane protein	-2,47
Q13686	Nucleic acid dioxygenase ALKBH1	-2,43
Q86TS9	39S ribosomal protein L52, mitochondrial	-2,42
Q96EA4	Protein Spindly	-2,41
O75157	TSC22 domain family protein 2	-2,37
Q9NW15	Anoctamin-10	-2,33
Q96IY1	Kinetochores-associated protein NSL1 homolog	-2,32
Q9NVM6	DnaJ homolog subfamily C member 17	-2,23
Q15013	MAD2L1-binding protein	-2,22
P23610	Factor VIII intron 22 protein	-2,10
Q9Y3D8	Adenylate kinase isoenzyme 6	-2,06
Q7L592	Protein arginine methyltransferase NDUF7, mitochondrial	1,96
O75582	Ribosomal protein S6 kinase alpha-5	2,11
P02462	Collagen alpha-1(IV) chain	2,14
A0PJW6	Transmembrane protein 223	2,15
Q9P003	Protein cornichon homolog 4	2,30
P16298	Serine/threonine-protein phosphatase 2B catalytic subunit beta isoform	2,33
Q9P0U3	Sentrin-specific protease 1	2,33
Q17RS7	Flap endonuclease GEN homolog 1	2,37
Q6F5E8	Capping protein, Arp2/3 and myosin-I linker protein 2	2,49
Q6UW68	Transmembrane protein 205	2,53
Q9BSY9	Deubiquitinase DES12	2,88
O75648	Mitochondrial tRNA-specific 2-thiouridylase 1	2,95
Q6N069	N-alpha-acetyltransferase 16, NatA auxiliary subunit	3,10
Q5BJF6	Outer dense fiber protein 2	3,27
Q16394	Exostosin-1	3,59
Q8N9N5	Protein BANP	3,87
P0CJ78	Zinc finger protein 865	3,90
O43353	Receptor-interacting serine/threonine-protein kinase 2	3,90
Q9UK58	Cyclin-L1	4,15
O43278	Kunitz-type protease inhibitor 1	4,30
Q9HBE1	POZ-, AT hook-, and zinc finger-containing protein 1	4,47
Q92581	Sodium/hydrogen exchanger 6	4,48
P78549	Endonuclease III-like protein 1	5,01
Q14145	Kelch-like ECH-associated protein 1	5,02
Q86SQ9	Dehydrolipoyl diphosphate synthase complex subunit DHDDS	5,03
Q9H7L9	Sin3 histone deacetylase corepressor complex component SDS3	5,11
Q96R72	Olfactory receptor 4K3	6,10
O75911	Short-chain dehydrogenase/reductase 3	7,51

Table 7. Regulated proteins identified in both KO/WT and KO/RES comparisons have the same trend of regulation.

UniProt ID	Protein name	PG.Quantit y KO/WT	PG.Quantit y KO/RES
P22033	Methylmalonyl-CoA mutase, mitochondrial	-8,01	-10,69
O95989	Diphosphoinositol polyphosphate phosphohydrolase 1	-6,21	-5,11
Q92558	Wiskott-Aldrich syndrome protein family member 1	-6,06	-5,73
Q96MW1	Coiled-coil domain-containing protein 43	-5,99	-5,87
Q9H008	Phospholysine phosphohistidine inorganic pyrophosphate phosphatase	-5,75	-5,15
Q6ZT21	Transmembrane protein with metallophosphoesterase domain	-5,32	-5,72
P13591	Neural cell adhesion molecule 1	-4,70	-4,03
P14649	Myosin light chain 6B	-4,59	-4,36
P16870	Carboxypeptidase E	-4,40	-3,57
Q96B97	SH3 domain-containing kinase-binding protein 1	-4,18	-4,61
Q9H999	Pantothenate kinase 3	-3,91	-3,85
P55854	Small ubiquitin-related modifier 3	-3,88	-3,91
Q96EQ0	Small glutamine-rich tetratricopeptide repeat-containing protein beta	-3,53	-3,06
O75157	TSC22 domain family protein 2	-3,52	-2,37
Q9UIL1	Short coiled-coil protein	-3,38	-4,27
Q96EA4	Protein Spindly	-2,75	-2,41
Q8N7R7	Cyclin-Y-like protein 1	-2,69	-2,93
O14618	Copper chaperone for superoxide dismutase	-2,57	-2,84
P23610	Factor VIII intron 22 protein	-2,23	-2,10
P78549	Endonuclease III-like protein 1	2,72	5,01
Q16394	Exostosin-1	3,59	3,59
Q8N9N5	Protein BANP	3,87	3,87
O43278	Kunitz-type protease inhibitor 1	4,30	4,30
O75582	Ribosomal protein S6 kinase alpha-5	4,39	2,11
Q14145	Kelch-like ECH-associated protein 1	5,02	5,02
Q6UW68	Transmembrane protein 205	6,44	2,53

Moreover, proteins coming from the KO vs WT comparison (Table 5) were then compared with those found regulated in MUT-KO from the LFQ experiment (*Results, 4.3.2*) to find the similarities. In detail, 5 proteins were found regulated in both experiments, 3 of which showed the same trend of regulation: tumor protein D53, neural cell adhesion molecule 1 and cadherin-1. Also other proteins, vimentin, protein lin-28 homolog B, brain acid soluble protein 1, redox-regulatory protein FAM213A, spindlin-1, and GDH/6PGL endoplasmic bifunctional protein, which were not included in the final list (Table 5) because their abundance values were below the threshold despite they were statistically significant, showed the same trend of regulation of the previous experiment. However, it is worth mentioning that vimentin was identified in the LFQ experiment (Table 3), validated by WB in the cells and in (MMA and CblC) patients' urines and by qRT-PCR in the cells (*Results, 4.3.5*), and lastly identified in the DIA experiment. These data may strongly encourage for the consideration of VIM as an important protein to focus on for further studies and a possible target for a designed therapy for MMA patients.

4.4. Mapping the interactome of MMACHC protein

4.4.1. Stable generation of MMACHC-FLAG and GFP-FLAG HepG2-expressing cell lines

In order to get insight into the precise role that MMACHC protein has in the formation of AdoCbl, cofactor of MUT protein, interactomics experiments were performed. HepG2 cell line was transfected and cultured in order to ensure stable expression of recombinant MMACHC-FLAG protein. A recombinant FLAG-tagged green fluorescent protein (GFP) was stably transfected in an independent HepG2 cell line to be used as control of false positive interactions. Figure 24 shows fluorescent images from GFP-FLAG cell line and the WB detection of both recombinant proteins using anti-FLAG antibody.

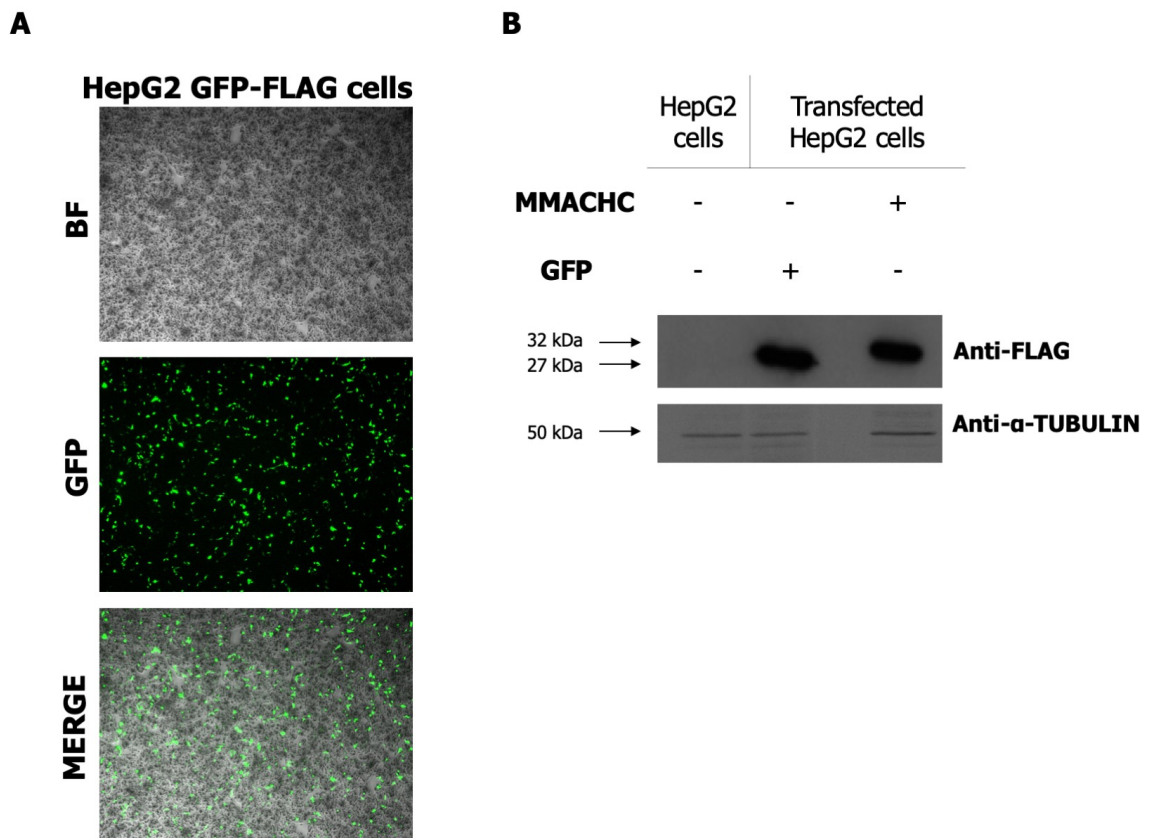


Figure 24. HepG2 cell line stably expresses GFP-FLAG and MMACHC-FLAG proteins. A) Microscopy analysis of HepG2 cell line expressing GFP protein. A Leica DMI 4000 B inverted microscope (10X objective) was used. B) GFP-FLAG and MMACHC-FLAG proteins are detectable in stably transfected HepG2 cells by WB using anti-FLAG antibody. In non-transfected HepG2 cells no signals were detected. Anti- α -tubulin was used as loading control. BF = phase-contrast bright field. GFP = green fluorescent protein.

4.4.2. Co-immunoprecipitation of MMACHC protein

MMACHC-FLAG protein was co-immunoprecipitated (IP) using magnetic anti-FLAG beads in order to isolate the “bait” and its cellular interactors. Parallel IP experiments were performed on GFP-FLAG HepG2-expressing cell line. All the experiments employed the use of three independent biological replicates per condition. Common interactors of both proteins will be assigned as random or non-specific interactors and not included in the final analysis. A first elution of IP complexes for both proteins (1st elution) was obtained by competition of FLAG peptide to isolate the IP complexes from the FLAG-beads used for IPs. Additionally, a non-specific 2nd elution was performed on the same samples as control that the majority of IP complexes were elute in the 1st elution. WB detection using anti-FLAG antibody revealed an enrichment of signals relative to GFP-FLAG and MMACHC-FLAG proteins in IP 1st elution compared to whole cell extracts. No MMACHC-FLAG signals were detected in the 2nd elution, showing that all the relative IP content was eluted in the 1st elution (Figure 25). IP 1st elution was used in the proteomic experiments for protein identification.

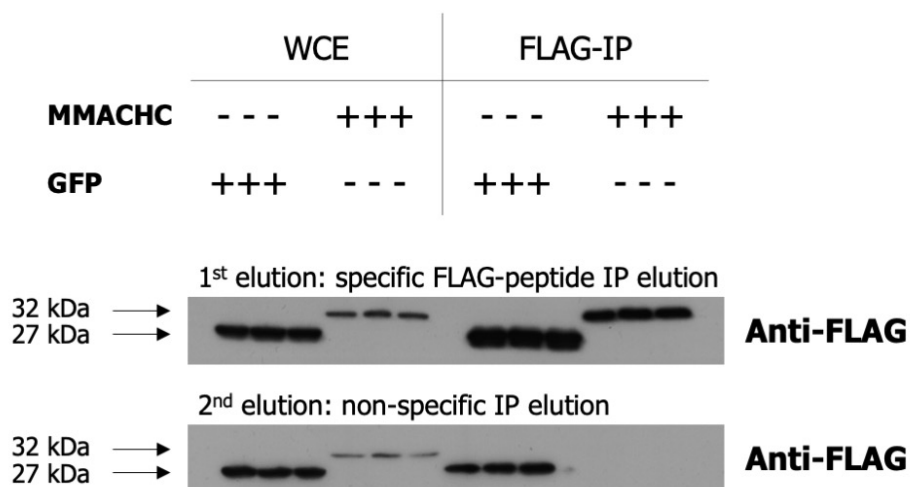


Figure 25. WB analysis of co-immunoprecipitation of MMACHC-FLAG and GFP-FLAG in transfected HepG2 cells. WB detection carried out using anti-FLAG antibody shows the enrichment of signals relative to GFP-FLAG and MMACHC-FLAG proteins in IP 1st elution compared to whole cell extracts of the same transfected cells. WCE = whole cell extract; FLAG-IP = co-immunoprecipitated samples.

4.4.3. MS-based identification of putative MMACHC interactors

The successfully obtained IP complexes for both FLAG-tagged proteins were used for subsequent LC-MS/MS-based protein identification. The experiment was carried out using two different strategies. Some aliquots of IP samples were resolved by SDS-PAGE (Figure 26) with following in-gel digestion and MS analysis. Two biological replicates were employed for this experiment. Other aliquots of the same samples were digested without prior electrophoretic separation using S-Trap columns and then analyzed by shotgun LC-MS/MS. Three biological replicates were employed for this experiment. The two generated lists of putative interactors were filtered as describe in *Material and Methods, 3.11*. Tables 8 and 9 show the identified putative interacting partners of MMACHC protein, including the UniProt ID, protein name, and number of peptides for each replicate of the experiments. Putative interactors of MMACHC protein will be validated performing WB analysis on IP complexes and reverse co-IP experiment by immunoprecipitating the putative interactor and revealing using MMACHC (or anti-FLAG) antibody.

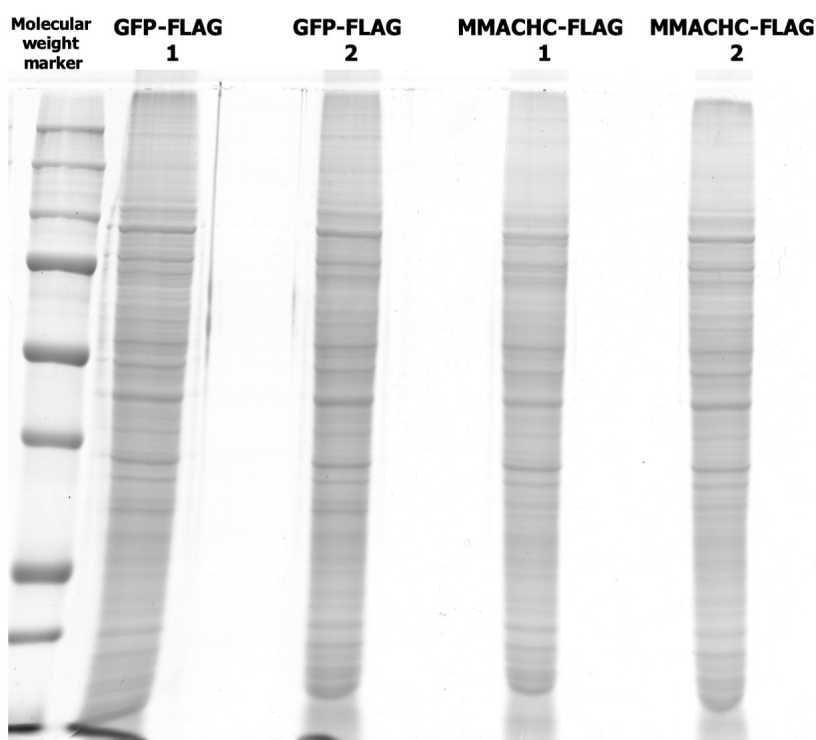


Figure 26. SDS-PAGE fractionation of GFP-FLAG and MMACHC-FLAG IPs. A 16 x 20 cm polyacrylamide gel was used to separate proteins. Coloration of fractionated samples was obtained with blue code staining reagent. Image acquisition was carried out using a scanning Densitometer S-800 (Bio-Rad). Ten bands for each lane were cut from the gel and digested by in situ hydrolysis.

Table 8. List of the putative interactors of MMACHC proteins identified in MMACHC-FLAG and GFP-FLAG IPs by gel-based LC-MS/MS.

UniProt ID	Protein name	GFP #peptides 2 biologic replicates	MMACHC #peptides 2 biologic replicates
Q9Y4U1	Methylmalonic aciduria and homocystinuria type C protein		11 10
Q9HA64	Ketosamine-3-kinase		6 6
Q13423	NAD(P) transhydrogenase, mitochondrial		5 10
Q9Y399	28S ribosomal protein S2, mitochondrial		5 8
Q00266	S-adenosylmethionine synthase isoform type-1		5 8
Q9NX63	MICOS complex subunit MIC19	1	5 5
Q9NVA2	Septin-11	1	5 3
P08590	Myosin light chain 3		5 2
P45379	Troponin T, cardiac muscle	1	5 2
O94776	Metastasis-associated protein MTA2	1	5 2
O75306	NADH dehydrogenase [ubiquinone] iron-sulfur protein 2, mitochondrial	1	4 5
Q96C19	EF-hand domain-containing protein D2		4 4
P52788	Spermine synthase		4 4
Q9HB07	UPF0160 protein MYG1, mitochondrial		4 4
Q08378	Golgin subfamily A member 3		4 4
Q9NP72	Ras-related protein Rab-18	1	4 4
P43897	Elongation factor Ts, mitochondrial	1	4 4
Q9NXA8	NAD-dependent protein deacetylase sirtuin-5, mitochondrial		4 3
Q9BVC6	Transmembrane protein 109		4 3
Q70IA6	MOB kinase activator 2		4 3
P41219	Peripherin	1	4 3
Q9Y3C8	Ubiquitin-fold modifier-conjugating enzyme 1		4 2
O75208	Ubiquinone biosynthesis protein COQ9, mitochondrial		4 2
O43681	ATPase ASNA1	1	4 2
Q15257	Serine/threonine-protein phosphatase 2A activator	1	3 7
O75915	PRA1 family protein 3		3 5
Q96AQ8	Mitochondrial calcium uniporter regulator 1		3 4
P53602	Diphosphomevalonate decarboxylase		3 4
Q9ULV4	Coronin-1C		3 4
Q99627	COP9 signalosome complex subunit 8	1	3 4
Q9NXS2	Glutamyl-peptide cyclotransferase-like protein	1	3 4
Q02750	Dual specificity mitogen-activated protein kinase kinase 1		3 3
O15126	Secretory carrier-associated membrane protein 1		3 3
Q9C0C9	E2/E3 hybrid ubiquitin-protein ligase UBE2O		3 3
Q86Y82	Syntaxin-12	1	3 3
Q92734	Protein TFG	1	3 3
A8MZ36	Envoplakin-like protein	1	3 3
Q9GZM8	Nuclear distribution protein nudE-like 1	1	3 3
Q14257	Reticulocalbin-2	1	3 3
Q15126	Phosphomevalonate kinase		3 3
Q9HC07	Transmembrane protein 165		3 2
P19429	Troponin I, cardiac muscle		3 2
Q92665	28S ribosomal protein S31, mitochondrial		3 2
P82979	SAP domain-containing ribonucleoprotein		3 2
Q13618	Cullin-3		3 2
Q96T51	RUN and FYVE domain-containing protein 1		3 2
O43617	Trafficking protein particle complex subunit 3	1	3 2
P51690	Arylsulfatase E	1	3 2
P20839	Inosine-5'-monophosphate dehydrogenase 1	1	3 2
P49590	Probable histidine--tRNA ligase, mitochondrial	1	3 2
Q9H943	Uncharacterized protein C10orf68	1	3 2
Q92882	Osteoclast-stimulating factor 1		3 2
Q9HBH5	Retinol dehydrogenase 14	1	2 8
Q7Z4V5	Hepatoma-derived growth factor-related protein 2		2 5
P00374	Dihydrofolate reductase		2 4
O43674	NADH dehydrogenase [ubiquinone] 1 beta subcomplex subunit 5, mitochondrial		2 4

Q3ZCQ8	Mitochondrial import inner membrane translocase subunit TIM50		1	2	4
Q9H3Z4	DnaJ homolog subfamily C member 5			2	3
Q92947	Glutaryl-CoA dehydrogenase, mitochondrial			2	3
Q86SE5	RNA-binding Raly-like protein			2	3
O15460	Prolyl 4-hydroxylase subunit alpha-2			2	3
P51857	3-oxo-5-beta-steroid 4-dehydrogenase			2	3
O43813	LanC-like protein 1			2	3
Q9Y3D3	28S ribosomal protein S16, mitochondrial	1		2	3
P82675	28S ribosomal protein S5, mitochondrial	1		2	3
P84157	Matrix-remodeling-associated protein 7		1	2	3
P42574	Caspase-3		1	2	3
Q14004	Cyclin-dependent kinase 13		1	2	3
Q9UBW8	COP9 signalosome complex subunit 7a			2	2
Q9GZN8	UPF0687 protein C20orf27			2	2
O75832	26S proteasome non-ATPase regulatory subunit 10			2	2
Q9C0E8	Protein lunapark			2	2
P61077	Ubiquitin-conjugating enzyme E2 D3			2	2
Q9GZT8	Putative GTP cyclohydrolase 1 type 2 NIF3L1			2	2
P46734	Dual specificity mitogen-activated protein kinase kinase 3			2	2
Q15526	Surfeit locus protein 1			2	2
Q8NDD1	Uncharacterized protein C1orf131			2	2
Q9NTG1	Polycystic kidney disease and receptor for egg jelly-related protein			2	2
Q9UDX5	Mitochondrial fission process protein 1	1		2	2
Q9UJW0	Dynactin subunit 4	1		2	2
Q9NS69	Mitochondrial import receptor subunit TOM22 homolog		1	2	2
Q9Y657	Spindlin-1		1	2	2
Q969U7	Proteasome assembly chaperone 2		1	2	2
Q8IY67	Ribonucleoprotein PTB-binding 1		1	2	2
Q16563	Synaptophysin-like protein 1		1	2	2
Q92600	Cell differentiation protein RCD1 homolog		1	2	2
Q9Y275	Tumor necrosis factor ligand superfamily member 13B		1	2	2
Q86UE4	Protein LYRIC		1	2	2

Table 9. List of the putative interactors of MMACHC proteins identified in MMACHC-FLAG and GFP-FLAG IPs by shotgun LC-MS/MS.

UniProt ID	Protein name	GFP #peptides 3 biologic replicates			MMACHC #peptides 3 biologic replicates		
Q9Y4U1	Methylmalonic aciduria and homocystinuria type C protein				11	13	15
Q8N110	Dedicator of cytokinesis protein 4				4	9	2
P16278	Beta-galactosidase	1			2	4	8
P49588	Alanine--tRNA ligase, cytoplasmic			1	4	6	2
P23458	Tyrosine-protein kinase JAK1				1	5	4
Q5JTZ9	Alanine--tRNA ligase, mitochondrial	1	1	1	3	3	3
P04792	Heat shock protein beta-1	1		1	2	4	3
Q3SY69	Mitochondrial 10-formyltetrahydrofolate dehydrogenase				4	4	5
P51812	Ribosomal protein S6 kinase alpha-3	1		1	1	5	2
Q9Y6N5	Sulfide:quinone oxidoreductase, mitochondrial	1	1	1	1	2	4
Q70IA6	MOB kinase activator 2				4	4	1
O94979	Protein transport protein Sec31A		1	1		5	2
P09651	Heterogeneous nuclear ribonucleoprotein A1				2	4	4
Q969G3	SWI/SNF-related matrix-associated actin-dependent regulator of chromatin subfamily E member 1				5	5	2
O95347	Structural maintenance of chromosomes protein 2			1	2	4	
P25205	DNA replication licensing factor MCM3				2	3	2

Q14141	Septin-6	1	1	1	3	4	2
Q8NI60	Chaperone activity of bc1 complex-like, mitochondrial			1	1	4	2
P84098	60S ribosomal protein L19		1		2	3	3
P28838	Cytosol aminopeptidase	1		1	1	3	2
P47755	F-actin-capping protein subunit alpha-2	1			1	2	4
O15160	DNA-directed RNA polymerases I and III subunit RPAC1				3	3	2
O60825	6-phosphofructo-2-kinase/fructose-2,6-bisphosphatase 2		1		2	2	2
Q9P270	SLAIN motif-containing protein 2		1		3	4	
P30086	Phosphatidylethanolamine-binding protein 1				2	3	3
P61163	Alpha-centractin	1	1	1	2	3	2
Q5SWX8	Protein odr-4 homolog				2	3	3
O00268	Transcription initiation factor TFIIID subunit 4	1			2	3	3
P10619	Lysosomal protective protein			1	2	3	2
Q13155	Aminoacyl tRNA synthase complex-interacting multifunctional protein 2	1			2	2	1
P30876	DNA-directed RNA polymerase II subunit RPB2	1		1	2	3	1
O43852	Calumenin				1	2	3
Q9NUI1	Peroxisomal 2,4-dienoyl-CoA reductase		1		3	2	2
P61221	ATP-binding cassette sub-family E member 1				1	3	2
Q16186	Proteasomal ubiquitin receptor ADRM1					3	3
O15269	Serine palmitoyltransferase 1				2	2	
Q96HP0	Dedicator of cytokinesis protein 6		1		1	2	
Q93009	Ubiquitin carboxyl-terminal hydrolase 7				2	1	2
Q15067	Peroxisomal acyl-coenzyme A oxidase 1					2	2
Q9UBF2	Coatomer subunit gamma-2					2	2
Q6PIW4	Fidgetin-like protein 1		1		2	2	
Q92947	Glutaryl-CoA dehydrogenase, mitochondrial				4	3	2
Q12769	Nuclear pore complex protein Nup160				2		2
O60341	Lysine-specific histone demethylase 1A				2	2	
P61204	ADP-ribosylation factor 3		1	1	2	2	
Q15005	Signal peptidase complex subunit 2	1	1	1	2	2	
P57088	Transmembrane protein 33	1			2	2	2
Q14103	Heterogeneous nuclear ribonucleoprotein D0	1	1	1	1	2	2
Q9Y676	28S ribosomal protein S18b, mitochondrial				2	2	1
O00567	Nucleolar protein 56				1	2	2

Making a comparison of the two lists obtained with the two different strategies, 2 proteins were found in common as MMACHC partners. One is MOB kinase activator 2 (MOB2) and the other is Glutaryl-CoA dehydrogenase, mitochondrial (GCDH).

Searching into the raw global lists for proteins that take part in biosynthetic and metabolic pathway of cobalamin or that are supposed to interact with it, the cob(I)yrinic acid a,c-diamide adenosyltransferase, mitochondrial (MMAB), simply called corrinoid adenosyltransferase, was identified in the gel-based experiment. This protein participates in the last step of AdoCbl formation by delivering the cofactor to MUT, together with MMAA protein (Plessl et al., 2017). MMAB was not included in the final list (Table 8) because was identified in both MMACHC-FLAG IPs with 1 peptide. MMAB was not identified in GFP-FLAG samples. Also the host cell factor 1 (HCFC1), a transcriptional co-regulator protein that modulates MMACHC expression, was identified with 1 peptide in MMACHC-FLAG IPs from gel-based experiment and for this not included in the final list (Table 8), and with 1 peptide in only one out of three

replicates in the shotgun experiment and for this not included in the final list (Table 9).

Very interestingly, S-adenosylmethionine synthase isoform type-1 (MAT1A) was identified in the first interactome (Table 8); this protein has an important role in cofactor (MeCbl) formation. In particular, when the MeCbl is used, the cobalt atom of the molecule becomes oxidized and MAT1A synthesizes S-adenosylmethionine that is used as methyl groups donor to restore MeCbl.

In addition to these observations, since it was proved only *in vitro* that MMACHC interacts with MMADHC (Froese et al., 2015) in a probable reduction process required in the formation of AdoCbl, the presence of this protein in MMACHC IPs was tested by WB. Figure 27 shows a specific signal for MMADHC only in the MMACHC immunoprecipitated samples and not in the control ones, confirming this still not completely clear literature datum. MMADHC was not identified by MS, fact probably due to the low abundance of this protein.

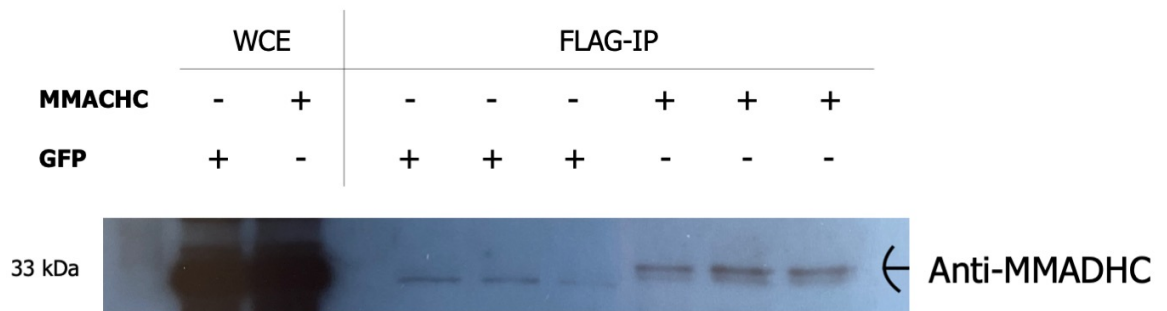


Figure 27. WB of MMADHC protein in GFP-FLAG and MMACHC-FLAG IPs. WB detection carried out using anti-MMADHC antibody showed specific signals for MMADHC protein in the MMACHC IP samples revealing their interaction. Whole cell extracts (WCE) were used as control.

5. DISCUSSION

The aim of this PhD project was to investigate and describe by proteomics and biochemical approaches the molecular alterations of the metabolic impairment caused by MMA in cellular models of disease. MMA is a rare inborn error of metabolism of propionyl-CoA due to mutations in methylmalonyl-CoA mutase enzyme, whose absence or reduced activity impairs the synthesis of succinyl-CoA, creating a block in the mitochondrial energy production within the Krebs cycle. In this form, MMA is presented as isolated MMA. Also mutations in the genes involved in the biosynthesis of MUT cofactor, the AdoCbl, can lead to MMA with or without homocystinuria, which can be less severe than the isolated type, even because the major responsiveness to therapeutic treatments. Then, the metabolites that accumulate as consequence of the disorder are thought to be responsible for other collateral damaging mechanisms, such as the inhibition of particular enzymes or the production of acidosis or the contribution to generate hyperammonemia and oxidative stress (Häberle et al., 2018). The mechanisms that underlie the pathophysiology of MMA in patients are not known due to the elevated heterogeneity of the phenotypes and the different impact that every mutation has on the single patient. Different patients sharing a similar genetic background often show different onset, different outcome and different severity of the symptoms. This could be somehow related to a different metabolic picture of these patients that is possible to investigate using the advanced mass spectrometric technologies in diagnostic laboratories. Despite the possible different metabolic alterations, common features are used as diagnostic biomarkers of the pathology or to discriminate the different subtypes of MMA.

The starting idea of this PhD project was to generate different kinds of engineered cell lines to reproduce the molecular alterations of MMA and study the eventual different response of each cell type to the metabolic damage produced. With the rapid progress of the MS-based proteomic knowledge and technical refinements, different label-free proteomics approaches have been used throughout the experimental procedures. Usual data-dependent and new data-independent acquisition techniques were employed in order to enlarge and better define the proteome of MMA.

5.1. MUT knockdown in SH-SY5Y cells induces alterations in proteins related to mitochondrial functionality

The present project started with the first attempt to generate a cell model for isolated MMA by knocking down MUT expression in SH-SY5Y neuroblastoma cell line (Costanzo et al., 2018). This cell line has been initially chosen because brain or neuronal damage is one of the most severe complications of the pathology. Thus, MUT protein expression was reduced by using specific siRNAs directed against MUT transcripts and, after 48 hours of treatment, it was

possible to achieve a reduction of MUT expression of about the 70%. The proteome of MUT-silenced SH-SY5Y cells (siRNA_MUT) was investigated with the aim to elucidate the molecular processes directly or not directly influenced by MUT knockdown. Quantitative proteomics based on spectral counts approach was applied to the MS identification after electrophoretic separation of the two compared proteomes (siRNA_MUT and WT) by SDS-PAGE. As result, 113 proteins were quantitatively detected as differentially regulated in MUT-silenced cells (Results, 4.1.2), and were subsequently analyzed by bioinformatic tools (Results, 4.1.3).

Within the molecular function GO term, the “oxidoreductase activity“ was one the most enriched category. This class included proteins such as electron transfer flavoprotein subunit alpha, mitochondrial (ETF_A), peroxiredoxin-6 (PRDX6), and peroxidase homolog (PXDN), all found to be less abundant in the siRNA_MUT condition. ETF_A, a crucial enzyme involved in mitochondrial fatty acid oxidation, accepts and transfers electrons from mitochondrial dehydrogenases, including the acyl-CoA dehydrogenases, to the membrane-bound ubiquinone oxidoreductase (Floyd et al., 2016). An example of defect of ETF_A is the glutaric acidemia type II, a rare metabolic organic acidemia characterized by accumulation and excretion of glutaric acid, but also lactic, ethylmalonic, butyric, isobutyric, 2-methylbutyric, and isovaleric acid. An impairment in the ETF_A-mediated processes, causative of metabolic alterations in glutaric acidemia, may also be contributing in the damaging mechanisms of MMA. Defects related to ETF_A reset mitochondrial fatty acid oxidation and affect the intracellular acidity, being the probable cause of the malformations of the brain and kidney found in patients (Stöckler et al., 1994; Gorgon, 2006). On the other hand, NADH-ubiquinone oxidoreductase 75 kDa subunit, mitochondrial (NDUS1), the largest subunit of complex I NADH dehydrogenase that transfers electrons from NADH to ubiquinone, resulted up-regulated in the proteomic list. While mutations of *NDUS1* gene cause metabolic reprogramming and disruption of the electron transfer (Ni et al., 2019), the alteration of the electron transfer system due to defective ETF_A could be probably modulated by the cells increasing the expression of NDUS1, as tentative to keep the respiratory chain functioning. In addition to this, PRDX6 and PXDN are proteins involved in the cell redox homeostasis, being peroxidases that catalyze the reduction of hydrogen peroxide and organic hydroperoxides to water and alcohols, respectively. It was reported that PRDX6 is involved in liver damage induced by oxidative stress (Tu et al., 2016). Recently, PXDN was identified as a protector against metabolic and oxidative stress in prostate cancer (Dougan et al., 2019). PRDX6 and PXDN down-regulation could affect the short-chain fatty acid and phospholipid hydroperoxides reduction with a lack in their protective role against oxidative stress. In fact, markers of oxidative stress are found increased in the urine and plasma of MMA patients (Manoli et al., 2005).

In the main biological processes coming from the bioinformatic analysis of the proteomic dataset, “metabolic process” resulted one of the most enriched categories. This included gamma-enolase (ENOG) and fructose bisphosphate

aldolase C (ALDOC), proteins involved in energetic metabolism, which resulted down-regulated in siRNA_MUT cells. In the previous proteomic investigation of the research group on livers from transplanted MMA patients, decreased levels of proteins involved in the energy metabolism, gluconeogenesis, and Krebs cycle anaplerosis were observed (Caterino et al., 2016). In line with the previous observations, the mitochondrial 2-oxoglutarate/malate carrier protein (M2OM) belongs to the mitochondrial carrier protein family, controls the transport of 2-oxoglutarate across the inner mitochondrial membrane, and regulates the malate-aspartate and oxoglutarate-isocitrate shuttles. It also takes part in the nitrogen metabolism. In addition, M2OM is responsible for glutathione uptake (Chen et al., 2000), and the glutathione deficiency is a complication of methylmalonic acidemia. Its down-regulation in this knockdown model of MMA may contribute to the impairment of the normal cell functions. Also the AMP deaminase 2 (AMPD2) that plays a critical role in energy metabolism and in the purine nucleotide cycle was found down-regulated. This protein was proved to play an evolutionary conserved role in the maintenance of cellular guanine nucleotide pools by regulating the feedback inhibition of adenosine derivatives on *de novo* purine synthesis. In neurodegenerative diseases, AMPD2 deficiency reflects a lack in neuroprotection mechanisms and consequent degeneration of tissues (Akizu et al., 2013).

Globally, these results are in line with the predicted and well-known alterations responsible for MMA pathophysiology. Nonetheless, a critical issue that can be raised in such experiments that employ transient gene silencing is that the modification of the proteome requires some time to become stable and, since the genetic modification is not stable itself, the proteome may rapidly change again for a fast recovery of protein expression levels. In addition, even if in this particular case no differences in the cell viability and apoptosis rate were detected (*Results, 4.1.1*), one concern is that a cell system tries to adapt somehow to the new genetic condition; for example, the activation of the interferon system that may lead to non-specific effects is a considered issue of RNA interference-based approaches (Aigner, 2006). Furthermore, it was not possible to assess whether 48 hours of silencing were a sufficient time to make the cells produce the “needed” quantity of methylmalonic acid, and other metabolites, which are actors in the damage mechanisms of MMA. Thus, since the transient reduction of MUT protein expression induced by siRNA may prevent to go into the deep of the molecular alterations of MMA, one solution was to create a stable total knockout cell model.

5.2. MUT knockout in SH-SY5Y and HEK293 cells

Logically, the first idea was then to create a stable knock out cell model using the CRISPR/Cas9 genome editing technology in the same human neuroblastoma SH-SY5Y cell line. Unfortunately, the CRISPR/Cas9 transfection experiment

was not successful. Transfected cells were not able to replicate and survive, floating dead in the culture plate. A possibility of technical issues was excluded by carrying out the experiment thrice in three different times. After the third tentative, it became necessary to realize that knocking out *MUT* gene in SH-SY5Y cell line would have been not possible. This was probably explainable according to the notion that methylmalonic acid, 2-methylcitric acid and other metabolites that accumulate as consequence of *MUT* absence/inactivity are toxic for neuronal cells (Jafari P et al., 2013). Another hypothesis could be that, even reproducing a gene mutation would be informative to study the biology of a disease, the mutation of an “important” gene, frequently, is not compatible with life in particular cells (Ding et al., 2013).

Thus, a parallel attempt to create a suitable cell model for MMA by knocking out *MUT* gene by CRISPR/Cas9 technology was made on the human embryonic kidney (HEK) 293 cell line, successfully. Cells (*MUT*-KO) well survived after the transfection and started to replicate in culture. Western blot analysis revealed the total absence of *MUT* protein in comparison with WT cells, while methylmalonic acid and propionylcarnitine, biomarkers for diagnosis of MMA (Häberle et al., 2018), resulted clearly increased in the new cell model. In addition, *MUT* knockout did not affect cell viability and proliferation (*Results, 4.3.1*), thus considering completely the possibility to employ it as cellular model for isolated MMA.

5.3. Proteomic analysis of HEK293 *MUT*-KO cells reveals impairment in metal homeostasis

A new comparative proteomic experiment was, then, designed for the *MUT*-KO cell line. Samples (4 replicates per condition) were digested using S-Trap columns and analyzed in technical triplicates by shotgun LC-MS/MS. A label-free analysis was performed using MaxQuant to address LFQ intensity values to each protein in each replicate. The differential proteome dataset resulted constituted by 178 proteins over a total of 4000 identified proteins. Before proceeding with bioinformatic analyses, HEK293 *MUT*-KO proteome was compared with that of SH-SY5Y siRNA_ *MUT* (*Results 4.1.2, Table 2*). From this comparison, no common protein was detected to have the same regulation. This was expected because in such experiments an overlap between two lists is truly improbable due to the different cell lines and genome modifications employed, and the different proteomic setup (LC and MS instruments, number of replicates, sample preparation, quantitative strategy). In addition, this is also explainable considering the different impact that MMA can have on different cell types.

Subsequently, *MUT*-KO proteomic dataset was analyzed by Cytoscape in a single cluster analysis that enriched three categories strictly related to metabolic pathways of propionyl-CoA metabolism: “Membrane lipid biosynthetic process”, “Cellular transition metal ion homeostasis”, and “Tetrapyrrole

metabolic process”. In particular, the “Cellular transition metal ion homeostasis” category included 7 key proteins acting in metal homeostasis: ferritin heavy chain (FTH1), nuclear receptor coactivator 4 (NCOA4), iron-responsive element-binding protein 2 (IREB2), ATP-binding cassette sub-family B member 6, mitochondrial (ABCB6), zinc transporter 9 (SLC30A9), and zinc transporter ZIP10 (SLC39A10).

Iron metabolism is a tightly regulated process controlled by a network of iron-dependent proteins; despite iron is essential for the survival of all organisms, the levels of free iron in a cell must be strictly controlled to avoid the generation of ROS via the Fenton reaction (Dixon and Stockwell, 2014). In this context, the role of FTH1 is to store iron atoms. When iron levels in the cell are low, FTH1 is degraded in the lysosome in order to release iron and let the cell use it, in an autophagic process called ferritinophagy. NCOA4 targets FTH1, by direct interaction, on the surface of autophagosomes for its degradation. The quantitative changes of FTH1 and NCOA4 depend on iron levels, even if the perfect correlation is still unknown. In conditions of normal homeostasis, when iron levels are high, NCOA4 abundance is low, thereby promoting FTH1 accumulation and iron capture. But when iron is low, NCOA4 levels increase to promote ferritinophagy. In contrast, when ferritinophagy occurs, both FTH1 and NCOA4 that targets FTH1 are degraded into the lysosome, reducing the levels of both proteins (Mancias et al., 2015). This latter situation may resemble the down-regulation of both FTH1 and NCOA4 in MUT-KO as a cause of an increase in the cellular levels of iron, which may also contribute to ROS production (*Results*, 4.3.7). Moreover, the reduction of FTH1 expression in MUT-KO may also be caused by an increase in the expression of IREB2 protein that, through the binding to iron-responsive elements (IRES) in ferritin mRNA, cause a repression of its mRNA translation (Moroishi et al., 2014). In addition, ABCB6 is reported to be a mitochondrial transporter involved in porphyrin transport, iron homeostasis, or resistance to cytotoxic agents (Paterson et al., 2007). Increased levels of iron into the cells may justify the up-regulation of this protein in MUT-KO dataset. Zinc transporter 9, Zinc transporter ZIP10, and Zinc transporter ZIP1 (which was not included in the same category by Cytoscape, but present in the proteomic list) are all involved in zinc homeostasis. ZIP1 and ZIP10 are involved in zinc uptake and influx and resulted both down-regulated while Zinc transporter 9 up-regulated in MUT-KO cells.

5.4. Proteomic analysis of HEK293 MUT-KO cells reveals impairment in mitochondrial metabolic pathways

In addition to the previous bioinformatics analysis, a subgroup of proteins (26) was recognized in the differential proteome as apparently belonging to mitochondrial compartment. Thus, it was clustered using STRING, which enriched interesting categories related to “metabolic pathways”, “cofactor metabolic process”, “oxidation-reduction process”, “fatty acid metabolism” and

“cellular transition metal ion homeostasis”. In the latter category, the above-mentioned FTH, NCOA4, ABCB6 and SLC30A9 were found. Several proteins belonging to the fatty acid metabolism were found regulated, suggesting a clear impairment in the regulation of fatty acids as consequence of MUT absence. Indeed, an up-regulation of the hydroxymethylglutaryl-CoA lyase (HMGCL), which uses the 3-hydroxy-3-methylglutaryl-CoA to produce acetyl-CoA and acetoacetate, results in the enhancement of ketogenesis, a feature of MMA (Rosario and Medina, 1982; Kim et al., 2019). Carnitine O-palmitoyltransferase 2 (CPT2) is a nuclear protein which is transported to the mitochondrial inner membrane where, together with carnitine palmitoyltransferase I, oxidizes long-chain fatty acids in the mitochondria. Defects of CPT2 are often reported as causative of inborn defect of fatty acid oxidation (Djouadi et al., 2019). On the other hand, an up-regulation of this protein may reflect an altered synthesis of long-chain fatty acids or other related species that engulf the mitochondrion and need to be eliminated. In support of this speculation, the up-regulation of nucleoside diphosphate-linked moiety X motif 19, mitochondrial (NUDT19) found by proteomics may increase the hydrolysis of fatty acyl-CoA esters. Furthermore, CPT2 up-regulation was found to increase mitochondrial reactive oxygen species, contributing to cellular damage (Brown et al., 2018). Not only with respect to mitochondria, the shuttling into the cells and the active manipulation of fatty acids can be also imputed at the up-regulation of the non-mitochondrial long-chain fatty acid transport protein 4 (SLC27A4). Finally, the down-regulation of glycine cleavage system H protein, mitochondrial (GCSH) is in line with the study of Kølvråa (1979), which demonstrated the inhibition of the glycine cleavage system by branched-chain amino acid metabolites that could explain the hyperglycinemia commonly found in MMA and PA patients.

5.5. Effects of MUT KO and MUT rescuing on cell adhesion, cytoskeleton and structural organization

MUT-KO cells were then engineered with a construct able to give stable expression of MUT protein, in order to generate an additional cell model, called MUT-Rescue, to control the specificity of KO effects. The rationale behind the creation of this new cell model is related to the fact that the effects that are visible in MUT-KO could be due the genetic modification or an eventual treatment. Instead, all the effects that are rescued after the introduction of MUT in KO cells are to be considered exclusively depending upon MUT absence. The stable expression of MUT in MUT-Rescue cell line was tested by western blot; in addition, MUT-Rescue showed no significant difference in cell viability compared with the other two cell types (Results, 4.3.4) convincing for its employment as additional control in all the following experiments.

According to the hints derived from ClueGO bioinformatic analysis that enriched the categories “membrane assembly” and “morphogenesis of an epithelial sheet”, a strong suggestion that processes related to extracellular

matrix deposition, cytoskeletal, cell junctions, and cell communication were altered as consequence of MUT knockout came out from a clear result obtained in both cell models (MUT-KO and MUT-Rescue) using WGA staining. WGA is a lectin that binds to N-acetyl-D-glucosamine and sialic acid residues labelling cell membrane (Monsigny et al., 1980). Interestingly, the glycosyltransferase EXT2 and the glycoproteins SDC2 and FN1 were found to be down-regulated in MUT-KO cells by proteomics, suggesting a possible effect of MUT knockout on glycoproteins distribution and organization. In fact, the intensity of fluorescence derived from WGA staining in MUT-KO resulted greatly diminished compared to WT and increased again after MUT-Rescue. Moreover, the completely different staining pattern of the three compared cell lines is suggestive of a structural modification that will probably impact the functioning of the cell systems through alteration of cell-cell junctions or cell architecture. WGA staining is presented very definite and delimits sharply the WT cell borders, while in MUT-KO cells it seems much more diffuse. Surprisingly, MUT-Rescue seems halfway between the other two cell types, suggesting that the reintroduction of MUT is not totally able to revert this effect. Also the down-regulation of alpha-1,2-mannosyltransferase ALG9 (ALG9) and probable C-mannosyltransferase DPY19L1 (DPY19L1) may be linked to alteration in glycoproteins formation, or the up-regulation of beta-1,3-glycosyltransferase (B3GALTL) to structural modifications acting on Notch pathway (Seidler et al., 2006; Kozma et al., 2006).

According to the above findings, 5 proteins were chosen from the proteomic dataset and validated by WB in MUT-KO cells in comparison with WT ones; the rescue of the expression levels of these proteins after the reintroduction of MUT was monitored in MUT-Rescue. Actually, the down-regulation of vimentin (VIM), syndecan-2 (SDC2), exostosin-2 (EXT2) and fibronectin (FN1), and the up-regulation of glutamine synthetase (GLUL) were validated in MUT-KO. Only EXT2 and VIM, but not SDC2, GLUL and FN1, seemed to show a trend of expression in MUT-Rescue similar to WT, suggesting that quantitative changes of these two proteins may be not due to a secondary alteration but strictly related to MUT deficiency in the MUT-KO model.

Then, speculating that VIM or EXT2 may have a role in such structural alterations, qRT-PCR analysis was performed to assess whether quantitative changes of these proteins may be related to a genetic or a protein regulation. A perfect overlap in the variation trend of expression both at gene and protein level was observed for VIM, thus suggesting that VIM down-regulation actually depends on a transcriptional regulation and is strictly related to MUT KO. EXT2 down-regulation in MUT-KO was confirmed also at gene level, while its gene expression was not reverted in MUT-Rescue cells. Moreover, VIM expression was tested by WB in the urine of two MUT patients. Assuming an expected trend similar to proteomic results in MUT-KO, a diminished expression of VIM was observed only in one out of two MUT patients analyzed. Surprisingly, very low expression levels of VIM were observed in the both MMA with homocystinuria cblC type patients used as additional controls (Results, 4.3.5). This may indicate

the involvement of VIM as a common regulative gene target altered in both isolated and Cbl-related MMA forms. In fact, Hannibal et al. (2011) identified an important down-regulation of VIM in a proteomic experiment on fibroblasts from cblC patients. Even in this context, the implication of *VIM* gene is not clear and, in general, it was difficult to investigate its importance in a wider cohort since the poor availability of patients' specimens due to the rarity of MMA.

Vimentin is an intermediate filament protein involved in cytoskeleton formation and its down-regulation can induce cytoskeleton reorganization with impairment of cell structure and cell-cell connections that may create alterations in the normal function of the tissue. Vimentin has key roles in cell adhesion by regulating integrin functions. Focal contacts (FC), or focal adhesions, are sites of close contact between cells and the extracellular matrix. VIM as intermediate filament is enrolled with microfilaments and microtubules in regulating FC through interaction with cytoskeleton. In vimentin-knocked down endothelial cells, FC were found significantly smaller than those observed in untreated cells, while the microtubule networks resulted normal. This evidence suggests a role for vimentin cytoskeleton in regulating adhesion upon direct control of FC (Tsuruta et al., 2003). Eckes et al. (2000) reported that in vimentin-knockout animals there is retardation in migration of fibroblasts following wounding, proposing that disruption of the VIM cytoskeleton may interfere with the ability of fibroblasts to adhere to matrix. Huo et al. (2016) in a vimentin-silenced ovarian cancer cell line found down-regulation of proteins involved in cytoskeleton organization and anchoring junction and tight junction. Amongst these proteins, they found the downregulation of cingulin (CGN), acting in the formation and regulation of tight junctions, in concordance with proteomic results in MUT-KO cells. Huo et al. also confirmed that destabilization of both anchoring and tight junctions may lead to the emergence of cancer stem cell promoting the up-regulation of the cancer stem cell markers ALDH1A1, while in MUT-KO cells the up-regulation of ALDH1A2 was found. Thus, an impairment of cell adhesion systems is becoming evident. In addition, also the down-regulation of neural cell adhesion molecule 1 (NCAM1) and protein CYR61 (CYR61) and the up-regulation of epithelial cell adhesion molecule (EPCAM) may contribute to the impairment of the structural organization of the cells by defective adhesion mechanisms.

Normal cells inhibit their growth and migration when cells adhere to each other. However, these properties are progressively lost in tumor cells, contributing to increased rates of cell proliferation and migration. Not surprisingly, E-cadherin (CDH1) down-regulation is relatively common in cancers of epithelial origin resulting in less intercellular contact and reduced cell polarity, promoting the epithelial-mesenchymal transition (EMT) process, a key mechanism for carcinogenesis and tumor invasion. In fact, current therapeutic strategies in some urogenital cancers are targeted to restoring the levels of E-cadherin (Song et al., 2019). A similar EMT process is activated in case of tissue repair or tissue fibrosis, and a specific pattern of expression of implicated proteins is recognized (Liu et al., 2015). In particular, EMT is characterized by

loss of epithelial markers, E-cadherin (CDH1), ZO-1, cytokeratin, and gain of mesenchymal markers, vimentin, metalloproteinase, fibronectin, α -smooth muscle actin, snail, and slug (Zeisberg et al., 2009). Contrarily with respect to this situation, in MUT-KO cell line there is a complete opposite trend of expression for some of the cited proteins: CDH1 is up-regulated, VIM and FN1 are down-regulated. In this context, Liu et al. (2015) showed the contribution of VIM in EMT process by mediating cytoskeletal organization and focal adhesion maturation. They knocked down VIM in a breast cancer cell line, which resulted in reduced cell proliferation, impaired wound healing, loss of directional migration, and increased large membrane extension. Vimentin depletion also induced reorganization of cytoskeleton and reduced focal adhesions. This extremely reinforces the idea that VIM may undergo quick transcriptional regulation in MUT-KO cell line. Nonetheless, even in a condition of impaired cytoskeletal and cell adhesion organization, the MUT-KO cell type does not acquire tumoral characteristics with regard to abnormal proliferation and invasion. On the contrary of EMT, MUT-KO proteome resembles much more the picture of a mesenchymal-epithelial transition (MET). In the enhancement of this statement comes the opposite trend of expression of EMT markers but also the down-regulation of Annexin A3 (ANXA3). In fact, Du et al. (2018) discovered that ANXA3 knockdown induced MET in breast cancer cells by decreasing mesenchymal markers expression, VIM and N-cadherin, and increasing epithelial markers expression, E-cadherin and γ -catenin. This may suggest a change in the normal cellular behavior of MUT-KO that modulates cell architecture and structure in order to metabolically adapt to the new acquired genetic condition; or, alternatively, the proteome alterations are the direct consequence of MUT absence that somehow has effect on cell adhesion and cell connections.

Cytoskeletal alterations may also be explained by the down-regulation of Epidermal growth factor receptor kinase substrate 8 (EPS8). EPS8 is a multi-functional actin-binding protein that regulates both dynamics and organization of actin cytoskeleton through diverse mechanisms: it modulates actin dynamics by direct binding, or indirectly via activation of tyrosine receptor-mediated Rac1. Specifically, it was demonstrated that Eps8 enhances neuronal cell proliferation and migration through the PI3K-Akt pathway and increases β -catenin levels with modulation of cell-cell adhesion, mimicking Wnt pathway (Stamatakou et al., 2015; Hinck et al., 1994). On the other hand, Eps8 silencing blocks the axon remodeling activity of Wnt3a. In this context, Protein wntless homolog (WLS), down-regulated in the LFQ proteomic experiment, is a conserved membrane protein that promotes the secretion of Wnt proteins and is identified as key member for Wnt3a-mediated communication between cultured human cells (Bänziger et al., 2006). Thus, a mechanism of cytoskeletal alteration may be addressed to inactivation of Wnt signalling by down-regulation of both EPS8 and WLS. In addition, in siRNA_MUT cells β -catenin also resulted down-regulated, in concordance with this speculation.

Members of 14-3-3 protein family are dimeric intracellular proteins that regulate cell cycle progression, apoptosis, and signal transduction. It has been shown that 14-3-3 proteins interact also with VIM head domain in a phosphorylation-dependent manner (Ivaska et al., 2007). In particular, proteomics of MUT-KO showed a down-regulation of 14-3-3 protein sigma (SFN). This protein, when bound to keratin 17, regulates protein synthesis and epithelial cell growth by stimulating Akt/mTOR pathway. Also the target of rapamycin complex subunit LST8 (MLST8), a subunit of both mTORC1 and mTORC2, was down-regulated in MUT-KO. Within mTORC1, MLST8 interacts directly with MTOR and enhances its kinase activity. It is possible that a transcriptional regulation that reduce the expression of VIM has impact on mTOR signaling by the impossibility to interact with some of 14-3-3 proteins.

In contrast with this, the Regulator complex protein LAMTOR4 (LAMTOR4) was up-regulated. As part of the Ragulator complex it is involved in amino acid sensing and activation of mTORC1. Activated by amino acids through a mechanism involving the lysosomal V-ATPase, the Ragulator functions as a guanine nucleotide exchange factor activating the small GTPases Rag. Activated Ragulator and Rag GTPases function as a scaffold recruiting mTORC1 to lysosomes where it is activated (Bar-Peled et al., 2012).

5.6. Production of ROS and hyperammonemia in MUT-KO

An assay to detect ROS was performed (Results, 4.3.7) and showed a significant increase in ROS levels in MUT-KO cells, if compared to WT. ROS levels decreased in MUT-Rescue cells, confirming the direct link between MUT and ROS production. A relevant increase in ROS levels was detected in all cell types after treatment with H₂O₂, but this increase was significantly higher for MUT-KO, thus suggesting that MUT-deficient cells are more sensitive to additional stress induced by H₂O₂ respect to controls. Additionally, the rescue of MUT protein is able to keep oxidative unbalance at the same levels of WT cells. This behaviour is in line with the knowledge that ROS and oxidative processes are unbalanced in MUT-deficient patients and responsible for most of the damage of MMA (Fontella et al., 2000; Fernandes et al., 2011).

As reported elsewhere (Häberle et al., 2018), hyperammonemia is a major complication of MMA, especially in brain and liver. To prevent hyperammonemia, high glutamine synthetase activity is found in the human liver, brain, and muscle (Häberle et al., 2005). Glutamine synthetase (GLUL), also called glutamate ammonia ligase, is an enzyme responsible for the synthesis of glutamine from glutamate and ammonia. This reaction explains the pivotal role of this enzyme in ammonia detoxification, interorgan nitrogen flux, and acid-base regulation. Glutamine deficiency caused by a defect of *GLUL* gene was reported to cause brain malformation in patients (Häberle et al., 2005). Here, a relevant up-regulation of GLUL was found by proteomics and validated in MUT-KO (Results, 4.3.5), where GLUL increases to protect cells from ammonia

toxicity. The fact that its expression was not rescued at normal levels after MUT reintroduction would explain that *GLUL* gene is not controlled by MUT expression and that the secondary metabolic adaptation of the cells to a probable higher level of ammonia regulates *GLUL* expression. In addition, it was recently found that treatment with glutamine resulted in an effect of protection of rats from ROS and oxidative damage (Hartmann et al., 2017). This could address a double role for *GLUL* up-regulation, in protecting cells from ammonia accumulation via incorporation in glutamine, and at the same time providing protection against oxidative damage.

5.7. Impact of propionate-induced stress in MUT-KO and siRNA_MUT cells

Results on siRNA_MUT and MUT-KO cells showed impairment of mitochondrial functionality by Neutral-Red and MTT assays performed in propionate-enriched culture medium (*Results*, 4.1.4; 4.3.6). From Neutral-Red assay no significant differences were detected in siRNA_MUT and between the three cell types (WT, MUT-KO and MUT-Rescue). In these experiments, 25 mM propionate caused significant reduction in MTT absorbance of MUT-KO cells, suggesting that a stress induced by propionate is able to induce reduction of mitochondrial functionality, measured from succinate dehydrogenase activity, in MUT-KO. In concordance with the major impact that the total absence of MUT protein can drive on the cells compared to its knockdown, this effect is more evident in MUT-KO respect to siRNA_MUT. The absence of MUT makes the cells more sensitive to this stress and this effect is not detectable in MUT-expressing cells. This is reasonable with the fact that metabolic instability in patients has the tendency to worsen, sometimes even after organ transplantation (Caterino et al., 2016; Chandler et al., 2009).

5.8. Exploring HEK293 MUT-KO and MUT-Rescue proteomes using Data-Independent Acquisition mass spectrometry

In order to have a comprehensive overview related to the proteomic investigation for all MMA cell models, a new Data-Independent Acquisition (DIA) proteomic experiment was performed on MUT-KO and MUT-Rescue. DIA experiment was designed in order to have a better identification coverage of proteomes and check rescue effect on protein expression levels also by a proteomic point of view. KO/WT and KO/RES comparisons were considered. Since this proteomic experiment has been only recently completed, no bioinformatic analysis or functional and validation assays have been performed. Despite this, the two protein lists generated from DIA experiment were intersected to find similarities, that means proteins that have the same trend of regulation in MUT-KO if compared to both WT and MUT-Rescue controls. As

assessed many times about the importance of MUT-Rescue control, the expression levels of such proteins are reverted after MUT reintroduction, being this way strictly related to MUT absence in MUT-KO. Among these proteins exostosin-1 (EXT1) was found up-regulated in MUT-KO and its levels are reverted in MUT-Rescue. EXT1 is a glycosyltransferase that forms a complex with EXT2 (which was validated to be down-regulated in MUT-KO, *Results*, 4.3.5) committed in the biosynthesis of heparan sulfates, thus reinforcing the hypothesis of proteoglycans or glycoproteins organization impairment. In light of this finding, the KO/WT list from DIA experiment (Table 5) was compared with that from LFQ experiment (Table 3). Despite the two methods were extremely different and not comparable (also considering the inclusion of a third set of samples, MUT-Rescue, in the global dataset), 5 proteins were found regulated in both experiments, 3 of which showed the same trend of regulation: tumor protein D53 (TPD52L1) and neural cell adhesion molecule 1 (NCAM1) were down-regulated while cadherin-1 (CDH1) was up-regulated. In addition, other proteins, such as vimentin, protein lin-28 homolog B, brain acid soluble protein 1, redox-regulatory protein FAM213A, spindlin-1, and GDH/6PGL endoplasmic bifunctional protein, which were not included in the final list (Table 5) because had abundance values below the imposed threshold, despite they were statistically significant, showed the same trend of regulation of the LFQ experiment. Once again, this let easily focus the attention on VIM, which was globally identified as down-regulated in the LFQ experiment, validated by WB in the cells and in urines from MMA and CblC patients and by qRT-PCR in the cells (*Results*, 4.3.5), and lastly identified in the DIA experiment. These data may strongly encourage for the consideration of VIM as an important protein to focus on for further studies and a possible target for a designed therapy for MMA patients.

5.9. Mapping the interactome of MMACHC protein

The role of MMACHC protein in the cell has not been completely cleared. It is known to act in the pathway devoted to the synthesis of cobalamin-derived cofactors, AdoCbl (MUT cofactor) and MeCbl (methionine synthase cofactor). Its interacting partners in this pathway or the correct sequence of events are still unknown. In order to get more insight into the role of MMACHC protein, interactomics experiments were performed by immunoprecipitation of MMACHC complexes followed by MS identification. Two strategies were used on the same samples: a gel-based and a shotgun LC-MS/MS analysis that produced two lists of interactors.

The two lists were compared in order to find common interactors of MMACHC possibly identified through two different sample preparation methods for MS analysis. In this context, 2 proteins were found in common as MMACHC partners. One is MOB kinase activator 2 (MOB2) and the other is glutaryl-CoA dehydrogenase, mitochondrial (GCDH). MOB2 is a regulator of

cell morphogenesis and polarized growth, can control cell cycle and is one of the proteins involved in Hippo signaling. Knockdown of Mob2 within the developing mouse cortex demonstrated its role in neuronal positioning (O'Neill et al., 2018; Gundogdu et al., 2019). As for now, no literature data seem to link this protein with MMACHC pathway. One possibility that may explain the interaction with this protein resides in its metal ion binding capability that MMACHC may use for the reduction of the cobalt atom of cobalamin. GCDH catalyzes the oxidative decarboxylation of glutaryl-CoA to crotonyl-CoA in the degradative pathway of lysine, hydroxylysine, and tryptophan. Interestingly, mutations in this enzyme are causative of another organic acidemia called glutaric acidemia type 1. MMA and glutaric acidemia type 1 may possibly have some intersecting pathways that are still unknown.

Interestingly, S-adenosylmethionine synthase isoform type-1 (MAT1A) was identified in the first interactome of MMACHC. MAT1A has a role in the formation of the cofactor (MeCbl) for methionine synthase. In particular, when the MeCbl is used, the cobalt atom of the molecule becomes oxidized and the methionine synthase reductase (MTRR) catalyzes the reductive methylation of cob(II)alamin to cob(I)alamin using S-adenosylmethionine (SAM) as a methyl donor. SAM is exactly synthesized by MAT1A, starting from methionine and ATP (Sloan et al., 2008; Froese et al., 2015). In addition to this, another interesting protein found in the first interactome of MMACHC (Table 8) is spermine synthase (SMS), which catalyzes the production of spermine from spermidine and decarboxylated SAM (Pegg and Michael, 2010). This finding may elucidate a new link between MMACHC and polyamines biosynthetic pathway.

Other two proteins identified in the first and second interactome definitely link MMACHC to folate and methionine metabolism: dihydrofolate reductase (DHFR) and mitochondrial 10-formyltetrahydrofolate dehydrogenase (ALDH1L2), respectively. DHFR is a key enzyme involved in the transformation of folate onto its biologically active form, the tetrahydrofolate, through the catalysis of two consecutive reduction reactions. DHFR reduces folate to dihydrofolate and this latter to tetrahydrofolate, using NADPH as electron donor. Tetrahydrofolate is involved in one-carbon metabolism, which includes the synthesis of thymidylate, purines, and pyrimidines for DNA synthesis. Tetrahydrofolate owns biological relevance because used to remethylate homocysteine to form methionine and SAM. On the other hand, ALDH1L2 is involved in the conversion of 10-formyltetrahydrofolate to tetrahydrofolate (Krupenko et al., 2010; Tjong and Mohiuddin, 2019).

In addition to these speculations, searching into the raw global lists for proteins that are known to take part in biosynthetic and metabolic pathway of cobalamin or that are supposed to interact with it, the cob(I)yrinic acid a,c-diamide adenosyltransferase, mitochondrial (MMAB), simply called corrinoid adenosyltransferase, was identified in the gel-based experiment. This protein participates in the last step of AdoCbl formation by delivering the cofactor to MUT, together with MMAA protein (Plessl et al., 2017). MMAB was not

included in the final list (Table 8) because identified in both MMACHC-FLAG IP replicates with 1 peptide, which is easily explainable with the natural low abundance of the protein. MMAB was not identified in GFP-FLAG samples. Also the host cell factor 1 (HCFC1), a transcriptional co-regulator protein that modulates MMACHC expression, was identified with 1 peptide in MMACHC-FLAG IPs from the gel-based experiment and for this not included in the final list (Table 8), and with 1 peptide in only one out of three replicates in the shotgun experiment and for this not included in the final list (Table 9). Finally, since it was proved *in vitro* that MMACHC interacts with MMADHC (Froese et al., 2015) in a probable reduction process required in the formation of AdoCbl, the presence of this protein in MMACHC IP complexes was tested by WB. This experiment actually confirmed a this still not completely clear literature datum. Despite all these interesting initial findings, both interactomes will be further investigated and functional experiments will confirm the interaction of MMACHC protein with some of the putative candidates produced in the two interactomes.

6. ACKNOWLEDGEMENTS

I would like to start this section informing the reader about the pride and the joy I can feel to have successfully undertaken, pursued and finally completed this PhD program. I am so proud of myself of being entitled of the highest academic degree and I wish myself good luck and a brilliant career in the future.

I am grateful and feel lucky to be part of this wonderful research group that someone once called “team M”, as for Michele, Margherita, Marianna.

First of all, I want to express my gratitude to Prof. Margherita Ruoppolo, my head, my supervisor, my tutor, our leader. You started training me in the 2015, when I was a young and enthusiastic guy with a thousand ideas in his mind and the will to conquer the world. Since the beginning you gave me trust and great responsibilities, teaching me everyday how to deal with problems and face the truth. We can discuss about science or people or silly things always in a constructive way. Your kindness, sympathy, apprehension, the way we joke at work, are the secret of our success as team and I am honored to have completed this important step of my scientific formation with you.

I am also pleased to thank the second person of this wonderful team, Dr. Marianna Caterino. What I most admire from you is your pragmatism and the ability you have to handle every kind of situation always preserving your rationality. We instantly had good feeling, creating a strong complicity that allowed us to make the impossible happen. In fact, the way we continue working together is extremely productive and stimulating and as we always like to say "never change a winning team!".

A particular acknowledgment goes to Dr. Armando Cevenini (Dino), for significantly contributing to get the best results for my project and for all the time spent with me in the lab - often late in the evening - in discussions, for giving me moral support or simply having a coffee together. One of the most kind, polite and generous person I have ever met in my life.

I am also very grateful for all the support I received for the collaborative work I undertook during my periods abroad in Europe as visiting researcher. I am so honored to have worked with prominent and expert people like you.

It is worth mentioning Dr. Ida Chiara Guerrera that hosted me in her lab in Paris, which has been possible thanks to a fellowship I won from the University of Naples “Federico II”.

Then, thanks to all the people from the group of Prof. Albert Sickmann, especially in the person of Dr. Laxmikanth Kollipara (Lucky). Without your friendship my stay in Dortmund would have been harder. Thank you for your scientific support and...for all the beers.

In the end, I want to acknowledge the person who I am most grateful to. She is the person by who I feel beloved everyday. When everything seemed to be lost, you encouraged me not to give up. I will always remember when you were the only one that believed in me, in my capabilities, in my preparation, in my stubbornness and obstinacy. You told me: “you must succeed, you will succeed!” and I hope you are proud of me now. You have been my strength during this path and not only, thanks my lovely Marianna.

7. REFERENCES

Aigner A. Gene silencing through RNA interference (RNAi) in vivo: strategies based on the direct application of siRNAs. *J Biotechnol.* 2006 Jun 25;124(1):12-25. Epub 2006 Jan 18. Review. PubMed PMID: 16413079.

Akizu N, Cantagrel V, Schroth J, Cai N, Vaux K, McCloskey D, Naviaux RK, Van Vleet J, Fenstermaker AG, Silhavy JL, Scheliga JS, Toyama K, Morisaki H, Sonmez FM, Celep F, Oraby A, Zaki MS, Al-Baradie R, Faqeih EA, Saleh MA, Spencer E, Rosti RO, Scott E, Nickerson E, Gabriel S, Morisaki T, Holmes EW, Gleeson JG. AMPD2 regulates GTP synthesis and is mutated in a potentially treatable neurodegenerative brainstem disorder. *Cell.* 2013 Aug 1;154(3):505-17. doi: 10.1016/j.cell.2013.07.005. PubMed PMID: 23911318; PubMed Central PMCID: PMC3815927.

Ballhausen D, Mittaz L, Boulat O, Bonafé L, Braissant O. Evidence for catabolic pathway of propionate metabolism in CNS: expression pattern of methylmalonyl-CoA mutase and propionyl-CoA carboxylase alpha-subunit in developing and adult rat brain. *Neuroscience.* 2009 Dec 1;164(2):578-87. doi: 10.1016/j.neuroscience.2009.08.028. Epub 2009 Aug 20. PubMed PMID: 19699272.

Bänziger C, Soldini D, Schütt C, Zipperlen P, Hausmann G, Basler K. Wntless, a conserved membrane protein dedicated to the secretion of Wnt proteins from signaling cells. *Cell.* 2006 May 5;125(3):509-22. PubMed PMID: 16678095.

Bar-Peled L, Schweitzer LD, Zoncu R, Sabatini DM. Ragulator is a GEF for therag GTPases that signal amino acid levels to mTORC1. *Cell.* 2012 Sep 14;150(6):1196-208. doi: 10.1016/j.cell.2012.07.032. PubMed PMID: 22980980; PubMed Central PMCID: PMC3517996.

Baumgartner MR, Hörster F, Dionisi-Vici C, Haliloglu G, Karall D, Chapman KA, Huemer M, Hochuli M, Assoun M, Ballhausen D, Burlina A, Fowler B, Grünert SC, Grünewald S, Honzik T, Merinero B, Pérez-Cerdá C, Scholl-Bürgi S, Skovby F, Wijburg F, MacDonald A, Martinelli D, Sass JO, Valayannopoulos V, Chakrapani A. Proposed guidelines for the diagnosis and management of methylmalonic and propionic acidemia. *Orphanet J Rare Dis.* 2014 Sep 2;9:130. doi: 10.1186/s13023-014-0130-8. Review. PubMed PMID: 25205257; PubMed Central PMCID: PMC4180313.

Berman HM, Westbrook J, Feng Z, Gilliland G, Bhat TN, Weissig H, Shindyalov IN, Bourne PE. The Protein Data Bank. *Nucleic Acids Res.* 2000 Jan 1;28(1):235-42. PubMed PMID: 10592235; PubMed Central PMCID: PMC102472.

Braissant O, McLin VA, Cudalbu C. Ammonia toxicity to the brain. *J Inherit Metab Dis.* 2013 Jul;36(4):595-612. doi: 10.1007/s10545-012-9546-2. Epub 2012 Oct 30. Review. PubMed PMID: 23109059.

Brown ZJ, Fu Q, Ma C, Kruhlak M, Zhang H, Luo J, Heinrich B, Yu SJ, Zhang Q, Wilson A, Shi ZD, Swenson R, Greten TF. Carnitine palmitoyltransferase gene upregulation by linoleic acid induces CD4⁺ T cell apoptosis promoting HCC development. *Cell Death Dis.* 2018 May 23;9(6):620. doi: 10.1038/s41419-018-0687-6. PMID: 29795111; PMCID: PMC5966464.

Bruderer R, Bernhardt OM, Gandhi T, Xuan Y, Sondermann J, Schmidt M, Gomez-Varela D, Reiter L. Optimization of Experimental Parameters in Data-Independent Mass Spectrometry Significantly Increases Depth and Reproducibility of Results. *Mol Cell Proteomics.* 2017 Dec;16(12):2296-2309. doi: 10.1074/mcp.RA117.000314. Epub 2017 Oct 25. PubMed PMID: 29070702; PubMed Central PMCID: PMC5724188.

Burkhart JM, Schumbrutzki C, Wortelkamp S, Sickmann A, Zahedi RP. Systematic and quantitative comparison of digest efficiency and specificity reveals the impact of trypsin quality on MS-based proteomics. *J Proteomics.* 2012 Feb 2;75(4):1454-62. doi: 10.1016/j.jprot.2011.11.016. Epub 2011 Nov 30. PubMed PMID:22166745.

Calvo, S.E., Klauser, C.R., Mootha, V.K. MitoCarta2.0: an updated inventory of mammalian mitochondrial proteins (2015). *Nucleic Acids Research* [doi: 10.1093/nar/gkv1003

Caterino M, Ruoppolo M, Mandola A, Costanzo M, Orrù S, Imperlini E. Protein-protein interaction networks as a new perspective to evaluate distinct functional roles of voltage-dependent anion channel isoforms. *Mol Biosyst.* 2017 Nov 21;13(12):2466-2476. doi: 10.1039/c7mb00434f. Review. PubMed PMID: 29028058.

Caterino M, Chandler RJ, Sloan JL, Dorko K, Cusmano-Ozog K, Ingenito L, Strom SC, Imperlini E, Scolamiero E, Venditti CP, Ruoppolo M. The proteome of methylmalonic acidemia (MMA): the elucidation of altered pathways in patient livers. *Mol Biosyst.* 2016 Feb;12(2):566-74. doi: 10.1039/c5mb00736d. PubMed PMID: 26672496; PubMed Central PMCID: PMC4858437.

Caterino M, Pastore A, Strozzi MG, Di Giovamberardino G, Imperlini E, Scolamiero E, Ingenito L, Boenzi S, Ceravolo F, Martinelli D, Dionisi-Vici C, Ruoppolo M. The proteome of cblC defect: in vivo elucidation of altered cellular pathways in humans. *J Inherit Metab Dis.* 2015 Sep;38(5):969-79. doi: 10.1007/s10545-014-9806-4. Epub 2015 Jan 14. PubMed PMID: 25585586.

Chandler RJ, Zerfas PM, Shanske S, Sloan J, Hoffmann V, DiMauro S, Venditti CP. Mitochondrial dysfunction in mutant methylmalonic acidemia. *FASEB J*. 2009 Apr;23(4):1252-61. doi: 10.1096/fj.08-121848. Epub 2008 Dec 16. PubMed PMID: 19088183; PubMed Central PMCID: PMC2660647.

Chandler RJ, Venditti CP. Genetic and genomic systems to study methylmalonic acidemia. *Mol Genet Metab*. 2005 Sep-Oct;86(1-2):34-43. Epub 2005 Sep 22. Review. PubMed PMID: 16182581; PubMed Central PMCID: PMC2657357.

Chen Z, Putt DA, Lash LH. Enrichment and functional reconstitution of glutathione transport activity from rabbit kidney mitochondria: further evidence for the role of the dicarboxylate and 2-oxoglutarate carriers in mitochondrial glutathione transport. *Arch Biochem Biophys*. 2000 Jan 1;373(1):193-202. PubMed PMID: 10620338.

Cohen SA, Michaud DP. Synthesis of a fluorescent derivatizing reagent, 6-aminoquinolyl-N-hydroxysuccinimidyl carbamate, and its application for the analysis of hydrolysate amino acids via high-performance liquid chromatography. *Anal Biochem*. 1993 Jun;211(2):279-87. PubMed PMID: 8317704.

Costanzo M, Cevenini A, Marchese E, Imperlini E, Raia M, Del Vecchio L, Caterino M, Ruoppolo M. Label-Free Quantitative Proteomics in a Methylmalonyl-CoA Mutase-Silenced Neuroblastoma Cell Line. *Int J Mol Sci*. 2018 Nov 13;19(11). pii: E3580. doi: 10.3390/ijms19113580. PubMed PMID: 30428564; PubMed Central PMCID: PMC6275031.

Costanzo M, Zacchia M, Bruno G, Crisci D, Caterino M, Ruoppolo M. Integration of Proteomics and Metabolomics in Exploring Genetic and Rare Metabolic Diseases. *Kidney Dis (Basel)*. 2017 Jul;3(2):66-77. doi: 10.1159/000477493. Epub 2017 Jun 30. Review. PubMed PMID: 28868294; PubMed Central PMCID: PMC5567043.

De Pasquale V, Costanzo M, Siciliano RA, Mazzeo MF, Pistorio V, Bianchi L, Marchese E, Ruoppolo M, Pavone LM, Caterino M. Proteomic Analysis of Mucopolysaccharidosis IIIB Mouse Brain. *Biomolecules*. 2020 Feb 26;10(3). pii: E355. doi: 10.3390/biom10030355. PubMed PMID: 32111039.

Deodato F, Boenzi S, Santorelli FM, Dionisi-Vici C. Methylmalonic and propionic aciduria. *Am J Med Genet C Semin Med Genet*. 2006 May 15;142C(2):104-12. Review. PubMed PMID: 16602092.

Ding Q, Lee YK, Schaefer EA, Peters DT, Veres A, Kim K, Kuperwasser N, Motola DL, Meissner TB, Hendriks WT, Trevisan M, Gupta RM, Moisan A, Banks E, Friesen M, Schinzel RT, Xia F, Tang A, Xia Y, Figueroa E, Wann A,

Ahfeldt T, Daheron L, Zhang F, Rubin LL, Peng LF, Chung RT, Musunuru K, Cowan CA. A TALEN genome-editing system for generating human stem cell-based disease models. *Cell Stem Cell*. 2013 Feb 7;12(2):238-51. doi: 10.1016/j.stem.2012.11.011. Epub 2012 Dec 13. PubMed PMID: 23246482; PubMed Central PMCID: PMC3570604.

Dionisi-Vici C, Rizzo C, Burlina AB, Caruso U, Sabetta G, Uziel G, Abeni D. Inborn errors of metabolism in the Italian pediatric population: a national retrospective survey. *J Pediatr*. 2002 Mar;140(3):321-7. PubMed PMID: 11953730.

Dixon SJ, Stockwell BR. The role of iron and reactive oxygen species in cell death. *Nat Chem Biol*. 2014 Jan;10(1):9-17. doi: 10.1038/nchembio.1416. Review. PubMed PMID: 24346035.

Djouadi F, Bastin J. Mitochondrial Genetic Disorders: Cell Signaling and Pharmacological Therapies. *Cells*. 2019 Mar 28;8(4). pii: E289. doi: 10.3390/cells8040289. Review. PubMed PMID: 30925787; PubMed Central PMCID: PMC6523966.

Dobson CM, Gradinger A, Longo N, Wu X, Leclerc D, Lerner-Ellis J, Lemieux M, Belair C, Watkins D, Rosenblatt DS, Gravel RA. Homozygous nonsense mutation in the MCEE gene and siRNA suppression of methylmalonyl-CoA epimerase expression: a novel cause of mild methylmalonic aciduria. *Mol Genet Metab*. 2006 Aug;88(4):327-33. Epub 2006 May 11. PubMed PMID: 16697227.

Dougan J, Hawsawi O, Burton LJ, Edwards G, Jones K, Zou J, Nagappan P, Wang G, Zhang Q, Danaher A, Bowen N, Hinton C, Otero-Marah VA. Proteomics-Metabolomics Combined Approach Identifies Peroxidase as a Protector against Metabolic and Oxidative Stress in Prostate Cancer. *Int J Mol Sci*. 2019 Jun 21;20(12). pii: E3046. doi: 10.3390/ijms20123046. PubMed PMID: 31234468; PubMed Central PMCID: PMC6627806.

Du R, Liu B, Zhou L, Wang D, He X, Xu X, Zhang L, Niu C, Liu S. Downregulation of annexin A3 inhibits tumor metastasis and decreases drug resistance in breast cancer. *Cell Death Dis*. 2018 Jan 26;9(2):126. doi: 10.1038/s41419-017-0143-z. PubMed PMID: 29374148; PubMed Central PMCID: PMC5833718.

Eckes B, Colucci-Guyon E, Smola H, Nodder S, Babinet C, Krieg T, Martin P. Impaired wound healing in embryonic and adult mice lacking vimentin. *J Cell Sci*. 2000 Jul;113 (Pt 13):2455-62. PubMed PMID: 10852824.

Eng JK, McCormack AL, Yates JR. An approach to correlate tandem mass spectral data of peptides with amino acid sequences in a protein database. *J Am*

Soc Mass Spectrom. 1994 Nov;5(11):976-89. doi: 10.1016/1044-0305(94)80016-2. PubMed PMID: 24226387.

Escher C, Reiter L, MacLean B, Ossola R, Herzog F, Chilton J, MacCoss MJ, Rinner O. Using iRT, a normalized retention time for more targeted measurement of peptides. *Proteomics*. 2012 Apr;12(8):1111-21. doi: 10.1002/pmic.201100463. PubMed PMID: 22577012; PubMed Central PMCID: PMC3918884.

Fernandes CG, Borges CG, Seminotti B, Amaral AU, Knebel LA, Eichler P, de Oliveira AB, Leipnitz G, Wajner M. Experimental evidence that methylmalonic acid provokes oxidative damage and compromises antioxidant defenses in nerve terminal and striatum of young rats. *Cell Mol Neurobiol*. 2011 Jul;31(5):775-85. doi: 10.1007/s10571-011-9675-4. Epub 2011 Mar 22. PubMed PMID: 21424830.

Filipowicz HR, Ernst SL, Ashurst CL, Pasquali M, Longo N. Metabolic changes associated with hyperammonemia in patients with propionic acidemia. *Mol Genet Metab*. 2006 Jun;88(2):123-30. Epub 2006 Jan 10. PubMed PMID: 16406646.

Floyd BJ, Wilkerson EM, Veling MT, Minogue CE, Xia C, Beebe ET, Wrobel RL, Cho H, Kremer LS, Alston CL, Gromek KA, Dolan BK, Ulbrich A, Stefely JA, Bohl SL, Werner KM, Jochem A, Westphall MS, Rensvold JW, Taylor RW, Prokisch H, Kim JP, Coon JJ, Pagliarini DJ. Mitochondrial Protein Interaction Mapping Identifies Regulators of Respiratory Chain Function. *Mol Cell*. 2016 Aug 18;63(4):621-632. doi: 10.1016/j.molcel.2016.06.033. Epub 2016 Aug 4. PubMed PMID: 27499296; PubMed Central PMCID: PMC4992456.

Fontella FU, Pulrolnik V, Gassen E, Wannmacher CM, Klein AB, Wajner M, Dutra-Filho CS. Propionic and L-methylmalonic acids induce oxidative stress in brain of young rats. *Neuroreport*. 2000 Feb 28;11(3):541-4. PubMed PMID: 10718311.

Froese DS, Kopec J, Fitzpatrick F, Schuller M, McCorvie TJ, Chalk R, Plessl T, Fettelschoss V, Fowler B, Baumgartner MR, Yue WW. Structural Insights into the MMACHC-MMADHC Protein Complex Involved in Vitamin B12 Trafficking. *J Biol Chem*. 2015 Dec 4;290(49):29167-77. doi: 10.1074/jbc.M115.683268. Epub 2015 Oct 19. PubMed PMID: 26483544; PubMed Central PMCID: PMC4705923.

Froese DS, Gravel RA. Genetic disorders of vitamin B₁₂ metabolism: eight complementation groups--eight genes. *Expert Rev Mol Med*. 2010 Nov 29;12:e37. doi: 10.1017/S1462399410001651. Review. PubMed PMID: 21114891; PubMed Central PMCID: PMC2995210.

Gordon N. Glutaric aciduria types I and II. *Brain Dev.* 2006 Apr;28(3):136-40. Epub 2005 Dec 20. Review. PubMed PMID: 16368216.

Green R, Allen LH, Bjørke-Monsen AL, Brito A, Guéant JL, Miller JW, Molloy AM, Nexo E, Stabler S, Toh BH, Ueland PM, Yajnik C. Vitamin B₁₂ deficiency. *Nat Rev Dis Primers.* 2017 Jun 29;3:17040. doi: 10.1038/nrdp.2017.40. Review. Erratum in: *Nat Rev Dis Primers.* 2017 Jul 20;3:17054. PubMed PMID: 28660890.

Gundogdu R, Hergovich A. MOB (Mps one Binder) Proteins in the Hippo Pathway and Cancer. *Cells.* 2019 Jun 10;8(6):569. doi: 10.3390/cells8060569. PMID: 31185650; PMCID: PMC6627106.

Häberle J, Chakrapani A, Ah Mew N, Longo N. Hyperammonaemia in classic organic acidurias: a review of the literature and two case histories. *Orphanet J Rare Dis.* 2018 Dec 6;13(1):219. doi: 10.1186/s13023-018-0963-7. Review. PubMed PMID: 30522498; PubMed Central PMCID: PMC6282273.

Häberle J, Görg B, Rutsch F, Schmidt E, Toutain A, Benoist JF, Gelot A, Suc AL, Höhne W, Schliess F, Häussinger D, Koch HG. Congenital glutamine deficiency with glutamine synthetase mutations. *N Engl J Med.* 2005 Nov 3;353(18):1926-33. PubMed PMID: 16267323.

Haijes HA, Jans JJM, Tas SY, Verhoeven-Duif NM, van Hasselt PM. Pathophysiology of propionic and methylmalonic acidurias. Part 1: Complications. *J Inher Metab Dis.* 2019 Sep;42(5):730-744. doi: 10.1002/jimd.12129. Epub 2019 Aug 7. Review. PubMed PMID: 31119747.

Hannibal L, DiBello PM, Jacobsen DW. Proteomics of vitamin B₁₂ processing. *Clin Chem Lab Med.* 2013 Mar 1;51(3):477-88. doi: 10.1515/cclm-2012-0568. Review. PubMed PMID: 23241609.

Hannibal L, DiBello PM, Yu M, Miller A, Wang S, Willard B, Rosenblatt DS, Jacobsen DW. The MMACHC proteome: hallmarks of functional cobalamin deficiency in humans. *Mol Genet Metab.* 2011 Jul;103(3):226-39. doi: 10.1016/j.ymgme.2011.03.008. Epub 2011 Mar 24. PubMed PMID: 21497120; PubMed Central PMCID: PMC3110603.

Hartmann RM, Licks F, Schemitt EG, Colares JR, do Couto Soares M, Zabet GP, Fillmann HS, Marroni NP. Protective effect of glutamine on the main and adjacent organs damaged by ischemia-reperfusion in rats. *Protoplasma.* 2017 Nov;254(6):2155-2168. doi: 10.1007/s00709-017-1102-3. Epub 2017 Apr 5. PubMed PMID: 28382390.

Heuberger K, Bailey HJ, Burda P, Chaikuad A, Krysztofinska E, Suormala T, Bürer C, Lutz S, Fowler B, Froese DS, Yue WW, Baumgartner MR. Genetic, structural, and functional analysis of pathogenic variations causing methylmalonyl-CoA epimerase deficiency. *Biochim Biophys Acta Mol Basis Dis.* 2019 Jun 1;1865(6):1265-1272. doi: 10.1016/j.bbadis.2019.01.021. Epub 2019 Jan 22. PubMed PMID: 30682498; PubMed Central PMCID: PMC6525113.

Hinck L, Nelson WJ, Papkoff J. Wnt-1 modulates cell-cell adhesion in mammalian cells by stabilizing beta-catenin binding to the cell adhesion protein cadherin. *J Cell Biol.* 1994 Mar;124(5):729-41. PubMed PMID: 8120095; PubMed Central PMCID: PMC2119963.

Huo Y, Zheng Z, Chen Y, Wang Q, Zhang Z, Deng H. Downregulation of vimentin expression increased drug resistance in ovarian cancer cells. *Oncotarget.* 2016 Jul 19;7(29):45876-45888. doi: 10.18632/oncotarget.9970. PubMed PMID: 27322682; PubMed Central PMCID: PMC5216767.

Ivaska J, Pallari HM, Nevo J, Eriksson JE. Novel functions of vimentin in cell adhesion, migration, and signaling. *Exp Cell Res.* 2007 Jun 10;313(10):2050-62. Epub 2007 Apr 14. Review. PubMed PMID: 17512929.

Jafari P, Braissant O, Zavadakova P, Henry H, Bonafé L, Ballhausen D. Brain damage in methylmalonic aciduria: 2-methylcitrate induces cerebral ammonium accumulation and apoptosis in 3D organotypic brain cell cultures. *Orphanet J Rare Dis.* 2013 Jan 8;8:4. doi: 10.1186/1750-1172-8-4. PubMed PMID: 23298464; PubMed Central PMCID: PMC3567978.

Kim S, Jeon JM, Kwon OK, Choe MS, Yeo HC, Peng X, Cheng Z, Lee MY, Lee S. Comparative Proteomic Analysis Reveals the Upregulation of Ketogenesis in Cardiomyocytes Differentiated from Induced Pluripotent Stem Cells. *Proteomics.* 2019 Apr;19(7):e1800284. doi: 10.1002/pmic.201800284. Epub 2019 Feb 26. PubMed PMID: 30724459.

Kölker S, Burgard P, Sauer SW, Okun JG. Current concepts in organic acidurias: understanding intra- and extracerebral disease manifestation. *J Inher Metab Dis.* 2013 Jul;36(4):635-44. doi: 10.1007/s10545-013-9600-8. Epub 2013 Mar 20. Review. PubMed PMID: 23512157.

Kølvraa S. Inhibition of the glycine cleavage system by branched-chain amino acid metabolites. *Pediatr Res.* 1979 Aug;13(8):889-93. PubMed PMID: 481963.

Kovachy RJ, Copley SD, Allen RH. Recognition, isolation, and characterization of rat liver D-methylmalonyl coenzyme A hydrolase. *J Biol Chem.* 1983 Sep 25;258(18):11415-21. PubMed PMID: 6885824.

Kozma K, Keusch JJ, Hegemann B, Luther KB, Klein D, Hess D, Haltiwanger RS, Hofsteenge J. Identification and characterization of abeta1,3-glucosyltransferase that synthesizes the Glc-beta1,3-Fuc disaccharide on thrombospondin type 1 repeats. *J Biol Chem*. 2006 Dec 1;281(48):36742-51. Epub 2006 Oct 10. PubMed PMID: 17032646.

Krupenko NI, Dubard ME, Strickland KC, Moxley KM, Oleinik NV, Krupenko SA. ALDH1L2 is the mitochondrial homolog of 10-formyltetrahydrofolate dehydrogenase. *J Biol Chem*. 2010 Jul 23;285(30):23056-63. doi: 10.1074/jbc.M110.128843. Epub 2010 May 24. PMID: 20498374; PMCID: PMC2906299.

la Marca G, Malvagia S, Pasquini E, Innocenti M, Donati MA, Zammarchi E. Rapid 2nd-tier test for measurement of 3-OH-propionic and methylmalonic acids on dried blood spots: reducing the false-positive rate for propionylcarnitine during expanded newborn screening by liquid chromatography-tandem mass spectrometry. *Clin Chem*. 2007 Jul;53(7):1364-9. Epub 2007 May 17. PubMed PMID: 17510301.

Larnaout A, Mongalgi MA, Kaabachi N, Khiari D, Debbabi A, Mebazza A, Ben Hamida M, Hentati F. Methylmalonic acidemia with bilateral globus pallidus involvement: a neuropathological study. *J Inherit Metab Dis*. 1998 Aug;21(6):639-44. PubMed PMID: 9762599.

Ledley FD, Lumetta M, Nguyen PN, Kolhouse JF, Allen RH. Molecular cloning of L-methylmalonyl-CoA mutase: gene transfer and analysis of mut cell lines. *Proc Natl Acad Sci U S A*. 1988 May;85(10):3518-21. PubMed PMID: 2453061; PubMed Central PMCID: PMC280243.

Lindblad B, Lindblad BS, Olin P, Svanberg B, Zetterström R. Methylmalonic acidemia. A disorder associated with acidosis, hyperglycinemia, and hyperlactatemia. *Acta Paediatr Scand*. 1968 Sep;57(5):417-24. PubMed PMID: 5706053.

Liu CY, Lin HH, Tang MJ, Wang YK. Vimentin contributes to epithelial-mesenchymal transition cancer cell mechanics by mediating cytoskeletal organization and focal adhesion maturation. *Oncotarget*. 2015 Jun 30;6(18):15966-83. PubMed PMID: 25965826; PubMed Central PMCID: PMC4599250.

Mancia F, Keep NH, Nakagawa A, Leadlay PF, McSweeney S, Rasmussen B, Bösecke P, Diat O, Evans PR. How coenzyme B12 radicals are generated: the crystal structure of methylmalonyl-coenzyme A mutase at 2 Å resolution. *Structure*. 1996 Mar 15;4(3):339-50. PubMed PMID: 8805541.

Mancias JD, Pontano Vaites L, Nissim S, Biancur DE, Kim AJ, Wang X, Liu Y, Goessling W, Kimmelman AC, Harper JW. Ferritinophagy via NCOA4 is required for erythropoiesis and is regulated by iron dependent HERC2-mediated proteolysis. *Elife*. 2015 Oct 5;4. doi: 10.7554/eLife.10308. PubMed PMID: 26436293; PubMed Central PMCID: PMC4592949.

Manoli I, Sloan JL, Venditti CP. Isolated Methylmalonic Acidemia. 2005 Aug 16 [updated 2016 Dec 1]. In: Adam MP, Ardinger HH, Pagon RA, Wallace SE, Bean LJH, Stephens K, Amemiya A, editors. *GeneReviews®* [Internet]. Seattle (WA): University of Washington, Seattle; 1993-2020. Available from <http://www.ncbi.nlm.nih.gov/books/NBK1231/>PubMed PMID: 20301409.

Manza LL, Stamer SL, Ham AJ, Codreanu SG, Liebler DC. Sample preparation and digestion for proteomic analyses using spin filters. *Proteomics*. 2005 May;5(7):1742-5. PubMed PMID: 15761957.

Mellacheruvu D, Wright Z, Couzens AL, Lambert JP, St-Denis NA, Li T, Miteva YV, Hauri S, Sardi ME, Low TY, Halim VA, Bagshaw RD, Hubner NC, Al-Hakim A, Bouchard A, Faubert D, Fermin D, Dunham WH, Goudreault M, Lin ZY, Badillo BG, Pawson T, Durocher D, Coulombe B, Aebersold R, Superti-Furga G, Colinge J, Heck AJ, Choi H, Gstaiger M, Mohammed S, Cristea IM, Bennett KL, Washburn MP, Raught B, Ewing RM, Gingras AC, Nesvizhskii AI. The CRAPome: a contaminant repository for affinity purification-mass spectrometry data. *Nat Methods*. 2013 Aug;10(8):730-6. doi: 10.1038/nmeth.2557. Epub 2013 Jul 7. PubMed PMID: 23921808; PubMed Central PMCID: PMC3773500.

Melo DR, Kowaltowski AJ, Wajner M, Castilho RF. Mitochondrial energy metabolism in neurodegeneration associated with methylmalonic acidemia. *J Bioenerg Biomembr*. 2011 Feb;43(1):39-46. doi: 10.1007/s10863-011-9330-2. Review. PubMed PMID: 21271280.

Mi H, Muruganujan A, Casagrande JT, Thomas PD. Large-scale gene function analysis with the PANTHER classification system. *Nat Protoc*. 2013 Aug;8(8):1551-66. doi: 10.1038/nprot.2013.092. Epub 2013 Jul 18. PubMed PMID: 23868073; PubMed Central PMCID: PMC6519453.

Millington DS, Stevens RD. Acylcarnitines: analysis in plasma and whole blood using tandem mass spectrometry. *Methods Mol Biol*. 2011;708:55-72. doi: 10.1007/978-1-61737-985-7_3. PubMed PMID: 21207283.

Monsigny M, Roche AC, Sene C, Maget-Dana R, Delmotte F. Sugar-lectin interactions: how does wheat-germ agglutinin bind sialoglycoconjugates? *Eur J Biochem*. 1980 Feb;104(1):147-53. PubMed PMID: 6892800.

Moroishi T, Yamauchi T, Nishiyama M, Nakayama KI. HERC2 targets the iron regulator FBXL5 for degradation and modulates iron metabolism. *J Biol Chem*. 2014 Jun 6;289(23):16430-41. doi: 10.1074/jbc.M113.541490. Epub 2014 Apr 28. PubMed PMID: 24778179; PubMed Central PMCID: PMC4047410.

Ni Y, Hagraas MA, Konstantopoulou V, Mayr JA, Stuchebrukhov AA, Meierhofer D. Mutations in NDUFS1 Cause Metabolic Reprogramming and Disruption of the Electron Transfer. *Cells*. 2019 Sep 25;8(10). pii: E1149. doi: 10.3390/cells8101149. PubMed PMID: 31557978; PubMed Central PMCID: PMC6829531.

O'Neill AC, Kyrousi C, Einsiedler M, Burtscher I, Drukker M, Markie DM, Kirk EP, Götz M, Robertson SP, Cappello S. Mob2 Insufficiency Disrupts Neuronal Migration in the Developing Cortex. *Front Cell Neurosci*. 2018 Mar 12;12:57. doi: 10.3389/fncel.2018.00057. eCollection 2018. PubMed PMID: 29593499; PubMed Central PMCID: PMC5857600.

Old WM, Meyer-Arendt K, Aveline-Wolf L, Pierce KG, Mendoza A, Sevinsky JR, Resing KA, Ahn NG. Comparison of label-free methods for quantifying human proteins by shotgun proteomics. *Mol Cell Proteomics*. 2005 Oct;4(10):1487-502. Epub 2005 Jun 23. PubMed PMID: 15979981.

Olsen JV, de Godoy LM, Li G, Macek B, Mortensen P, Pesch R, Makarov A, Lange O, Horning S, Mann M. Parts per million mass accuracy on an Orbitrap mass spectrometer via lock mass injection into a C-trap. *Mol Cell Proteomics*. 2005 Dec;4(12):2010-21. Epub 2005 Oct 24. PubMed PMID: 16249172.

Ombro D, Giocaliere E, Forni G, Malvagia S, la Marca G. Expanded newborn screening by mass spectrometry: New tests, future perspectives. *Mass Spectrom Rev*. 2016 Jan-Feb;35(1):71-84. doi: 10.1002/mas.21463. Epub 2015 May 7. Review. PubMed PMID: 25952022.

Paterson JK, Shukla S, Black CM, Tachiwada T, Garfield S, Wincovitch S, Ernst DN, Agadir A, Li X, Ambudkar SV, Szakacs G, Akiyama S, Gottesman MM. Human ABCB6 localizes to both the outer mitochondrial membrane and the plasma membrane. *Biochemistry*. 2007 Aug 21;46(33):9443-52. Epub 2007 Jul 28. PubMed PMID: 17661442.

Pegg AE, Michael AJ. Spermine synthase. *Cell Mol Life Sci*. 2010 Jan;67(1):113-21. doi: 10.1007/s00018-009-0165-5. Epub 2009 Oct 27. PMID: 19859664; PMCID: PMC2822986.

Perkins DN, Pappin DJ, Creasy DM, Cottrell JS. Probability-based protein identification by searching sequence databases using mass spectrometry data. *Electrophoresis*. 1999 Dec;20(18):3551-67. PubMed PMID: 10612281.

Plessl T, Bürer C, Lutz S, Yue WW, Baumgartner MR, Froese DS. Protein destabilization and loss of protein-protein interaction are fundamental mechanisms in cblA-type methylmalonic aciduria. *Hum Mutat.* 2017 Aug;38(8):988-1001. doi: 10.1002/humu.23251. Epub 2017 Jun 6. PubMed PMID: 28497574.

Pupavac M, Watkins D, Petrella F, Fahiminiya S, Janer A, Cheung W, Gingras AC, Pastinen T, Muenzer J, Majewski J, Shoubridge EA, Rosenblatt DS. Inborn Error of Cobalamin Metabolism Associated with the Intracellular Accumulation of Transcobalamin-Bound Cobalamin and Mutations in ZNF143, Which Codes for a Transcriptional Activator. *Hum Mutat.* 2016 Sep;37(9):976-82. doi: 10.1002/humu.23037. Epub 2016 Jul 12. PubMed PMID: 27349184.

Quintana AM, Yu HC, Brebner A, Pupavac M, Geiger EA, Watson A, Castro VL, Cheung W, Chen SH, Watkins D, Pastinen T, Skovby F, Appel B, Rosenblatt DS, Shaikh TH. Mutations in THAP11 cause an inborn error of cobalamin metabolism and developmental abnormalities. *Hum Mol Genet.* 2017 Aug 1;26(15):2838-2849. doi: 10.1093/hmg/ddx157. PubMed PMID: 28449119; PubMed Central PMCID: PMC5886234.

Ribeiro LR, Della-Pace ID, de Oliveira Ferreira AP, Funck VR, Pinton S, Bobinski F, de Oliveira CV, da Silva Fiorin F, Duarte MM, Furian AF, Oliveira MS, Nogueira CW, Dos Santos AR, Royes LF, Figuera MR. Chronic administration of methylmalonate on young rats alters neuroinflammatory markers and spatial memory. *Immunobiology.* 2013 Sep;218(9):1175-83. doi: 10.1016/j.imbio.2013.04.008. Epub 2013 Apr 19. PubMed PMID: 23726524.

Rosario P, Medina JM. Stimulation of ketogenesis by propionate in isolated rat hepatocytes: an explanation for ketosis associated with propionic acidaemia and methylmalonic acidaemia? *J Inher Metab Dis.* 1982;5(1):59-62. PubMed PMID: 6820416.

Ruoppolo M, Caterino M, Albano L, Pecce R, Di Girolamo MG, Crisci D, Costanzo M, Milella L, Franconi F, Campesi I. Targeted metabolomic profiling in rat tissues reveals sex differences. *Sci Rep.* 2018 Mar 16;8(1):4663. doi: 10.1038/s41598-018-22869-7. PubMed PMID: 29549307; PubMed Central PMCID: PMC5856765.

Scolamiero E, Cozzolino C, Albano L, Ansalone A, Caterino M, Corbo G, di Girolamo MG, Di Stefano C, Durante A, Franzese G, Franzese I, Gallo G, Giliberti P, Ingenito L, Ippolito G, Malamisura B, Mazzeo P, Norma A, Ombrone D, Parenti G, Pellicchia S, Pecce R, Pierucci I, Romanelli R, Rossi A, Siano M, Stoduto T, Villani GR, Andria G, Salvatore F, Frisso G, Ruoppolo M. Targeted metabolomics in the expanded newborn screening for inborn errors of

metabolism. *Mol Biosyst.* 2015 Jun;11(6):1525-35. doi: 10.1039/c4mb00729h. PubMed PMID: 25689098.

Seetharam B, Li N. Transcobalamin II and its cell surface receptor. *Vitam Horm.* 2000;59:337-66. Review. PubMed PMID: 10714245.

Seidler DG, Faiyaz-Ul-Haque M, Hansen U, Yip GW, Zaidi SH, Teebi AS, Kiesel L, Götte M. Defective glycosylation of decorin and biglycan, altered collagen structure, and abnormal phenotype of the skin fibroblasts of an Ehlers-Danlos syndrome patient carrying the novel Arg270Cys substitution in galactosyltransferase I (beta4GalT-7). *J Mol Med (Berl).* 2006 Jul;84(7):583-94. Epub 2006 Apr 1. PubMed PMID: 16583246.

Shannon P, Markiel A, Ozier O, Baliga NS, Wang JT, Ramage D, Amin N, Schwikowski B, Ideker T. Cytoscape: a software environment for integrated models of biomolecular interaction networks. *Genome Res.* 2003 Nov;13(11):2498-504. PubMed PMID: 14597658; PubMed Central PMCID: PMC403769.

Shindo N, Nojima S, Fujimura T, Taka H, Mineki R, Murayama K. Separation of 18 6-aminoquinolyl-carbamyl-amino acids by ion-pair chromatography. *Anal Biochem.* 1997 Jun 15;249(1):79-82. PubMed PMID: 9193711.

Sloan JL, Carrillo N, Adams D, Venditti CP. Disorders of Intracellular Cobalamin Metabolism. 2008 Feb 25 [updated 2018 Sep 6]. In: Adam MP, Ardinger HH, Pagon RA, Wallace SE, Bean LJH, Stephens K, Amemiya A, editors. *GeneReviews®* [Internet]. Seattle (WA): University of Washington, Seattle; 1993-2020. Available from <http://www.ncbi.nlm.nih.gov/books/NBK1328/PubMed> PMID: 20301503

Song Y, Ye M, Zhou J, Wang ZW, Zhu X. Restoring E-cadherin Expression by Natural Compounds for Anticancer Therapies in Genital and Urinary Cancers. *Mol Ther Oncolytics.* 2019 May 17;14:130-138. doi: 10.1016/j.omto.2019.04.005. eCollection 2019 Sep 27. Review. PubMed PMID: 31194121; PubMed Central PMCID: PMC6551504.

Stamatakou E, Hoyos-Flight M, Salinas PC. Wnt Signalling Promotes Actin Dynamics during Axon Remodelling through the Actin-Binding Protein Eps8. *PLoS One.* 2015 Aug 7;10(8):e0134976. doi: 10.1371/journal.pone.0134976. eCollection 2015. PubMed PMID: 26252776; PubMed Central PMCID: PMC4529215.

Stöckler S, Radner H, Karpf EF, Hauer A, Ebner F. Symmetric hypoplasia of the temporal cerebral lobes in an infant with glutaric aciduria type II (multiple

acyl-coenzyme A dehydrogenase deficiency). *J Pediatr.* 1994 Apr;124(4):601-4. PubMed PMID: 8151478.

Sun ZJ, Wang Y, Cai Z, Chen PP, Tong XJ, Xie D. Involvement of Cyr61 in growth, migration, and metastasis of prostate cancer cells. *Br J Cancer.* 2008 Nov 18;99(10):1656-67. doi: 10.1038/sj.bjc.6604712. Epub 2008 Oct 21. PubMed PMID: 18941464; PubMed Central PMCID: PMC2584944.

Szklarczyk D, Gable AL, Lyon D, Junge A, Wyder S, Huerta-Cepas J, Simonovic M, Doncheva NT, Morris JH, Bork P, Jensen LJ, Mering CV. STRING v11: protein-protein association networks with increased coverage, supporting functional discovery in genome-wide experimental datasets. *Nucleic Acids Res.* 2019 Jan 8;47(D1):D607-D613. doi: 10.1093/nar/gky1131. PubMed PMID: 30476243; PubMed Central PMCID: PMC6323986.

Takahashi-Iñiguez T, García-Hernandez E, Arreguín-Espinosa R, Flores ME. Role of vitamin B12 on methylmalonyl-CoA mutase activity. *J Zhejiang Univ Sci B.* 2012 Jun;13(6):423-37. doi: 10.1631/jzus.B1100329. Review. PubMed PMID: 22661206; PubMed Central PMCID: PMC3370288.

Tjong E, Mohiuddin SS. Biochemistry, Tetrahydrofolate. [Updated 2019 Apr 21]. In: StatPearls [Internet]. Treasure Island (FL): StatPearls Publishing; 2019 Jan-. Available from: <https://www.ncbi.nlm.nih.gov/books/NBK539712/>

Trotter TN, Yang Y. Matricellular proteins as regulators of cancer metastasis to bone. *Matrix Biol.* 2016 May-Jul;52-54:301-314. doi: 10.1016/j.matbio.2016.01.006. Epub 2016 Jan 22. Review. PubMed PMID: 26807761; PubMed Central PMCID: PMC4875810.

Tsuruta D, Jones JC. The vimentin cytoskeleton regulates focal contact size and adhesion of endothelial cells subjected to shear stress. *J Cell Sci.* 2003 Dec 15;116(Pt 24):4977-84. PubMed PMID: 14625391.

Tu Q, Xiong Y, Fan L, Qiao B, Xia Z, Hu L, Wang Y, Peng G, Ye Q. Peroxiredoxin 6 attenuates ischemia- and hypoxia-induced liver damage of brain-dead donors. *Mol Med Rep.* 2016 Jan;13(1):753-61. doi: 10.3892/mmr.2015.4587. Epub 2015 Nov 19. PubMed PMID: 26647763; PubMed Central PMCID: PMC4686087.

Villani GR, Gallo G, Scolamiero E, Salvatore F, Ruoppolo M. "Classical organic acidurias": diagnosis and pathogenesis. *Clin Exp Med.* 2017 Aug;17(3):305-323. doi: 10.1007/s10238-016-0435-0. Epub 2016 Sep 9. Review. PubMed PMID: 27613073.

Watkins D, Rosenblatt DS. Failure of lysosomal release of vitamin B12: a new complementation group causing methylmalonic aciduria (cblF). *Am J Hum Genet.* 1986 Sep;39(3):404-8. PubMed PMID: 3766542; PubMed Central PMCID: PMC1683971.

Wiśniewski JR, Zougman A, Nagaraj N, Mann M. Universal sample preparation method for proteome analysis. *Nat Methods.* 2009 May;6(5):359-62. doi:10.1038/nmeth.1322. Epub 2009 Apr 19. PubMed PMID: 19377485

Yu HC, Sloan JL, Scharer G, Brebner A, Quintana AM, Achilly NP, Manoli I, Coughlin CR 2nd, Geiger EA, Schneck U, Watkins D, Suormala T, Van Hove JL, Fowler B, Baumgartner MR, Rosenblatt DS, Venditti CP, Shaikh TH. An X-linked cobalamin disorder caused by mutations in transcriptional coregulator HCFC1. *Am J Hum Genet.* 2013 Sep 5;93(3):506-14. doi: 10.1016/j.ajhg.2013.07.022. PubMed PMID: 24011988; PubMed Central PMCID: PMC3769968.

Zeisberg M, Neilson EG. Biomarkers for epithelial-mesenchymal transitions. *J Clin Invest.* 2009 Jun;119(6):1429-37. doi: 10.1172/JCI36183. Epub 2009 Jun 1. Review. PubMed PMID: 19487819; PubMed Central PMCID: PMC2689132.

Zsengellér ZK, Aljinovic N, Teot LA, Korson M, Rodig N, Sloan JL, Venditti CP, Berry GT, Rosen S. Methylmalonic acidemia: a megamitochondrial disorder affecting the kidney. *Pediatr Nephrol.* 2014 Nov;29(11):2139-46. doi: 10.1007/s00467-014-2847-y. Epub 2014 May 28. PubMed PMID: 24865477.

8. LIST OF PUBLICATIONS

1. De Pasquale V*, **Costanzo M***, Siciliano RA, Mazzeo MF, Pistorio V, Bianchi L, Marchese E, Ruoppolo M, Pavone LM, Caterino M. *Proteomic analysis of mucopolysaccharidosis IIIB mouse brain*. *Biomolecules*. 2020 Feb 26;10(3). pii: E355. doi: 10.3390/biom10030355. PubMed PMID: 32111039.
*equal contribution
2. Caterino M, Ruoppolo M, Villani GRD, Marchese E, **Costanzo M**, Sotgiu G, Dore S, Franconi F, Campesi I. *Influence of Sex on Urinary Organic Acids: A Cross-Sectional Study in Children*. *Int. J. Mol. Sci.* 2020 Jan 16;21(2). pii: E582. doi: 10.3390/ijms21020582. PubMed PMID: 31963255.
3. Giacco A, Delli Paoli G, Senese R, Cioffi F, Silvestri E, Moreno M, Ruoppolo M, Caterino M, **Costanzo M**, Lombardi A, Goglia F, Lanni A, de Lange P. *The saturation degree of fatty acids and their derived acylcarnitines determines the direct effect of metabolically active thyroid hormones on insulin sensitivity in skeletal muscle cells*. *FASEB J.* 2019 Feb;33(2):1811-1823. doi: 10.1096/fj.201800724R. Epub 2018 Sep 11. PubMed PMID: 30204501.
4. **Costanzo M**, Cevenini A, Marchese E, Imperlini E, Raia M, Del Vecchio L, Caterino M, Ruoppolo M. *Label-Free Quantitative Proteomics in a Methylmalonyl-CoA Mutase-Silenced Neuroblastoma Cell Line*. *Int J Mol Sci.* 2018 Nov 13;19(11). pii: E3580. doi: 10.3390/ijms19113580. PubMed PMID: 30428564; PubMed Central PMCID: PMC6275031.
5. Ruoppolo M, Caterino M, Albano L, Pecce R, Di Girolamo MG, Crisci D, **Costanzo M**, Milella L, Franconi F, Campesi I. *Targeted metabolomic profiling in rat tissues reveals sex differences*. *Sci Rep.* 2018 Mar 16;8(1):4663. doi: 10.1038/s41598-018-22869-7. PubMed PMID: 29549307; PubMed Central PMCID: PMC5856765.
6. Caterino M, Zacchia M, **Costanzo M**, Bruno G, Arcaniolo D, Trepiccione F, Siciliano RA, Mazzeo MF, Ruoppolo M, Capasso G. *Urine Proteomics Revealed a Significant Correlation Between Urine-Fibronectin Abundance and Estimated-GFR Decline in Patients with Bardet-Biedl Syndrome*. *Kidney Blood Press Res.* 2018;43(2):389-405. doi: 10.1159/000488096. Epub 2018 Mar 8. PubMed PMID: 29539623.
7. Caterino M, Ruoppolo M, Mandola A, **Costanzo M**, Orrù S, Imperlini E. *Protein-protein interaction networks as a new perspective to evaluate distinct functional roles of voltage-dependent anion channel isoforms*. *Mol*

Biosyst. 2017 Nov 21;13(12):2466-2476. doi: 10.1039/c7mb00434f.
Review. PubMed PMID: 29028058.

8. **Costanzo M**, Zacchia M, Bruno G, Crisci D, Caterino M, Ruoppolo M. *Integration of Proteomics and Metabolomics in Exploring Genetic and Rare Metabolic Diseases*. *Kidney Dis (Basel)*. 2017 Jul;3(2):66-77. doi: 10.1159/000477493. Epub 2017 Jun 30. Review. PubMed PMID: 28868294; PubMed Central PMCID: PMC5567043.

9. ABBREVIATIONS

AdoCbl	adenosylcobalamin
Cas9	caspase-9
Cbl	cobalamin
CoA	coenzyme A
CRISPR	clustered regularly interspaced short palindromic repeats
DDA	data-dependent analysis
DDT	DL-Dithiothreitol
DIA	data-independent analysis
EXT2	exostosin-2
FBS	fetal bovine serum
FN1	fibronectin
GA	glutaric acidemia
GC-MS	gas chromatography – mass spectrometry
GFP	green fluorescent protein
GLUL	glutamine synthetase
GO	gene ontology
H ₂ DCFDA	2',7'-Dichlorodihydrofluorescein diacetate
HEK293	human embryonic kidney 293
HepG2	human hepatocellular carcinoma
IAA	iodoacetamide
IP	immunoprecipitation
KO	knockout
LC-MS/MS	liquid chromatography – tandem mass spectrometry
LFQ	label-free quantification
MeCbl	methylcobalamin
MMA	methylmalonic acidemia
MMACHC	methylmalonic aciduria and homocystinuria type C protein
MRM	multiple reaction monitoring
MTT	3-(4,5-dimethylthiazol-2-yl)-2,5-diphenyltetrazolium bromide
MUT	methylmalonyl-CoA mutase
NR	neutral red
NSAF	normalized spectral abundance factor
PA	propionic acidemia
PBS	phosphate buffered saline
qRT-PCR	quantitative real-time polymerase chain reaction
RES	rescue
ROS	reactive oxygen species
SAF	spectral abundance factor
SH-SH5Y	human bone marrow neuroblastoma
siRNA	small interfering ribonucleic acid

SDC2	syndecan-2
SDS-PAGE	sodium dodecyl sulfate - polyacrylamide gel electrophoresis
TCEP	tris(2-carboxyethyl)phosphine
VIM	vimentin
WB	western blot
WGA	wheat germ agglutinin
WT	wild type